



University of Adelaide  
Department of Geology and Geophysics

Automatic Interpretation of Gravity Data Over Step Faults  
with Example for South Australia  
Lidia E. Swietlik B.Sc. (Hons)  
January, 1993

A thesis submitted to the University of Adelaide in fulfilment of the requirements for the  
degree of Master of Science.

Awarded 1994

# Contents

1	Introduction	1
2	Faults	3
2.1	Introduction	3
2.2	Fault - Geology	6
2.3	Simple Faults	7
2.3.1	Description	7
2.3.2	Classification and Relation to Stress	14
2.3.3	Thrust Faults	15
2.3.4	Transcurrent Faults	16
2.3.5	Normal Faults	17
2.3.6	Dynamical Theory	19
2.4	Complex Faults	21
2.5	Reasons for Going into Details	27
3	Gravity Effect of Simple Fault Structure	28
3.1	Approximation of Fault Structure by Semi-Infinite Horizontal Slab	30
3.2	Fault_Structure Program	38
3.2.1	Input Data	39
3.2.1.1	Observed gravity	40

3.2.1.2	Parameter for the fault structure . . . . .	40
3.2.2	Calculating Data . . . . .	43
3.2.3	Minimalization of the Difference between Observed and Calculated Gravity Data . . . . .	44
3.2.4	Output Data . . . . .	45
3.2.5	Relevant Subroutines Called by FAULT_STRUCTURE Program . . . . .	46
3.2.5.1	The subroutine: GRAVITY_OUT0 . . . . .	46
3.2.5.2	The subroutine: GRAVITY_OUT1 . . . . .	47
3.2.5.3	The subroutine: GRAVITY_0 . . . . .	48
3.2.5.4	The subroutine: GRAVITY_1 . . . . .	49
3.2.5.5	The subroutine: GRADIENT_0 . . . . .	50
3.2.5.6	The subroutine: GRADIENT_1 . . . . .	51
3.2.5.7	The subroutine: MODEL . . . . .	52
4	Adelaide City Area as the Example of Using the Fault_Structure Program . . . . .	53
4.1	Introduction . . . . .	53
4.2	Regional Geology . . . . .	54
4.3	The Para Fault Zone . . . . .	58
4.4	Gravity data . . . . .	58
4.5	Profiles . . . . .	61
4.6	Theoretical Model of Underground Structure Based on Gravity Survey . . . . .	61
4.7	Previous Work Based on Drilling . . . . .	61
4.8	Commentaries . . . . .	65
5	New Information about Faults in the Frome Embayment in South Australia Section of the Eromanga Basin . . . . .	68
5.1	Introduction . . . . .	68
5.1.1	Historical Note - Eromanga Basin in South Australia . . . . .	70

5.2	The Study Area .....	71
5.3	Gravity Data .....	73
5.4	Profiles .....	73
5.5	Theoretical model of underground structure .....	78
5.6	Commentaries .....	90
6	Conclusions .....	98
A	Mathematical Formula for Simple Shapes .....	A-1
A.1	Fundamental Theory .....	A-1
A.1.1	Force of Gravitation .....	A-1
A.1.2	Acceleration of Gravity .....	A-2
A.1.3	Gravitational Potential .....	A-2
A.1.4	Three-Dimensional Potential .....	A-3
A.1.5	Two Dimensional Potential .....	A-4
A.2	Gravity Effects of Simple Two-dimensional Bodies .....	A-5
A.2.1	Thin Dipping Sheet .....	A-5
A.2.2	Thick Prism .....	A-7
A.2.3	Semi-Infinite Horizontal Slab .....	A-9
B	Computer Programs .....	B-1
B.1	FAULT_STRUCTURE Program .....	B-1
B.2	Subroutine GRAVITY_0 .....	B-11
B.3	Subroutine GRAVITY_1 .....	B-12
B.4	Subroutine GRAVITY_OUT0 .....	B-13
B.5	Subroutine GRAVITY_OUT1 .....	B-14
B.6	Subroutine GRADIENT_0 .....	B-15
B.7	Subroutine GRADIENT_1 .....	B-16

B.8 Subroutine MAXGR .....	B-17
B.9 Subroutine MODEL .....	B-19
C Initial and Output Data for Theoretical Models .....	C-1
C.1 Adelaide City Area .....	C-1
C.1.1 Gravity Data from File OBS_GRAV.DAT .....	C-1
C.1.2 Output Data from File OUT_INF.DAT .....	C-2
C.1.3 Output Data from File OUT_GR.DAT .....	C-3
C.1.4 Output Plot from File PLOT1.PLT .....	C-4
C.1.5 Output Data from File PLOT2.PLT .....	C-5
C.2 Eromanga Basin - Line no.13a .....	C-6
C.2.1 Gravity Data from File OBS_GRAV.DAT .....	C-6
C.2.2 Output Data from File OUT_INF.DAT .....	C-7
C.2.3 Output Data from File OUT_GR.DAT .....	C-8
C.2.4 Output Plot from File PLOT1.PLT .....	C-9
C.2.5 Output Data from File PLOT2.PLT .....	C-10
C.3 Eromanga Basin - Line no.12a .....	C-11
C.3.1 Gravity Data from File OBS_GRAV.DAT .....	C-11
C.3.2 Output Data from File OUT_INF.DAT .....	C-12
C.3.3 Output Data from File OUT_GR.DAT .....	C-13
C.3.4 Output Plot from File PLOT1.PLT .....	C-14
C.3.5 Output Data from File PLOT2.PLT .....	C-15
C.4 Eromanga Basin - Line no.3; One Fault .....	C-16
C.4.1 Gravity Data from File OBS_GRAV.DAT .....	C-16
C.4.2 Output Data from File OUT_INF.DAT .....	C-17
C.4.3 Output Data from File OUT_GR.DAT .....	C-18
C.4.4 Output Plot from File PLOT1.PLT .....	C-19
C.4.5 Output Data from File PLOT2.PLT .....	C-20

C.5	Eromanga Basin - Line no.3; Two Faults .....	C-21
C.5.1	Gravity Data from File OBS_GRAV.DAT .....	C-21
C.5.2	Output Data from File OUT_INF.DAT .....	C-22
C.5.3	Output Data from File OUT_GR.DAT .....	C-23
C.5.4	Output Plot from File PLOT1.PLT .....	C-24
C.5.5	Output Data from File PLOT2.PLT .....	C-25
C.6	Eromanga Basin - Line no.11 .....	C-26
C.6.1	Gravity Data from File OBS_GRAV.DAT .....	C-26
C.6.2	Output Data from File OUT_INF.DAT .....	C-27
C.6.3	Output Data from File OUT_GR.DAT .....	C-28
C.6.4	Output Plot from File PLOT1.PLT .....	C-29
C.6.5	Output Data from File PLOT2.PLT .....	C-30
D	Abbreviations .....	D-1
	Bibliography .....	95

# List of Figures

2.1: Terminology for fault plane ( d - dip )	7
2.2: Nature of movement	8
2.3: Rotation movement	9
2.4: Net slip, dip slip, and strike slip	10
2.5: Apparent displacement in vertical section equals the net slip	11
2.6: Apparent displacement in a vertical section gives erroneous impression that hanging wall has gone up	12
2.7: Apparent displacement in vertical section equals net slip	13
2.8: Fault is parallel to bedding, and hence there is no apparent displacement	13
2.9: Planes of actual faulting - Thrust Faults	15
2.10: Reverse Fault	16
2.11: Planes of actual faulting - Transcurrent Faults	17
2.12: Planes of actual faulting - Normal Fault	18
2.13: Normal Fault	19
2.14: Deformation caused by transcurrent faults	20
2.15: Contraction and extension faults	21
2.16: Block diagram to show the main features of extension faults	22
2.17: The appearance of an extension basin in cross-section	23
2.18: A detachment fault in cross-section, north-central Montana	23
2.19: Interpretation of the sequence of generation of extension faults	24

2.20: Structure characteristics of planar high-angle normal fault zones such as those bounding grabens in terrains that have been inhomogeneously extended by small percentage .....	24
2.21: Block diagram to show the main features of thrust faults .....	25
2.22: Imbricate zone in map and section. Near Lochcarron, Scotland .....	26
3.1: Actual geological structure .....	28
3.2: Theoretical model .....	29
3.3: Gravity effect of the vertical fault .....	30
3.4: Gravity effect of two vertical faults .....	31
3.5: Gravity effect of two normal faults .....	32
3.6: Gravity effect of two normal faults .....	33
3.7: Gravity effect of two vertical faults (small distance between them) .....	34
3.8: Gravity effect of two vertical faults (large distance between them) .....	34
3.9: Gravity effect of two vertical faults .....	35
3.10: Gravity effect of two vertical faults (big difference between the depth) .....	36
3.11: Gravity effect of two normal faults (big difference between the depth) .....	37
3.12: Theoretical model .....	38
4.1: The St Vincent Basin .....	54
4.2: Regional geological map .....	55
4.3: Geological section across Adelaide region .....	56
4.4: Summary of geology .....	57
4.5: Intersections and structure contours of Precambrian bedrock .....	59
4.6: Map of Adelaide showing position of Para Fault and approximate line of survey .....	60
4.7: Theoretical model .....	62
4.8: The observed and calculated gravity data for theoretical model .....	63
4.9: Geological section .....	64



4.10: Location plan of bores and gravity survey line .....	66
5.1: Locations of geological contributions .....	71
5.2: Study Area Location .....	72
5.3: The Bouguer anomaly map for Lake Frome area .....	74
5.4: The profile of line no. 3 .....	75
5.5: The profile of line no. 12a .....	76
5.6: The profile of line no. 13a .....	77
5.7: The theoretical model for line no. 13a .....	79
5.8: Observed and calculated gravity for line no. 13a .....	80
5.9: The theoretical model for line no. 12a .....	81
5.10: Observed and calculated gravity for line no. 12a .....	82
5.11: First theoretical model for line no. 3 .....	83
5.12: Observed and calculated gravity for line no. 3 (one fault) .....	84
5.13: Second theoretical model for line no. 3 .....	85
5.14: Observed and calculated gravity for line no. 3 (two faults) .....	86
5.15: The profile of line no. 11 .....	87
5.16: The theoretical model for line no. 11. ....	88
5.17: Observed and calculated gravity for line no. 11 .....	89
A.1: Gravity effect of a thin sheet of infinite strike length .....	A-6
A.2: Gravity effect of a thick prism of infinite strike length .....	A-7

# Statement

This thesis contains no material which has been accepted for the award of any other degree or diploma in any university and, to the best of my knowledge, no material previously published or written by another person, except where due reference is made in the text.

I consent to the thesis being made available for photocopying and loan where applicable if accepted for the award of the degree.

  
Lidia E. Swietlik

January, 1993

# Acknowledgments

Firstly, I would like to thank my supervisor, Professor David Boyd for his invaluable advice, encouragement, useful comments, suggestions and patience from start to finish of this project.

Special thanks Dr. Shanti Rajagopalan for her assistance in many areas and help over the time I have known her.

Dr. Peter Brooker, Dr. John Pain and Mr. Andy Mitchell are thanked for some helpful information and access to their software programs.

Thanks to the staff and my colleagues of Department of Geology and Geophysics for their discussion and help.

I am grateful to the South Australian Department of Mines and Energy for supplying the magnetic tapes with the gravity data that I used.

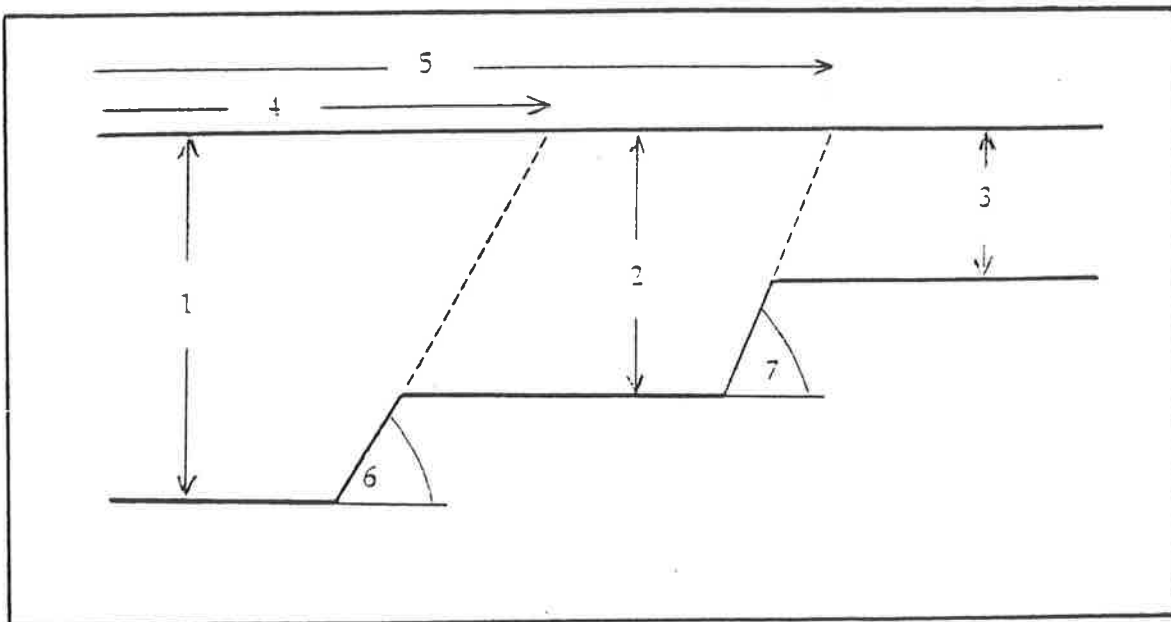
I wish to thank the Defence Science and Technology Organisation for granting me study time which allowed me to complete the thesis and thanks to the staff of DSTO particularly to Dr. Ray Janus for his useful comments and interest.

Finally, I would like to thank my family, especially my husband for encouragement and inspiration when I needed it.

## Abstract

A program called FAULT STRUCTURE has been written which will obtain the best match of observed gravity data to a simple step fault using the following criteria for the best match based on the minimum total difference between the observed values and calculated values of gravity data.

The operating instructions allow for seven possible variables in the geometry of the faults



If any of the variables is known the accuracy of the solution and the speed obtaining the solution is increased.

This method has been applied and shown to work well with ideal data and ideal data with 10% noise. It has also been applied to real data and examples from the Paralana Fault, Mount Painter and Para Fault, Adelaide City and suburbs.

A major problem in testing the area was to find step faults in which the exact positions, throws and dips of the faults with sufficient precision to test the method properly.

Program FAULT STRUCTURE provides rapid accurate theoretical modelling of step fault structures. The method can be used as an additional source of information in the research of the faults which form the edges of sedimentary basins and in which the geology of the basin with the density contrast is well defined and simple. Although as a theoretical tool program FAULT STRUCTURE is not 100% accurate, when used it will make underground models more realistic. In exploration activities having such a model will save time and money.

Program FAULT\_STRUCTURE would provide better instruments for more accurate theoretical modelling of faults structures. This method can be used as an additional source of information in the research of the faults.

The original contributions of this research are to be found in chapter 3 and expanded in Appendix C and the demonstration that it works is shown in chapter 4 and 5.

There is nothing original in chapter 2 and the geology is elementary. It is written and included because understanding the simple geometry of faults is so important in understanding the limitations in applying the interpretation method development.

# Chapter 1

## Introduction

This thesis is about the use of the gravity method to obtain better information about faults. Faults are common and sometimes fairly simple geological structure and knowledge of the geometry can contribute to the understanding of the operation of the stresses which produced the folds and faults in the area. Very often geologists are not able to observe faults and must infer or assume the indication of the faults. The actual gravitational effect of faults is observed directly: if there is a density contrast between rocks on either side of the fault then there will be a gravity anomaly and from the shape of this anomaly it is possible to deduce information about the dip of the fault plane and consequently of the nature of the faults providing the anomaly. This new information is important for geologists trying to understand the tectonic development of a region.

The mathematical formula for the gravity anomaly due to a simple fault has been known for many years (Heiland 1940). The form of the expression normally used for computing the effect was published by Talwanii (1959).

In this thesis the simple slab formula is used in a program written for a VAX main frame to obtain the best model of a simple structure involving two faults in which the variables are the depth of the faulted surface and the angle of dip of the faults.

This simple approach makes use of the considerable computing power of the VAX main frame. The method will also be effective on the faster P.C.s available today (1992).

It was the purpose of this research to be practical. If any method is to be useful must be tested first on theoretical data without and with the addition of noise. It must then be applied to real data to discover if there are any new difficulties encountered.

The tests on real data was first tried with gravity data from the Eromanga Basin, (see figure 5.12). It is part of data set which was provided on a magnetic tape by SADME. Much of the gravity data was collected during the decade interval 1955 and 1965 by the petroleum exploration Co. Delhi Petroleum. This data was collected at 2 km spacing on a wider grid of approximately 20 km square. Gravity data in Adelaide area was collected by SADME as part of a study of the structure of the Adelaide city region. Observations were made at close intervals-often stations were 50 or 100 metres apart. Additional gravity observation were made by students and staff from the Department of Geology and Geophysics of the University of Adelaide.

Although a lot of work was done with the data from the Eromanga Basin and results were obtained, it was not possible to use this work to test the method as not enough was known about the faults covered by the survey. Later tests were done using data from the Adelaide and Willunga Basin where the faults are better known but even here it was not possible to get exact information about the faults to test the method fully.

This research was started in April 1985 but had to be deferred in January 1988 due to family problems which made it impossible to continue . In 1990 my new employer DSTO granted me study time of half day per week which allowed me to complete this thesis.



## Chapter 2

### Faults

#### 2.1 Introduction

As this thesis is concerned with discovering further information about the character and nature of faults it is necessary to consider what faults are, why they are important and what kind of information can be obtained from them.

The gravity anomaly shape is related to the "shape" of the fault and the shape of the fault is related to the stresses which caused the fracture of the rocks which produced this fault - it is therefore appropriate to examine classification of faults types which occur in nature and also necessary to provide an explanation for the different types of faults in order to understand how the results of the analysis of the gravity data will be used.

A gravity anomaly depends on the existence of a density contrast between rocks on either side of the fault: therefore the gravity study starts with the situation in which the biggest density contrast occurs, as this is likely to be the easiest problem. This is usually between the high density basement rocks and the lower density sediments - justification for this choice of problem will be provided in later chapters.



To solve the problems of the direction of earlier stresses it is important to understand the origin of fault and to be able to describe them as clearly as possible. That is the purpose of this chapter.

There are three fundamental structures which affect rocks, folds, faults and unconformities. They are so basic in geology that they are introduced in every elementary text book on geology but they are also so complex that specialist studies have yet to exhaust the variety in which they are expressed.

Folds are the result of ductile deformation of rocks, deformation in which there are no discontinuities.

Faults in contrast are the result of brittle deformation which results in the rupture and dislocation of bodies which have at one time been in contact. Both are the result of regional stressing of the rocks.

Unconformities mark another type of dislocation, a dislocation in time, in which younger rocks are laid on the eroded surface of older rocks. Although unconformities are a different type of feature it is important to note that in the field the distinction between faults and unconformities is not necessarily obvious.

Faults may be observed at the surface in quarries and in road cuttings and occasionally in stream beds but on the whole observation of outcrops of faults are rare and there are many faults which are deduced from the outcrop pattern of the rocks but which are not themselves observed. Consequently much has often to be assumed about the inclination of the fault which may be important for a geologist who is trying to understand the development of the geological structure of an area.

Faults are often seen underground in mines: they were first recognised and seriously studied in coal mines because of the serious consequences they had in displacing the coal seams. It was probably at this time that the significance of the dip of the fault and the implied direction of movement was appreciated and for this reason a classification of faults into normal, reverse and thrust faults was introduced. This classification was made long before the mechanics of fault formation was understood.

The relationship between the stresses in the earth crust and the actual movement along fault planes was developed by E.M.Anderson (1942) and from his conclusions about the nature of regional stresses and the understanding of fault patterns arose. From this there has come a proliferation of studies which is outside the scope of this review because they are concerned with aspects of detailed fault descriptions about which the gravity response of the faults which responds to the large scale feature of the faults can give little assistance.

Faults have a potential to be a target for gravity surveys and some of them will be explored. In this research the problem is best approached in its simpler forms, that is where there is one or at most two faults which separate rock groups with a substantial difference in density between the rocks and where it is assumed the density variations within the bodies is not great. It was considered that there was no point in trying to solve complex problems until the method had been tested and proved on simple ones.

The special problem, which is considered in more detail here is one in which there is a basin of younger sedimentary rocks with a faulted margin and lying within a basement of older and probably metamorphosed basement and denser rocks.

Examples of such basin structure are widespread. In South Australia examples have been examined from the Telfer Basin at Leigh Creek, the Adelaide Tertiary basin and the Wilunga Basin south of Adelaide as well as the western edge of Eromanga Basin and Mt Painter. Other examples of gravity profiles over rift valleys boundary faults in Western Australia , East Africa and Germany have also been studied.

It is appropriate to comment on the description of the problem used above as being " simpler ". No geophysical interpretation is simple, some are just less complex than others. In some cases the assumption of simplicity is not unreasonable and allows workable conclusions to be drawn. In this case assumptions are made about a uniform density within the sediments. If the basin is shallow and the sediments are mainly sands, this assumption is likely to give useful results; if however the basin is one or more kilometre deep and the sediments include a substantial volume of clay, the densities of the rock within the basin are likely to increase considerably with the compression due to the weight of overlying rocks and the simple problem becomes less simple.

Similarly, there may be substantial density contrasts within the basement rocks and this too will invalidate the assumption of a simple density contrast between the basement and the basin fill.

Faults are often very complicated but as the gravity method responds to large masses of rock the "appearance" of the fault to the gravity method is usually a simpler structure.

## 2.2 Fault - Geology

Faults are perhaps the most frustrating structures to deal with on a map. On the one hand, they are tremendously important features, in both academic and industrial work. They can, for example, interfere with the predictions of the mining geologist and cause special problems for the civil engineer. Even non-geologist may well know something about faults, if only the devastating effects of earthquakes that can arise from earth movements along them.

Faults are known because they are actually seen in surface outcrops, mine and boreholes. Faults are recognised on geological maps by the displacement of outcrops of rocks which are otherwise continuous and by the juxtaposition of rocks of different ages each side of the fault.

Often, however, the fault is not seen but has to be inferred from other evidence such as unexpected rocks in contact, a break in the pattern of the rocks, from topography such as escarpments or very straight rivers. The fracturing of rocks adjacent to a fault plane makes them less resistant to weathering so that the outcrop of a fault is commonly marked by an erosional feature - stream, valley, lake, escarpment, or coast line. Large faults which bring together rocks of different lithology may be further marked by a contrast between areas of differing topography, vegetation, and land use.

Although faults may be very common in some areas the different rocks separated by the fault plane along which movement has taken place may not actually be seen in any place and it is necessary to infer the presence of the faults. As a result it can be very difficult to get exact information about the fault ( see for example Adelaide city fault described by J. Selby and J. Lindsay (1982) and investigated in chapter no. 4 ).

This may also be true underground or in a drill hole because faulted rock is soft and breaks easily, also the fault plane is not a simple uniform sheet but is distorted and what you see in the mine or the drill hole is not necessarily typical of the dip of the whole fault.

Geologists solve this difficult problem by making a range of different types of observations of small scale structures associated with faults and this is used along with geophysical observations to get the best picture and detailed information about the fault.

## 2.3 Simple Faults

### 2.3.1 Description

Faults may be complicated but as the gravity method responds to large masses of rock the "appearance" of the fault to the gravity method is usually a simpler structure. Faults are recognised in geology by the abrupt ending of a sedimentary layer (such as a coal seam in mine), by observation of the broken rocks in the fault plane itself; it was the need of miners to predict where to dig or drill for the extension of a faulted coal seam that led to the study of faults.

Faults are ruptures along which the opposite walls have moved past each other. The essential feature is differential movement parallel to the surface of the fracture. Some faults are only a few inches long, and the total displacement is measured in fractions of an inch. At the other extreme, there are faults that are hundreds of miles long with a displacement measured in miles or even tens of miles.

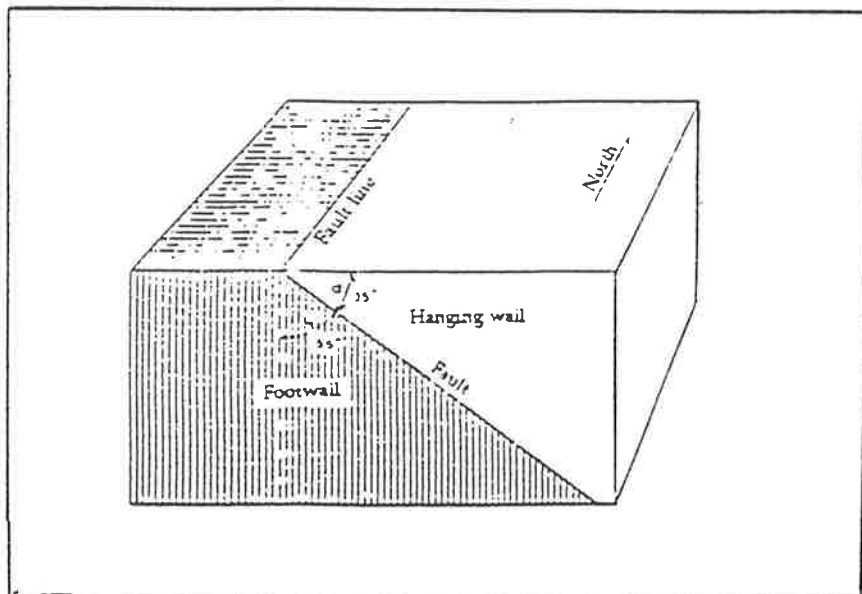


Figure 2.1: Terminology for fault plane ( d - dip ).

The strike and dip of the fault are measured in the same way as they are for bedding or jointing. The strike is a trend of horizontal line in the plane of the fault. The dip is the angle between a horizontal surface and the plane of the fault, and is measured in a vertical plane that strikes at right angles to the fault. The intersection of the fault with the surface of the earth is known as the fault line, fault trace or fault outcrop. In most instances, the fault line, is shown on a map as reasonably straight or sinuous but often the actual position of the fault is not known with precision. If the dip of the fault is low and the topographic relief high, the fault line may be exceedingly irregular.

The movements along faults may be translatory or rotational. In translatory movements there has been no rotation of the blocks relative to each other; all straight lines on opposite sides of the fault and outside the dislocated zone that were parallel before the displacement, are parallel afterwards.

In figure 2.2 two points a and a' contiguous before faulting, have been separated by the faulting. The right-hand block has moved directly down the dip of the fault relative to the left-hand block. The lines bc and c'd which were parallel before faulting, are also parallel after faulting. In diagram B the right hand block has moved diagonally down the fault, the lines bc and c'd parallel to each other before faulting are also parallel after faulting.

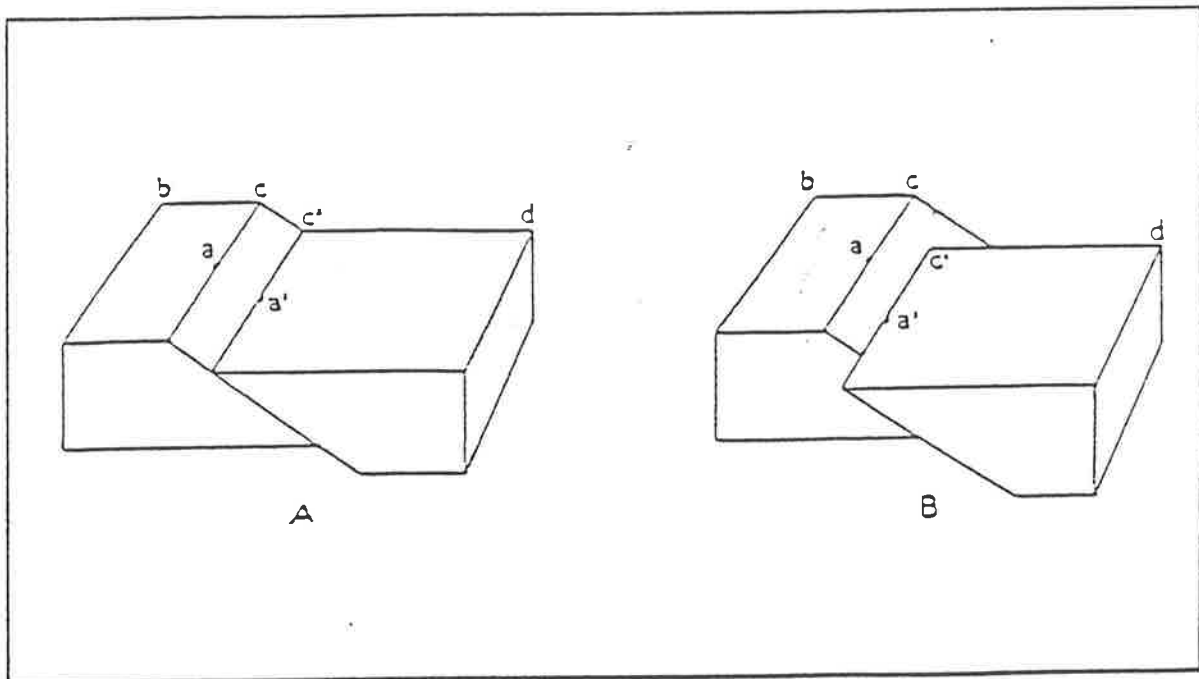


Figure 2.2: Nature of movement.

Those movements in which some straight lines on opposite sides of the fault and outside the dislocated zone, parallel before the displacement, are no longer parallel afterwards. In diagram C the right-hand block has gone down relative to the left-hand block, but the displacement increases toward the front. At point there has been no displacement, but b and b' were contiguous before faulting. Lines ca and ad parallel before faulting, are not parallel after faulting.

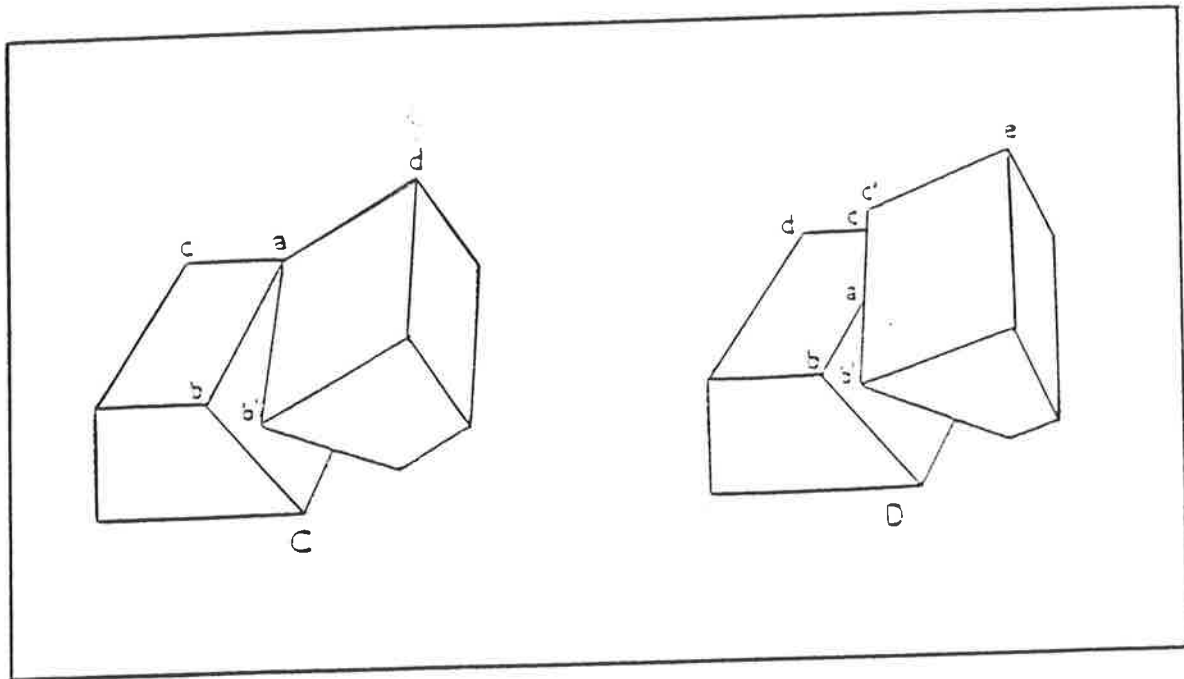


Figure 2.3: Rotation movement.

In diagram D the back part of the right-hand block has gone up relative to the left-hand block, but the forward part of the right-hand block has gone down. The lines dc and c'e parallel before faulting, are no longer parallel after faulting. A line within the fault plane and separating that part of the right-hand block that has gone up from that part that has gone down, is known as the hinge or hinge line. Faults in themselves never offer any direct evidence as to which block actually moved. The next diagram (see figure 2.4) illustrates some of the various kinds of relative movements that may take place along a translatory fault. In part A the hanging wall has moved directly down the dip relative to the footwall. In part B the hanging wall has moved parallel to the strike, in part C the hanging wall

has moved diagonally down the fault plane. In D the hanging wall has moved directly up the dip of the fault, and in E the hanging wall has moved diagonally up the fault plane.

The term slip is used to indicate the relative displacement of formerly adjacent points on opposite sides of the fault and it is measured on the fault surface. The net slip  $ab$  (see figure 2.4) is the total displacement and is the distance measured on the fault surface between two formerly adjacent points situated on opposite walls of the fault.

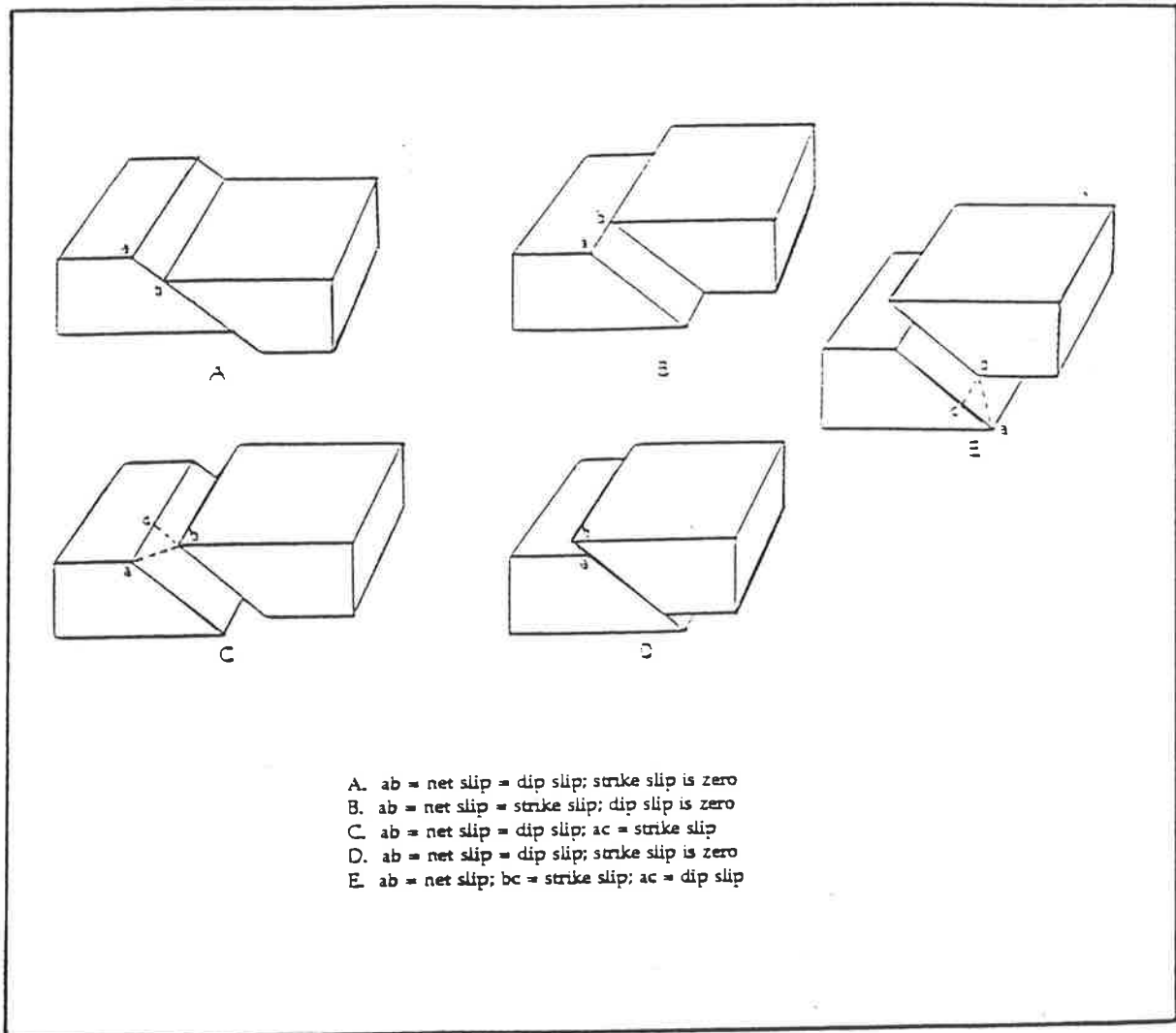


Figure 2.4: Net slip, dip slip, and strike slip.

The strike-slip is the component of the net slip parallel to the strike of the fault, as indicated by  $ac$  in diagram C. The dip-slip is the component of the net slip measured parallel to the dip of the fault plane;  $bc$  in figure 2.4 C.

In figure 2.4 A and D the dip slip equals the net slip, and the strike slip is zero. In figure 2.4 B the strike slip equals the net slip  $ab$ , and the dip slip is zero. In fig 2.4 E the movement is diagonal, there is both a dip slip  $ac$ , and strike slip  $bc$ , component to the net slip  $ab$ .

The above discussion has not considered the effects of relative movements on the disrupted strata or veins. The apparent movement of the disrupted strata may be very different from the net slip. This point is very important because the net slip is what is interpreted from the gravity survey data. The apparent movement is a function of many variables and depends not only on the net slip, but also on the strike and dip of the fault, the strike and dip of the disrupted strata and the attitude of the surface on which the observations are made. It is possible for the apparent movement to be zero, although the net slip may be great.

The next figures show the relationship between the net slip and the apparent movement under different conditions.

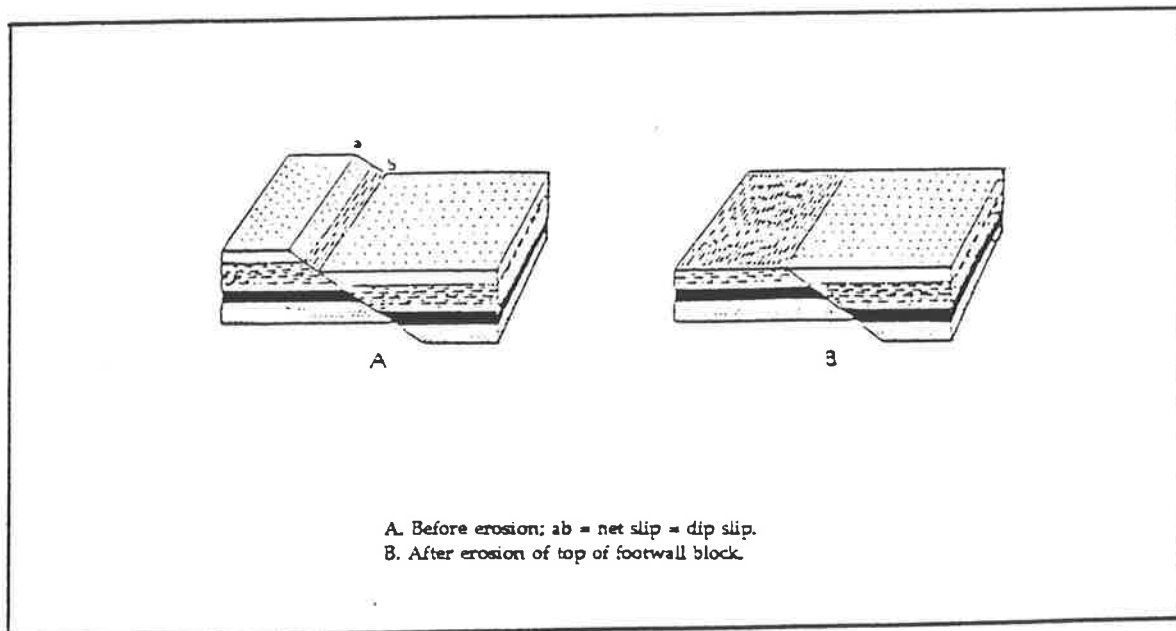


Figure 2.5: Apparent displacement in vertical section equals the net slip, (M. P. Billing).



In figure 2.5 the beds are horizontal and the net slip is directly down the dip. Diagram A illustrates relations before erosion and diagram B shows the relations after the left-hand block has been eroded to the level of the right-hand block. On the map, the upper surface of figure 2.5 B, different beds outcrop on opposite sides of the fault. On the front of the blocks, the apparent movement equals the net slip. A dip valley or an artificial opening such as a quarry or mine, might produce an exposure of this sort.

Below are some pictures of possible relative movements along faults and effects on disrupted strata, and because there could be a lot of different configurations, I chose only a few as illustration of the problem.

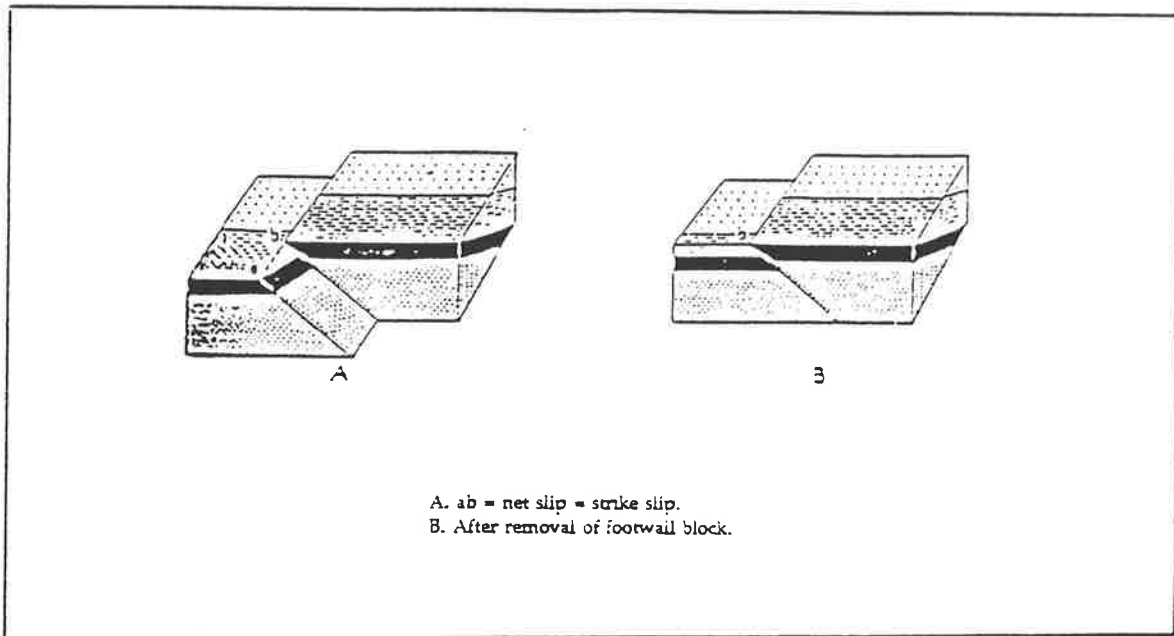


Figure 2.6: Apparent displacement in a vertical section gives erroneous impression that hanging wall has gone up, (M. P. Billings).

In figure 2.6, the net slip is parallel to the strike of the fault. Diagram A shows the relations before erosion; diagram B indicates the relations after the front of the left-hand block has been eroded back to coincide with the front of the right-hand block. On the map, the apparent movement equals the net slip, but the apparent movement on the front of the block, diagram B, gives the false impression that the hanging wall has moved up.

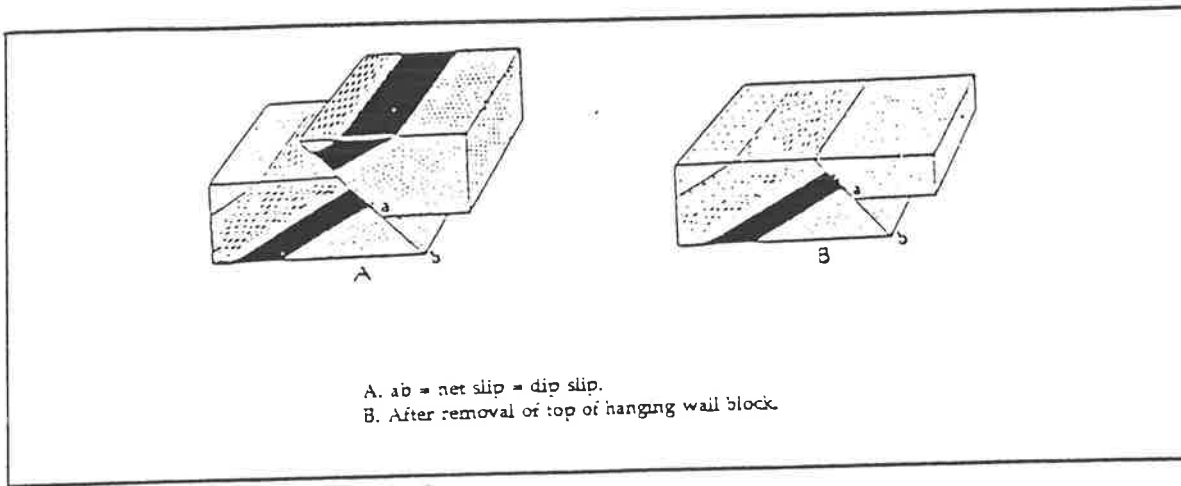


Figure 2.7: Apparent displacement in vertical section equals net slip, (M. P. Billings).

Figure 2.7 illustrates a fault that strikes parallel to the strike of the strata, but the hanging wall has moved up relative to the footwall. The net slip is the same as the apparent movement on the front of the block in diagram A. If the right hand block is eroded to the level of the left-hand block, the bed shown in solid black does not crop out on the surface.

Figure 2.8 is the special case in which the fault and the strata have not only the same strike, but have also the same dip. It is obvious that, in such a or cases, the apparent movement on the map and in the cross section is zero, regardless of the value of the net slip.

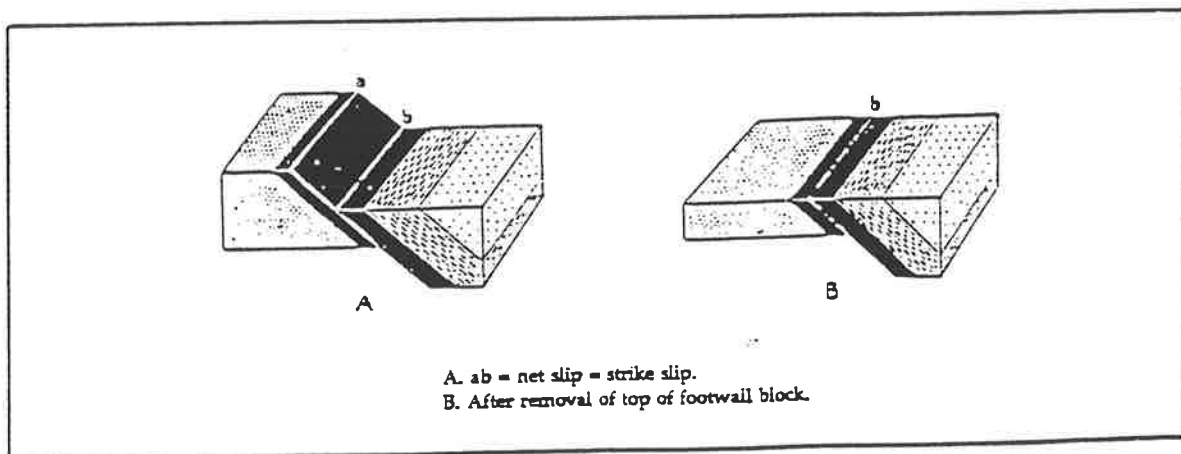


Figure 2.8: Fault is parallel to bedding, and hence there is no apparent displacement, (M. P. Billings).

These examples have been cited in great detail to emphasise that the apparent movement may be very deceiving and it is essential to understand this when interpreting the gravity data. Moreover, it is disconcerting to realise, that even if we know the dip and strike of the fault, the dip and strike of the disrupted strata and the apparent movement, it is impossible to determine the net slip.

### 2.3.2 Classification and Relation to Stress

The classification of faults is based on strike and dip of the fault plane and the relative direction of movement of the rocks on either side of the fault. This results in three types of faults:

- reverse/thrust faults
- transcurrent faults
- normal faults

These definitions are not intended to be critical, or to include every case of faulting. It may be said, that the majority of faults can easily be assigned to one or other of the three classes.

The above subdivision refers only to faulting and this is not the only type of fracture which geologists have to deal with.

The following assumptions were first set forth by E. M. Anderson (1942) to explain the origin of faults: one of the principal directions of stress is, in normal circumstances, nearly vertical. The other two principal directions must then be nearly horizontal, and these were fairly constant in direction, for long distances, during certain geological epochs.

Three relations between the magnitudes of the principal stresses are possible:

1. There may be increase of pressure in all horizontal directions.
2. There may be increase of pressure in one horizontal direction,  
with relief of pressure in the horizontal direction at right angles
3. There may be relief of pressure in all horizontal directions.

### 2.3.3 Thrust Faults

Suppose there is an increase of pressure in all horizontal directions and there is one horizontal direction along which pressure is greatest. This maximum pressure is P. Then R, the minimum pressure, will be vertical, and the intermediate pressure, Q, will be in horizontal direction. There will be two sets of planes across which tangential stress is at a maximum. Both sets will have their "strike" parallel to Q, and perpendicular to P. They will dip at angles of  $45^\circ$ , in opposite directions. Suppose now that the stresses are so great as to lead to actual fracture. In that case, the planes of faulting will also strike parallel to Q, but they will be inclined at less than  $45^\circ$  to the direction of P, that is to the horizontal. They should form two series which dip in opposite directions in the vertical plane which contains the greatest pressure, at approximately the same angles.

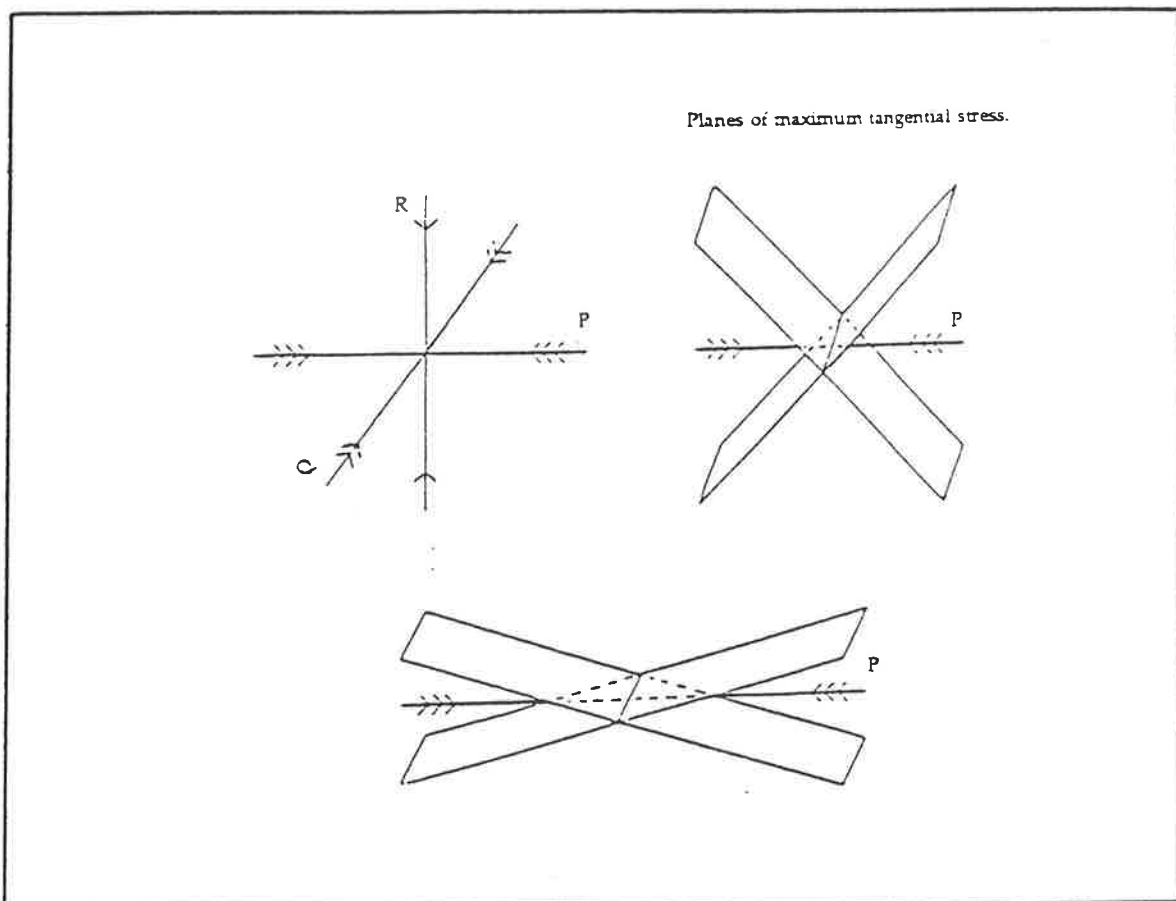


Figure 2.9: Planes of actual faulting - Thrust Faults, (E. M. Anderson).

A reverse fault then, is one in which the rocks above the fault plane move up relative to rocks below. A reverse fault in which the dip is so small that the overlying block is pushed predominantly horizontally is a thrust fault.

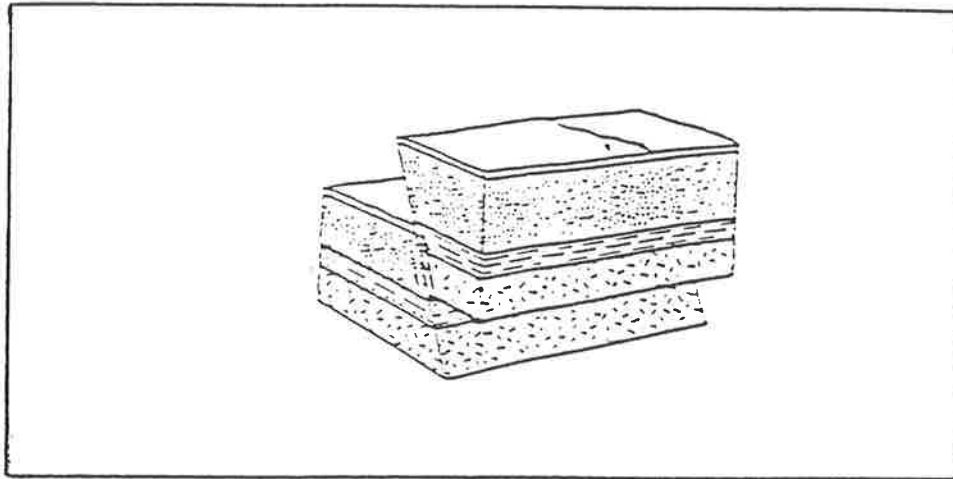


Figure 2.10: Reverse Fault.

Thrusts are faults which are inclined, in theory, at well under  $45^{\circ}$  to the horizon, and in field experience it is found that they are sometimes nearly horizontal.

The rock which forms the overlying layer has been impelled directly, or almost directly, up the slope of the fault plane. As the slope is a low one, the movement is nearly more horizontal than vertical, and a thrust fault may therefore be classed as tangential. Some low angle faults are not easily detected by gravity surveys.

### 2.3.4 Transcurrent Faults

In the second case, there is an increase of pressure in one horizontal direction, and a relief of pressure in a horizontal direction at right angles to the first. The maximum pressure,  $P$ , is then horizontal; the intermediate principal pressure is vertical, while the third principal direction, which may correspond

to extension, or to the smallest pressure, is horizontal and at right angles to P. The planes of maximum tangential stress are in this case vertical, and inclined at angles of  $45^\circ$  to the directions of P and R. The planes of actual faulting will deviate from these positions so as to form smaller angles with P.

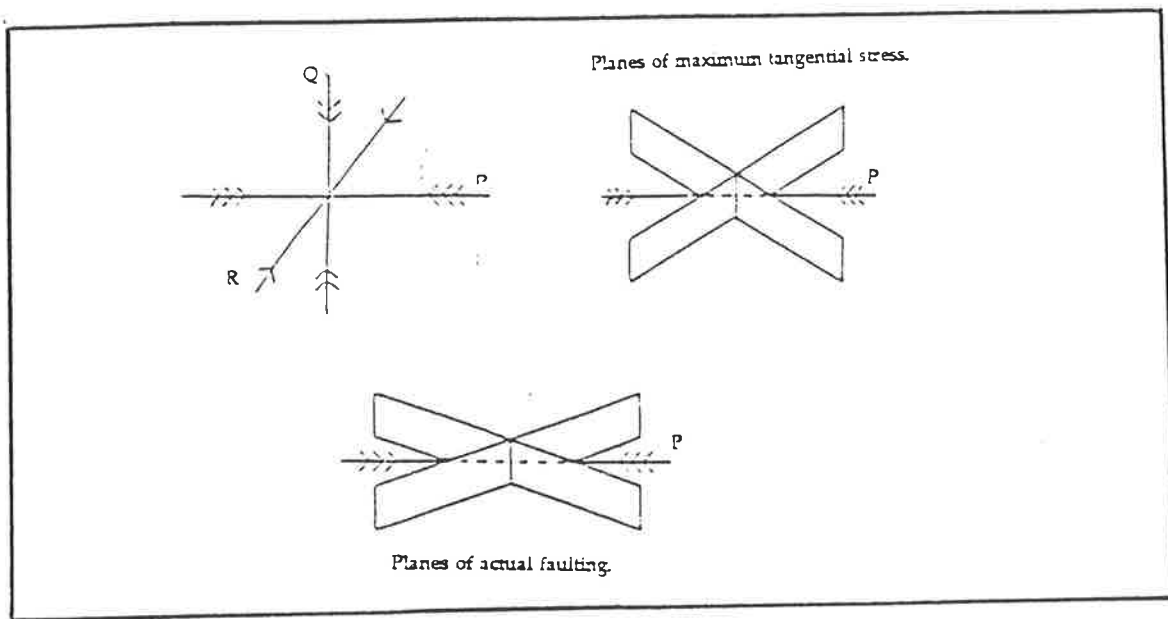


Figure 2.11: Planes of actual faulting - Transcurrent Faults, (E. M. Anderson).

A Transcurrent fault is a nearly vertical fracture, along which the separated segments have slid in a horizontal or nearly horizontal manner. Here again there is "tangential" movement.

### 2.3.5 Normal Faults

In the third case there is relief of pressure in all horizontal directions. The greatest pressure is then the vertical pressure which is due to gravity. It can seldom happen that the pressures or tensions, in

all horizontal directions, are equal. The planes of maximum tangential stress will in this case strike parallel to Q, and perpendicular to R, and they will dip in opposite directions at 45°. The planes of actual faulting will deviate from these positions so as to form smaller angles with P the vertical pressure. The result will be a double series of fault planes, dipping in opposite directions at angles of more than 45°, and striking at right angles to the direction in which relief of pressure is greatest. Motion will take place along these planes in the manner characteristic of normal faults.

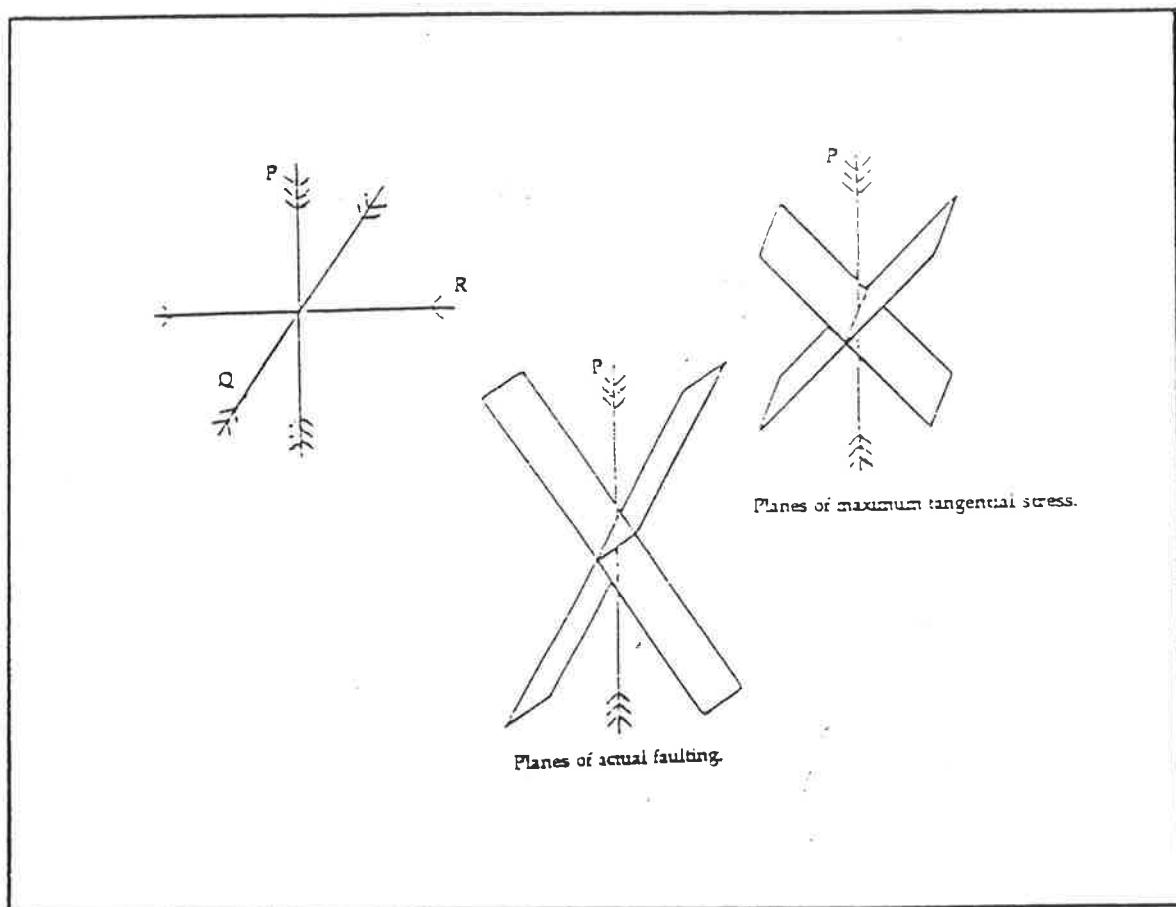


Figure 2.12: Planes of actual faulting - Normal Fault, (E. M. Anderson).

Faults need a further characterisation, since the movement can be up or down, or right or left. A normal fault is one in which the rock above the fault plane move down relative to the rocks below.

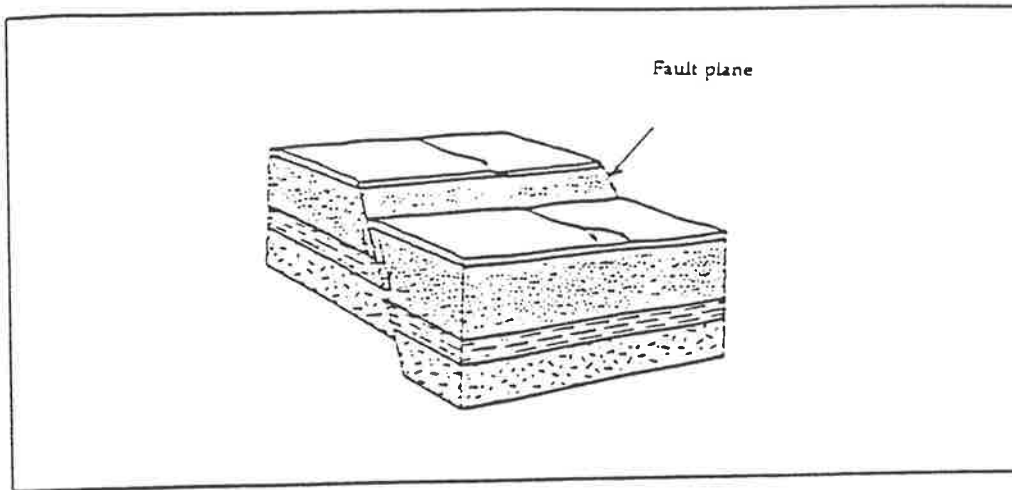


Figure 2.13: Normal Fault.

Normal faults are, in theory, steep, but not vertical. Their angle is usually found to be well over  $45^\circ$ . The overlying block has, in this case, moved directly, or almost directly, down the slope of the fault-plane. The movement is more nearly vertical than horizontal.

### 2.3.6 Dynamical Theory

The effect of all faulting is to relieve stress, and bring conditions nearer to what has been defined as the standard state. In the case of thrusting, it is easy to see that relief will eventuate, but this is not so apparent with regard to a single transcurrent fault. Where a number of such faults cross each other, the effect can be visible. Figure 2.14 illustrates the case of transcurrent faults formed under a north-south pressure together with an east-west tension, and shows how relief is afforded by a general distortion. Regarded as a vertical section, the same diagram will apply to the case of normal faulting. It also shows the directions of motion that must occur along any single or double series of transcurrent faults. It will be noticed that along any of the north-westerly members, motion is always to be right along what an observer would regard as the distant side of a fault plane.



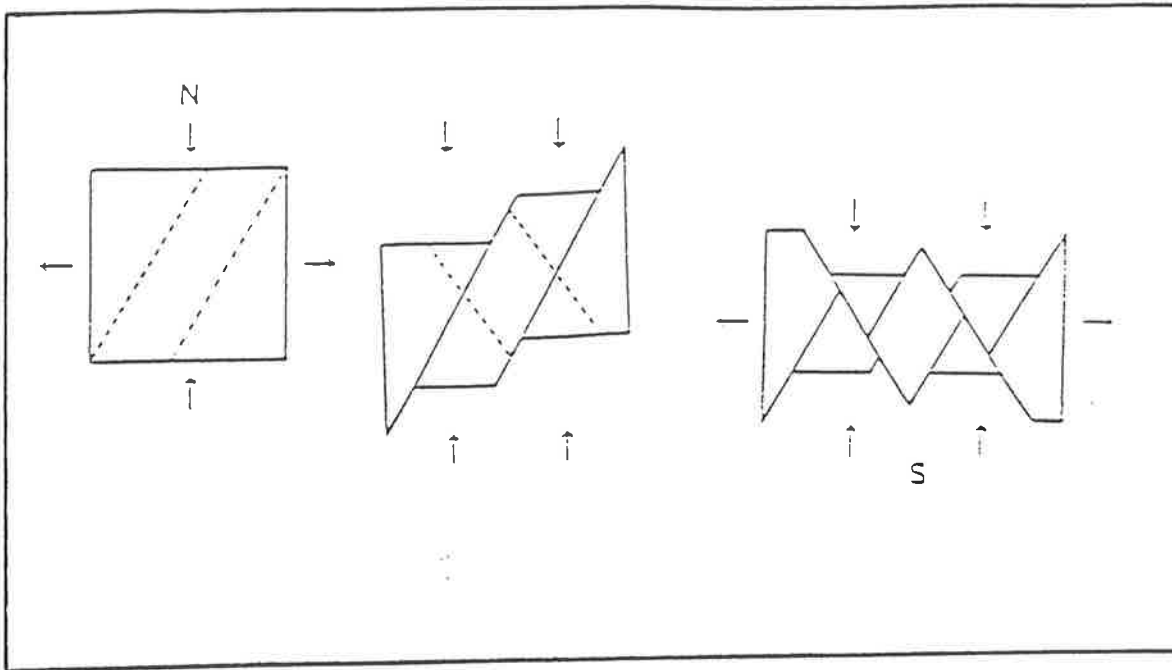


Figure 2.14: Deformation caused by transcurrent faults, (E. M. Anderson).

It follows from the dynamical theory that thrust planes and normal faults of the same age can never occur in association. The same does not apply to thrusts and transcurrent faults. It may happen that a large meridional pressure is contemporaneous with an east-west pressure which is only a little greater than the standard or vertical. These conditions may give rise to thrusting. A slight decrease of the east-west pressure may then cause it to become less than standard, and if the north-south pressure continues, there may be formation of transcurrent faults. The same general conditions may thus give rise to systems of faults which are not parallel. As related positions, faults which are parallel, are not always due to the same conditions. A system of faults with axes running to the north-east, is typically due to pressures directed between south-east and north-west. A fault which strikes north-east may be formed in four different ways. It may be due to the same stresses which have produced folding, but only if it is an overthrust. It may, on the other hand, be a normal fault, in which case it indicates a decrease of pressure from south-east to north-west. Or it may be a transcurrent fault, formed either by an increase of pressure in a direction somewhat south of west and north of east, accompanied by relief from north to south, or an increase of pressure directed west of south and east of north, with relief from west to east.

## 2.4 Complex Faults

This part of the thesis is about the complex faults which are too complicated to find all parameters of the structure using gravitational methods. The FAULT\_STRUCTURE program may be applied to a part of the fault system structure which consists of an isolated simple fault or two faults.

These are the kinds of faults where the use of FAULT\_STRUCTURE program is not appropriate.

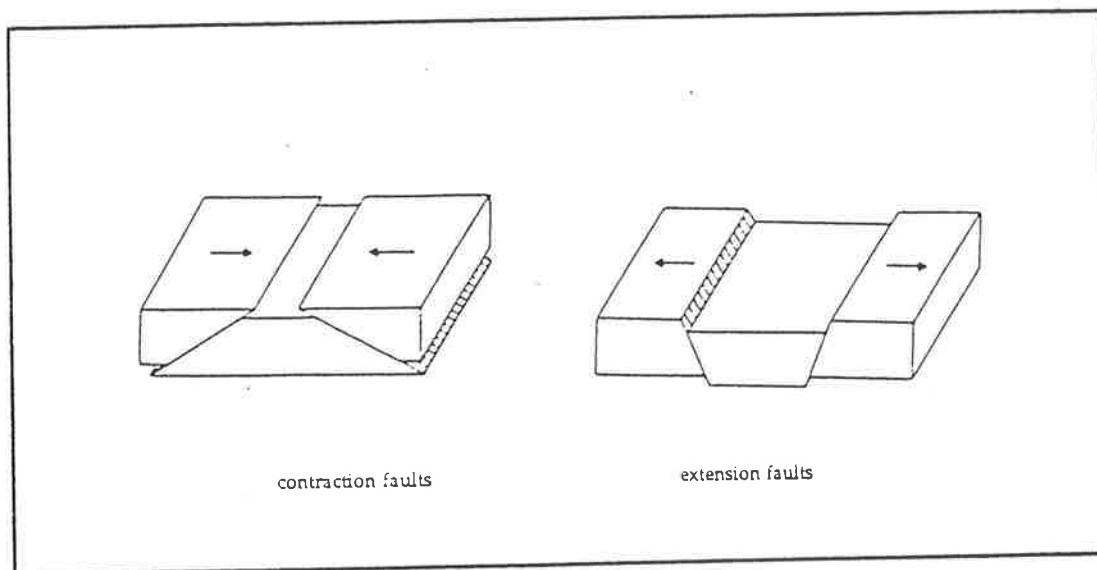


Figure 2.15: Contraction and extension faults.

There are areas of the earth which have been 'pulled apart' or 'compressed' where faults are numerous and dominated by one or other particular type. Extension and contraction faults occur in groups, to form the complex faults. Sometimes the fault is a wide zone rather than a thin sheet with sharp edges or fault planes bend due to stronger and weaker rock layers. Fault systems can be considered in plan on a map - a set of faults makes up system which includes step faults and graben or rift valleys. Faults are also seen as a response to irregularities in the basement of sedimentary basin. Most faults are

known only close to the surface, seismic surveys suggest that a lot of faults flatten out at depths of a few kilometres.

The extension faults are dip-slip faults which dip at a low angle towards their downthrow side. They are therefore normal faults of shallow inclination. This form requires that higher rocks are brought down next to lower (younger over older) which is the exact opposite of thrusts (see figure 2.16). In cross-section the transport direction will be down dip. Their overall effect is to attenuate or pull out the stratigraphic sequence laterally, so that it becomes thinner but more really extensive. Extension faults therefore tend to form basins rather than linear belts.

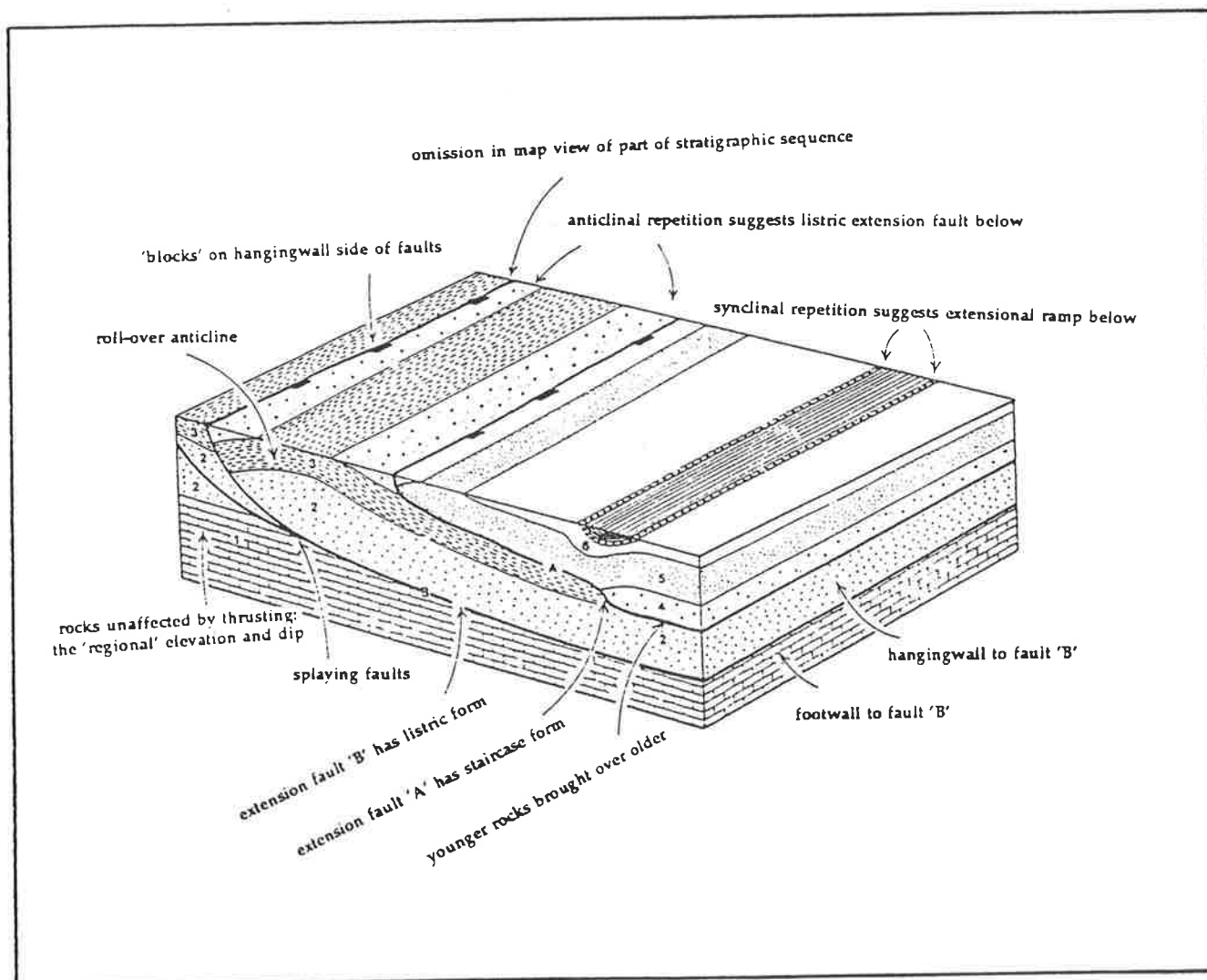


Figure 2.16: Block diagram to show the main features of extension faults, (A. Maltman).

Extension faults occur in groups, to form extensional basins. The faults may interlink and have minor splay faults. The resulting basin is by no means necessarily symmetrical. The variable distribution of displacements can produce complex basin shapes. Arrays of high-angle extension faults can form imbricate zones. The faults root into a basal, low-angle detachment fault. This is normally at depth, but may reach the surface at its tips. There are areas of the earth where such large, low-angle faults occur more or less singly. Below are some examples of extension faults.

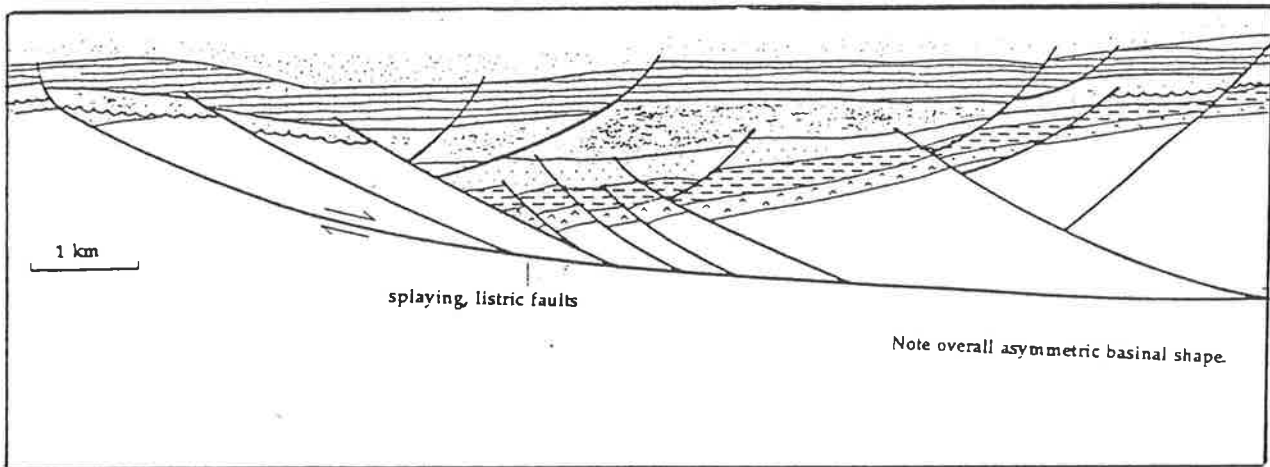


Figure 2.17: The appearance of an extension basin in cross-section, Witch Ground, North Sea, (A. Maltman).

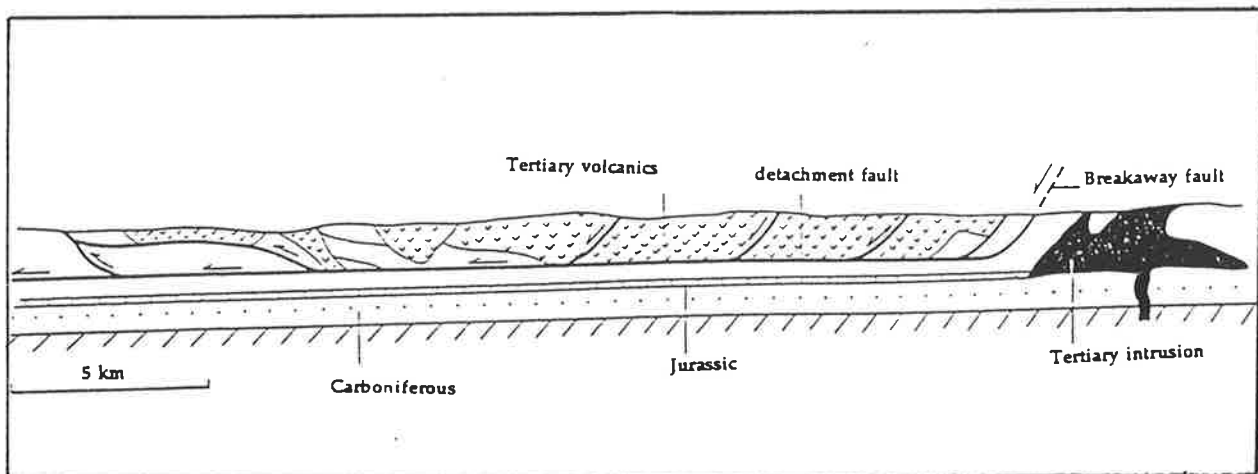


Figure 2.18: A detachment fault in cross-section, north-central Montana, (A. Maltman).

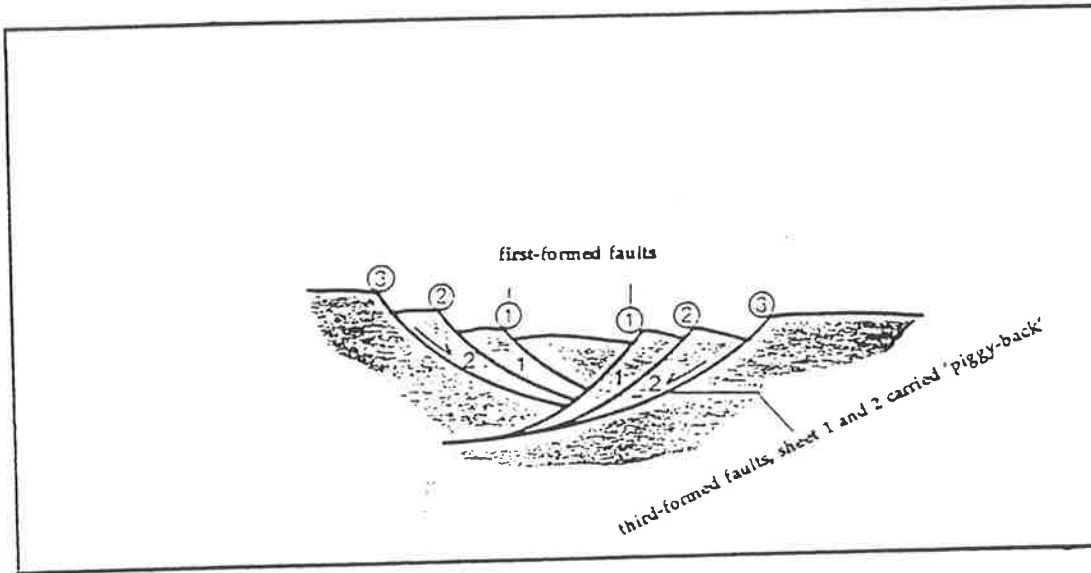


Figure 2.19: Interpretation of the sequence of generation of extension faults, (A. Maltman).

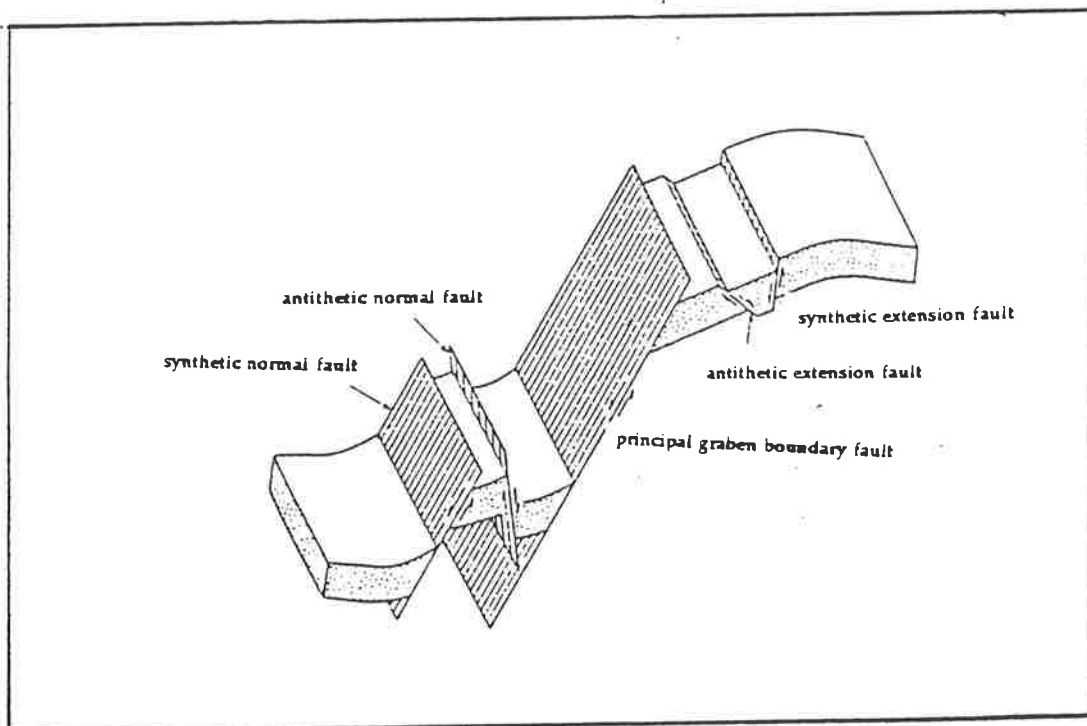


Figure 2.20: Structures characteristics of planar high-angle normal fault zones such as those bounding grabens in terrains that have been inhomogeneously extended by small percentage, (P. L. Hancock).

There are long, linear zones made up of faults which have essentially a reverse fault geometry but are of shallow inclination. They are called thrust faults, and the zones in which they predominate are called thrust belts. Their overall effect, along with any associated reverse faults, is to telescope together the stratigraphic sequence, producing a thick stack of beds and decreasing their horizontal extent. Hence, all these faults can be referred to as contraction faults. They have attracted much attention, partly because of the intriguing problem of understanding how the rocks can actually accomplish large amounts of contraction, and partly because in recent years some thrust belts have been the scene of intensive oil exploration. Thrust faults are low-angle dip-slip faults, along which the hangingwall has been upthrown (see figure 2.21). They are therefore essentially reverse faults and low-angle reverse faults are sometimes called thrusts.

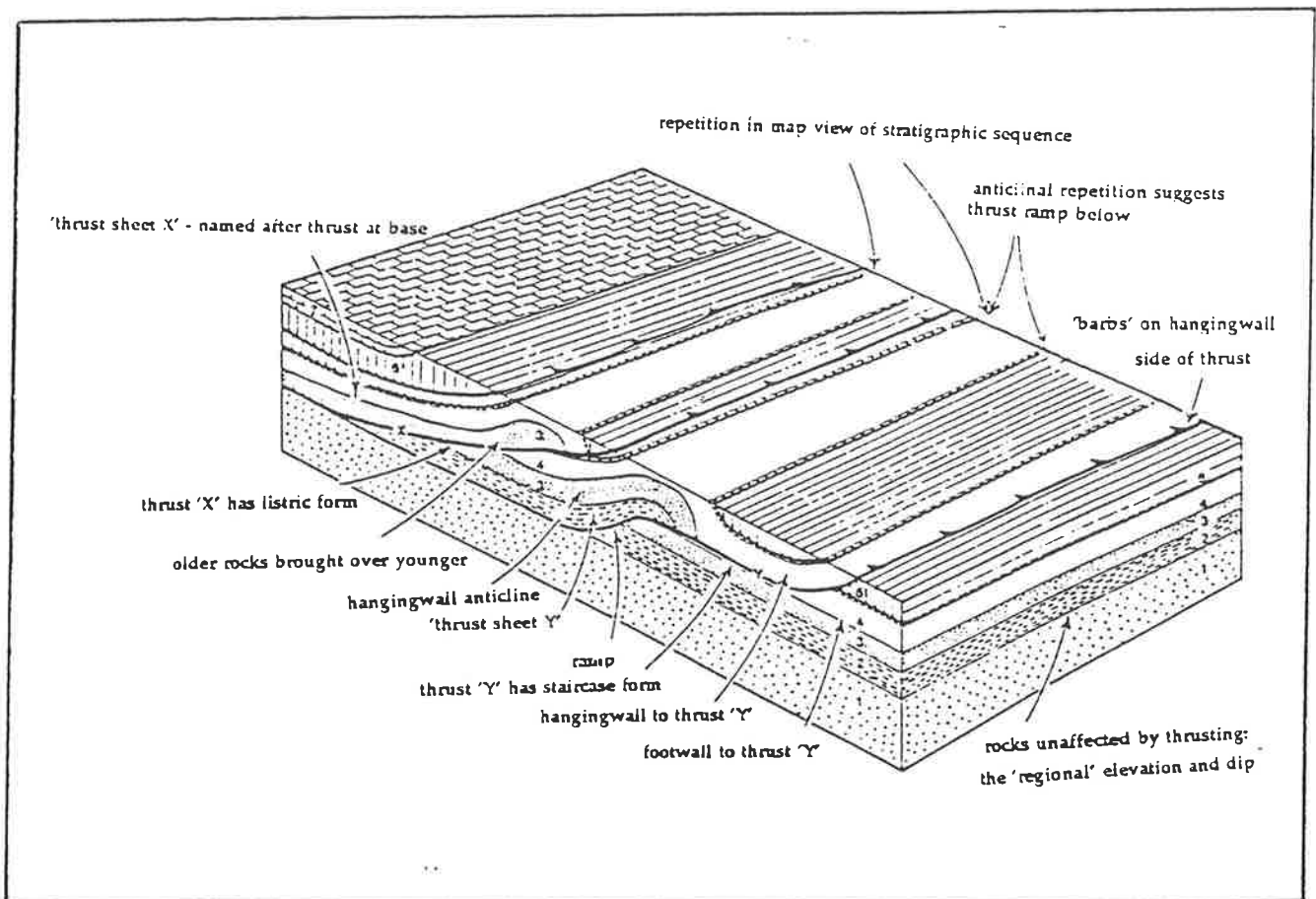


Figure 2.21: Block diagram to show the main features of thrust faults, (A. Maltman).

Thrusts rarely occur as isolated faults. Typically they are in groups, which together with splaying and interlocking smaller thrusts and folds, form the long, linear zones known as fold-and-thrust belts or simply thrust belts. Families of closely spaced splaying reverse faults called imbricate zones may also be involved (see figure 2.22).

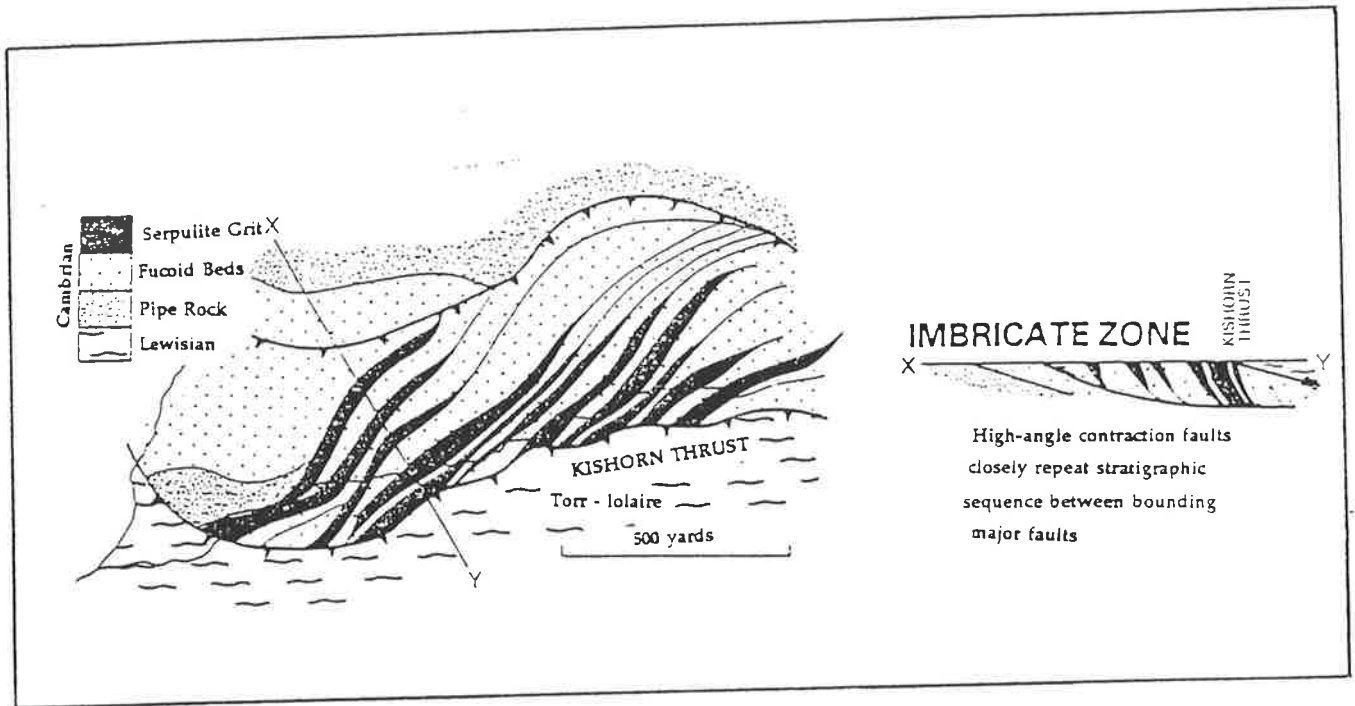


Figure 2.22: Imbricate zone in map and section. Near Lochcarron, Scotland, (A. Maltman).

The displacements on the major thrusts of the belts may be substantial and are typically measured in kilometres of movement.

The low dip of the thrust faults towards the upthrow side results in bringing more deeply buried rocks up and over shallow rocks. It is a general property of thrusts that they bring older rocks over younger. The hangingwall of a thrust is commonly called a thrust sheet and named after the fault at its base.

## 2.5 Reasons for Going into Details About Faults

Nothing original is being written in chapter 2, it can all be found in text books but unless the geometry of faults is clearly understood it is difficult to interpret the gravity, that is why this section is part of the thesis.

1. Gravity can provide information about the position, dip and throw of faults that geologist can not obtain by observation.
2. Using gravity to study faults it is very important to have as much information as possible about the shape of fault, also as much detail of position of the fault.
3. Gravity surveys show only present position of rocks, it is important to have some knowledge of the sequence of events by which rocks obtained this present position.
4. The reason behind the study of faults is to better understand the stresses which have operated in the geological past in the region.



## Chapter 3

# Gravity Effect of Simple Fault Structure

The basic mathematics for the attraction of a fault is found in most intermediate text books (Heiland, Terford et. al.). The mathematical development is provided in Appendix A ( Mathematical Formula for Simple Shapes ) which may be read first before this chapter.

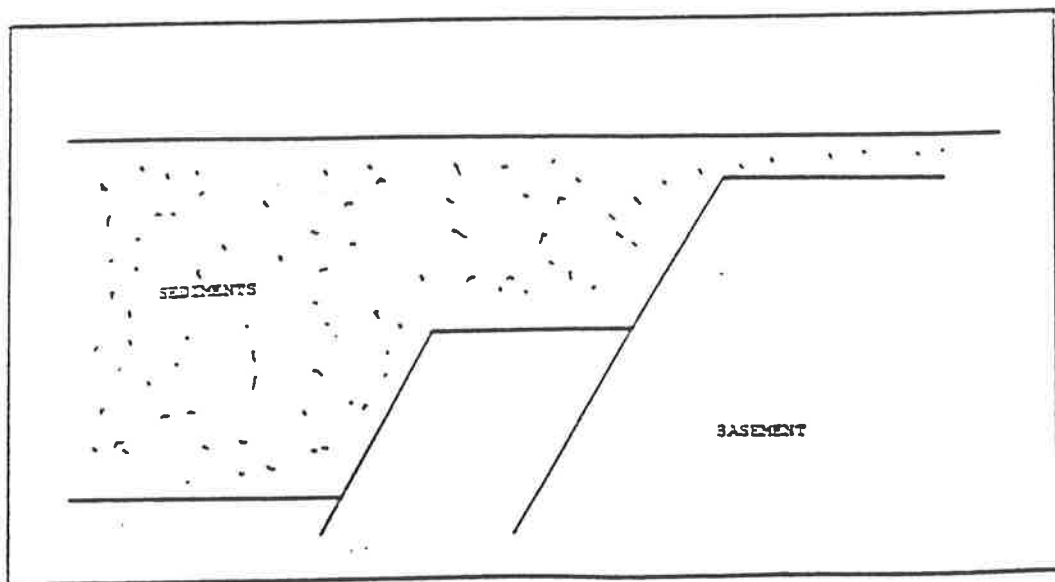


Figure 3.1: Actual geological structure.

Usually it is better to start with a simple problem. If the simple problem cannot be solved, it is rare that a solution would be found to a more complex version of the problem. The initial task is to develop a model which consists of two adjacent faults, a main fault and an adjacent step fault. The actual geological structure can be represented as on figure number 3.1.

For the purpose of the gravity survey we may regard the above as equivalent to two masses with a density contrast.

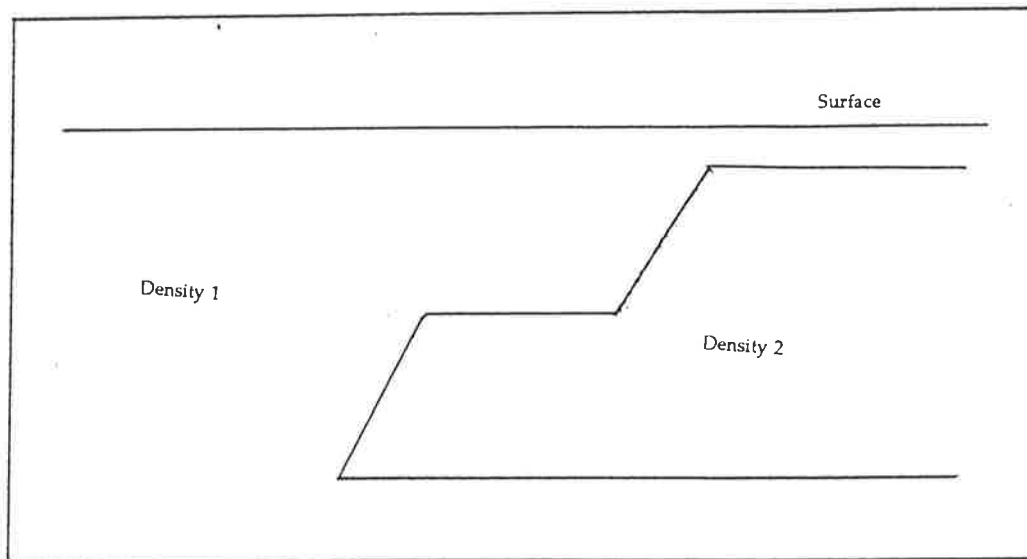


Figure 3.2: Theoretical model.

The geometrical model for two faults affecting the basement is shown in figure 3.2 and is obtained by adding the gravitational effect of two horizontal slabs. This simple model is used to show more clearly the problem. If the faults are well separated the individual gravitational effect is evident. If however the faults are closer the effects merge and the curve has the appearance of that due to a single fault. The resolution of the faults and the accuracy with which the various parameters can be determined also depends on the amplitude of the separate horizontal slab anomalies, the "noise" level ( due to various sources including accuracy of observations, geological noise from soil thickness variation and density variation within the sediments and the basement rocks ).

### 3.1 Approximation of Fault Structure by Semi-Infinite Horizontal Slab

The fault structure with the large throw can be approximated by the semi-infinite horizontal slab (see Appendix A, eq. no. A.21). Figure 3.3 represents a simple structure with the vertical fault and the gravity effect for this fault.

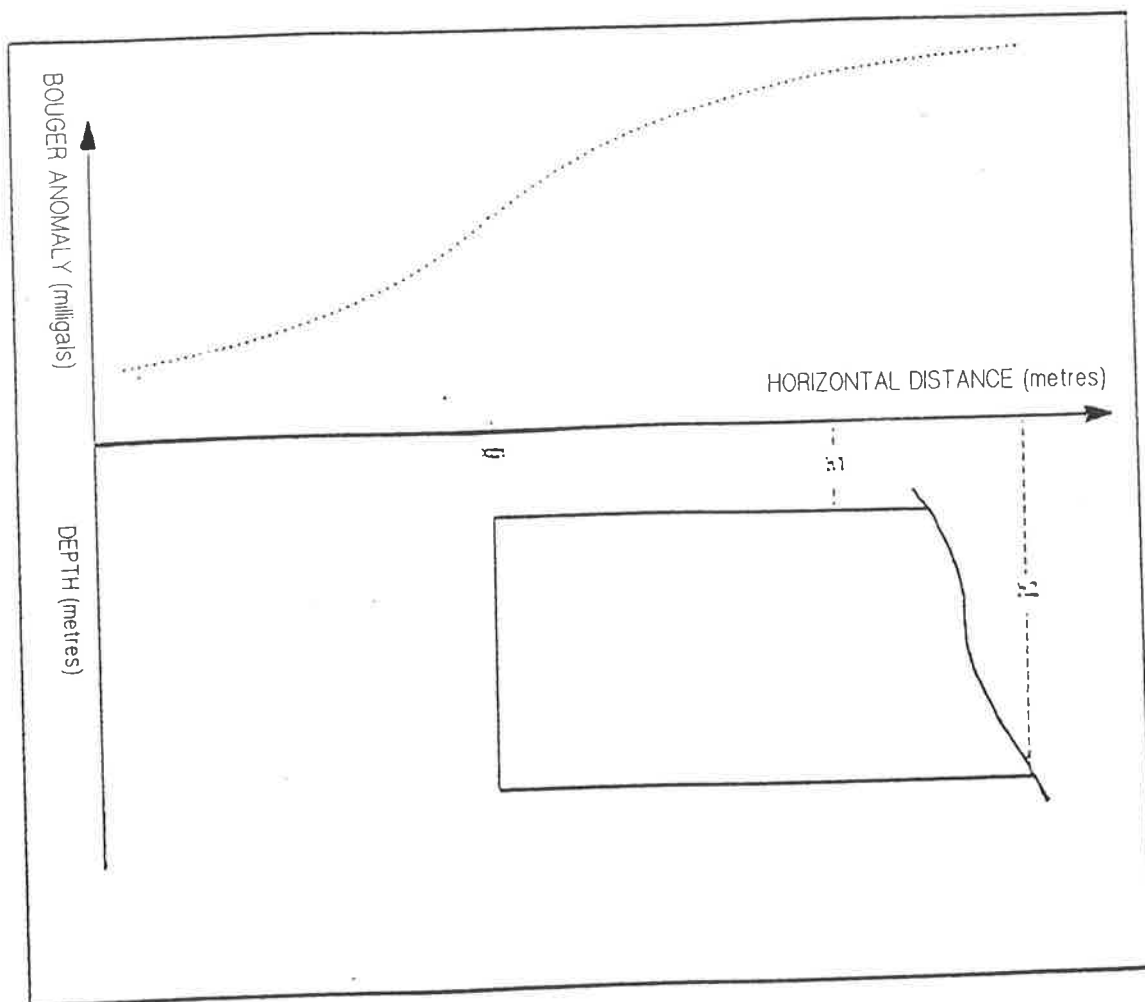


Figure 3.3: Gravity effect of the vertical fault.

But the same gravity effect is obtained for two semi-infinite horizontal slab. The faulted block can be divided into two parts and the gravity effect for both can be calculated, as is shown in Figure 3.4.

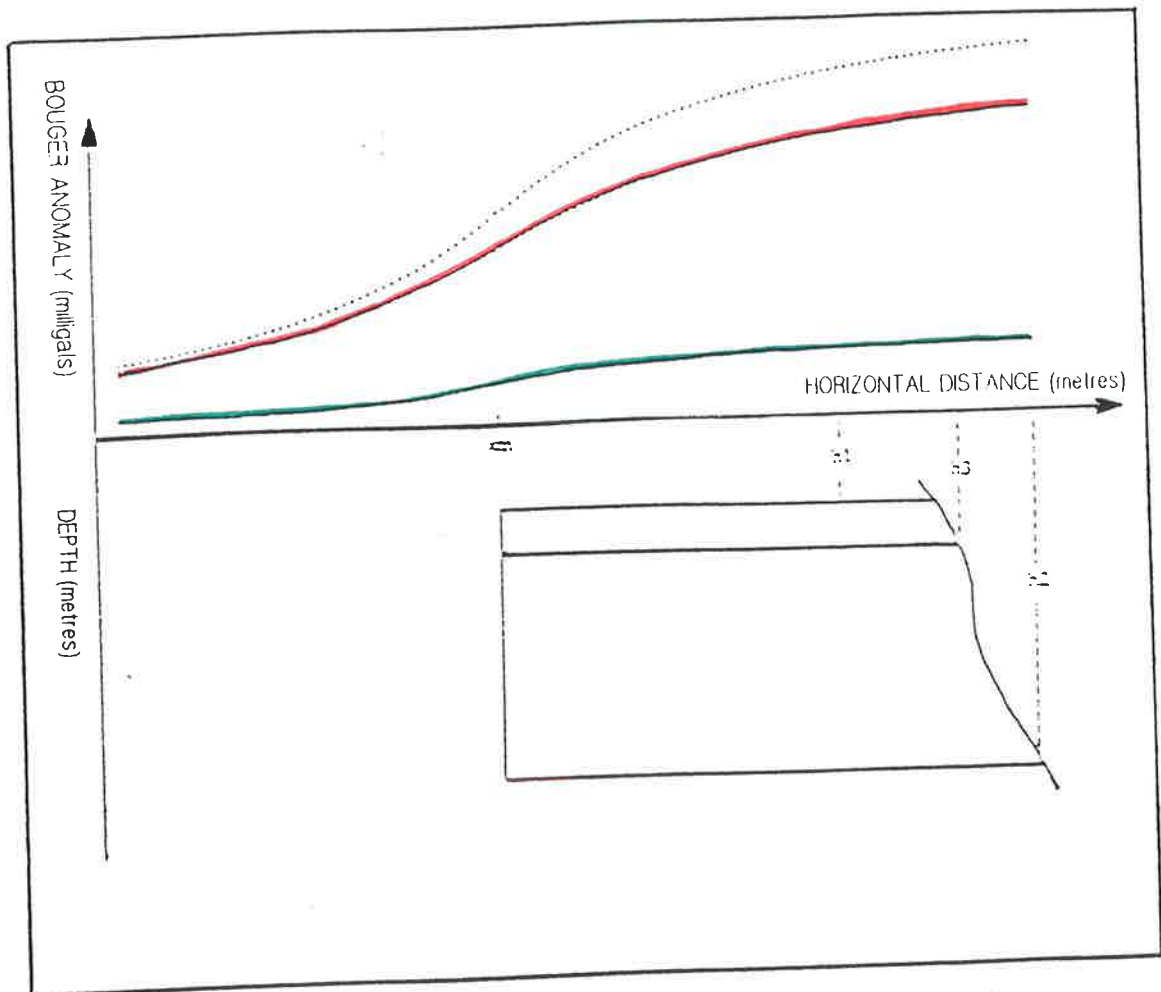


Figure 3.4: Gravity effect of two vertical faults.

The green line is the gravity effect due to the upper block. The red line is the gravity effect for the lower block shown in red. If we add the gravity effect for both blocks we obtain just the same gravity effect as for the fault which has the parameters  $h_1$ ,  $h_2$ ,  $x_m$ .

Figure 3.5 represents the example for the normal fault. Similarly to the vertical, the normal fault can be divided into two parts:

1. first indicated by  $h_1, h_3, x_m, \alpha$
2. second indicated by  $h_3, h_2, x_m, \alpha$

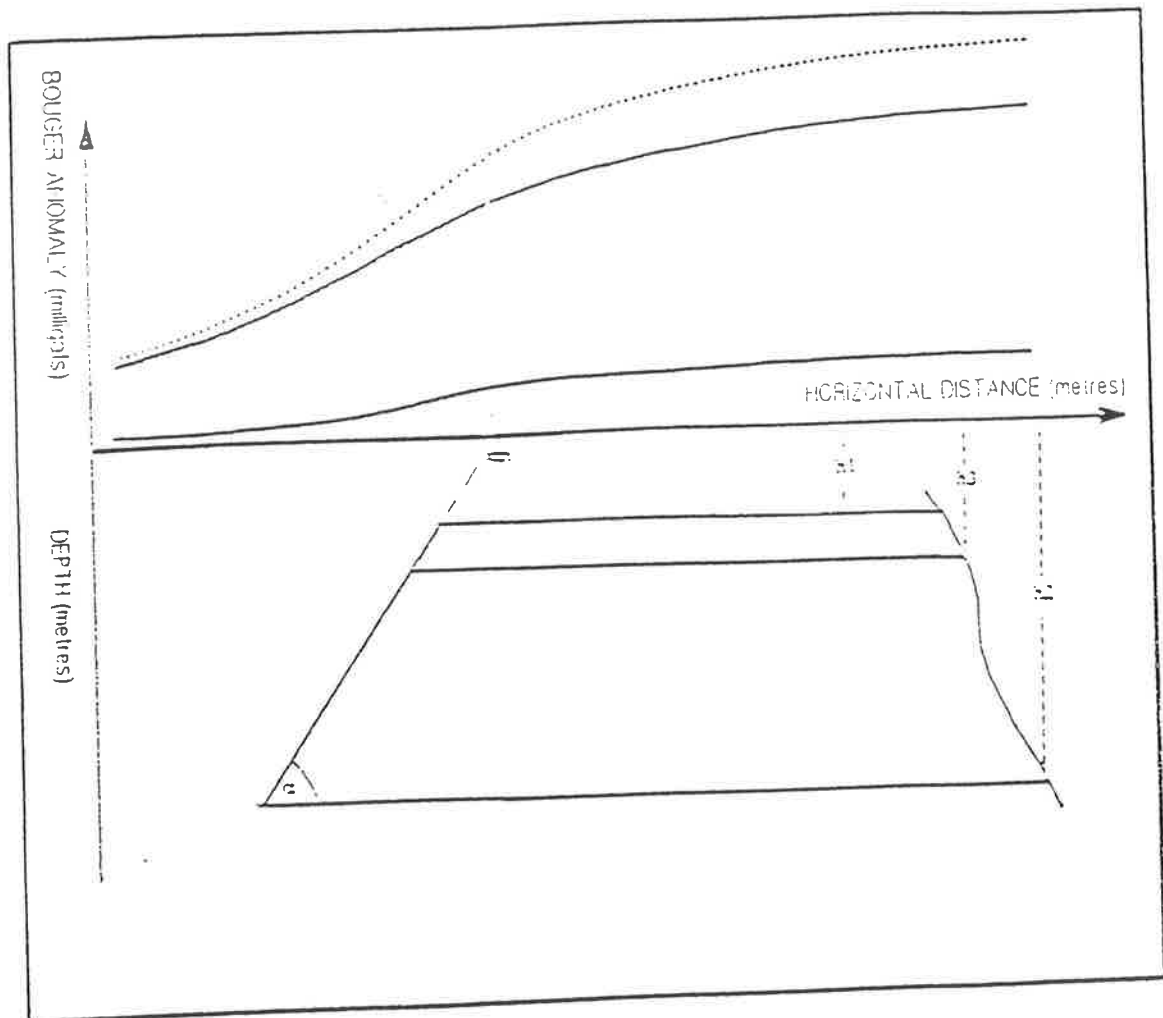


Figure 3.5 Gravity effect of two normal faults.

Adding up the gravity effects for both parts of the fault we obtain the same gravity effect as for one fault with  $h_1, h_2, x_m, \alpha$ .

Figure 3.6 shows a more complicated structure:

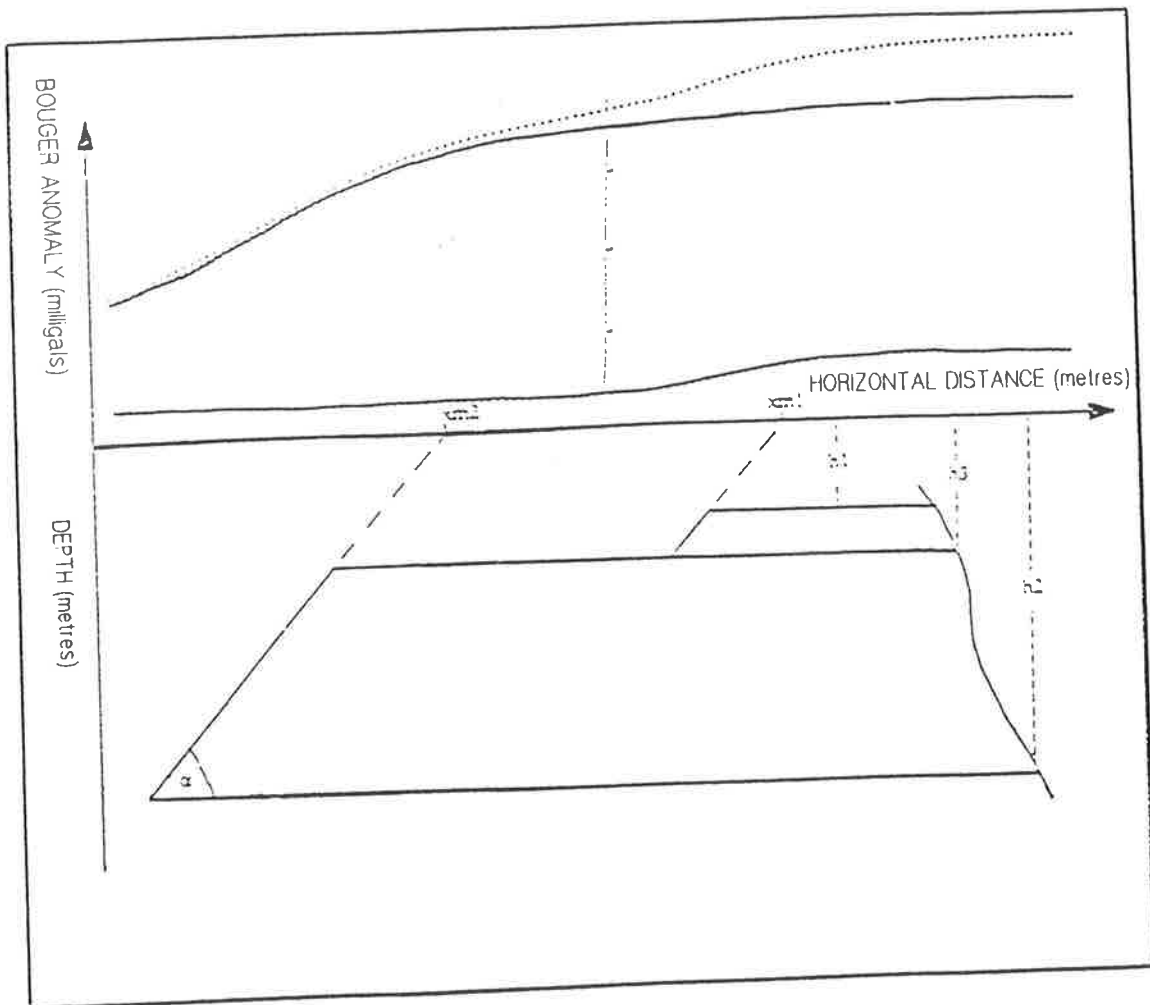


Figure 3.6: Gravity effect of two normal faults.

Considering previous examples the gravity effect for this structure can be calculated as the sum of the gravity effects for two different faults:

1.  $h_1, h_3, x_{m1}, \alpha$
2.  $h_3, h_2, x_{m2}, \alpha$

Below are a few more examples of the vertical faults, where the depths of the faults were the same but the distance between them different.

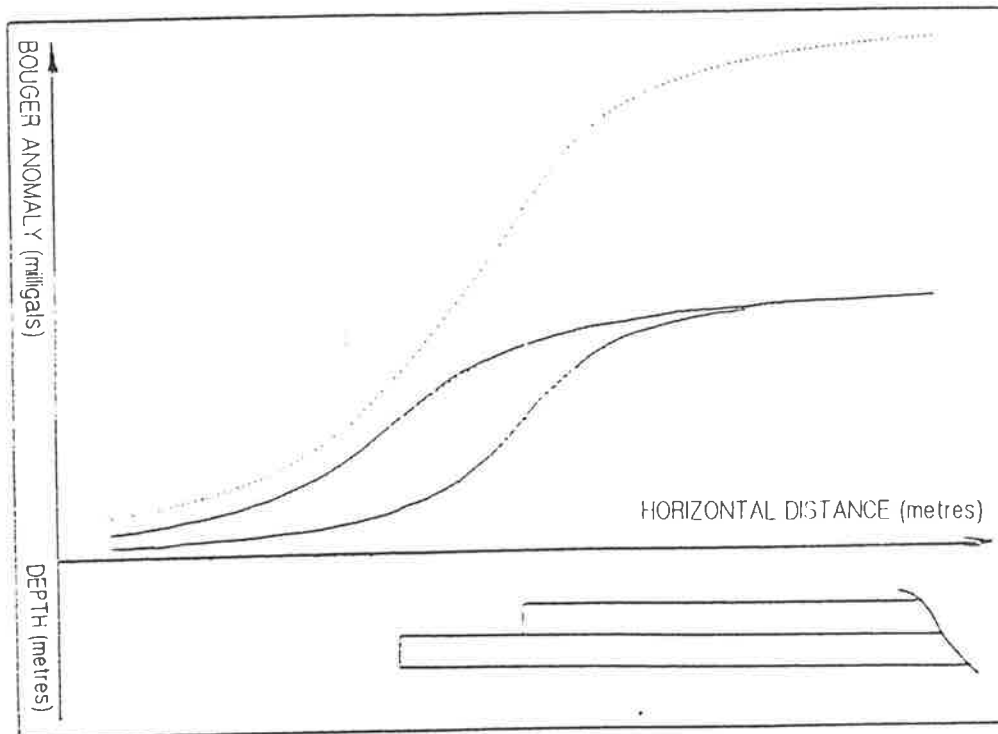


Figure 3.7: Gravity effect of two vertical faults (small distance between them).

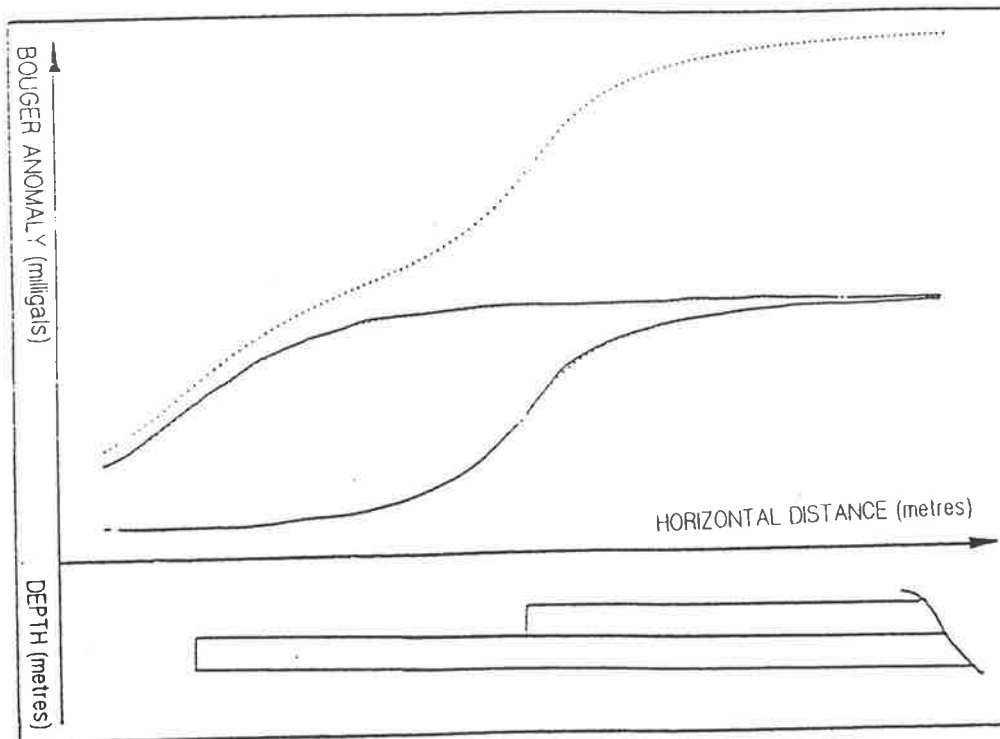


Figure 3.8: Gravity effect of two vertical faults (large distance between them).

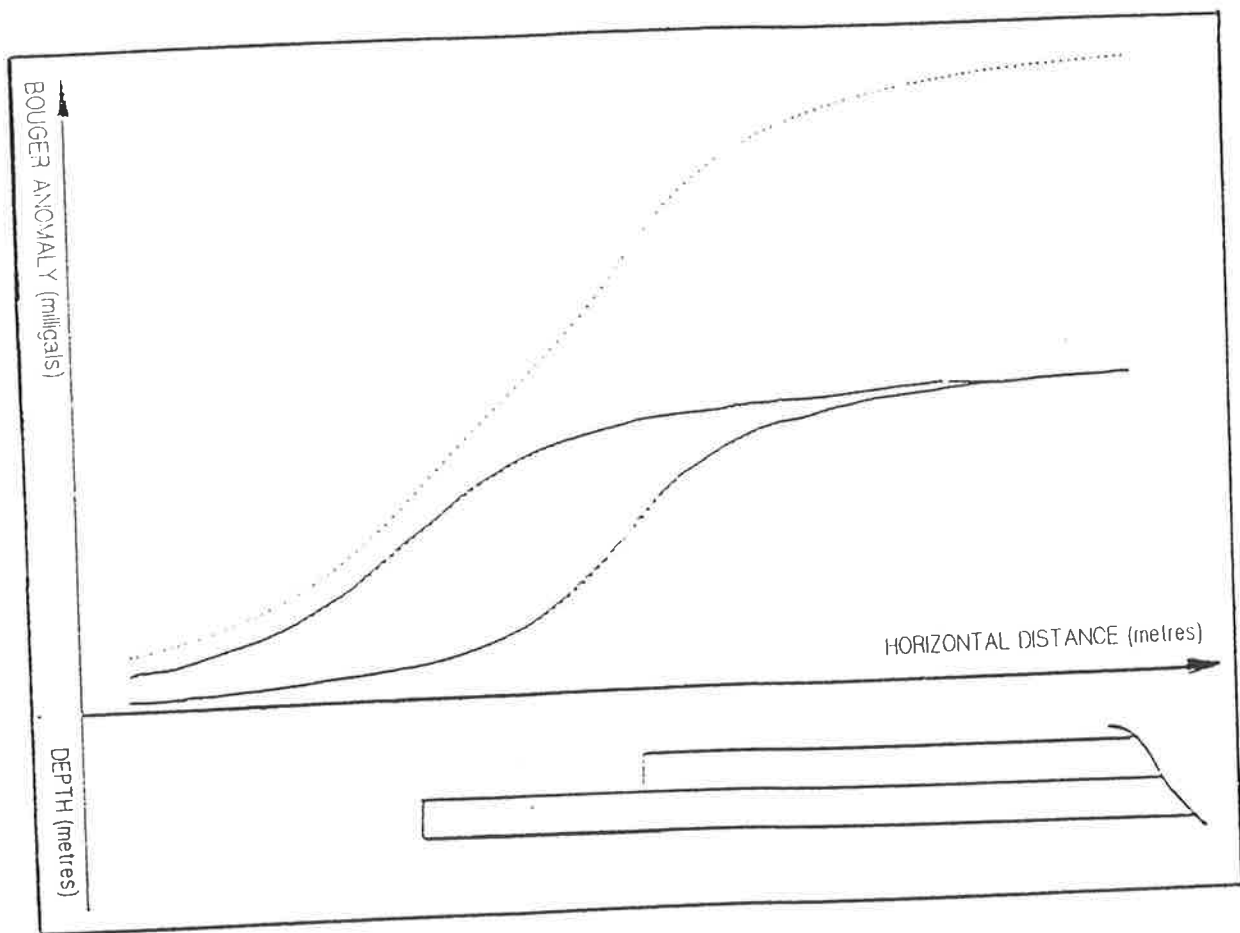


Figure 3.9: Gravity effect of two vertical faults.

As can be observed from figure 3.7 sometimes the profile gives information which appears to be from one fault but it must be remembered that an almost identical gravity effect is given by two faults with a small distance between each fault. This observation is a foundation of the computer program which finds the parameters for two faults.



Below is an example of vertical faults, where the depths of the faults are very different.

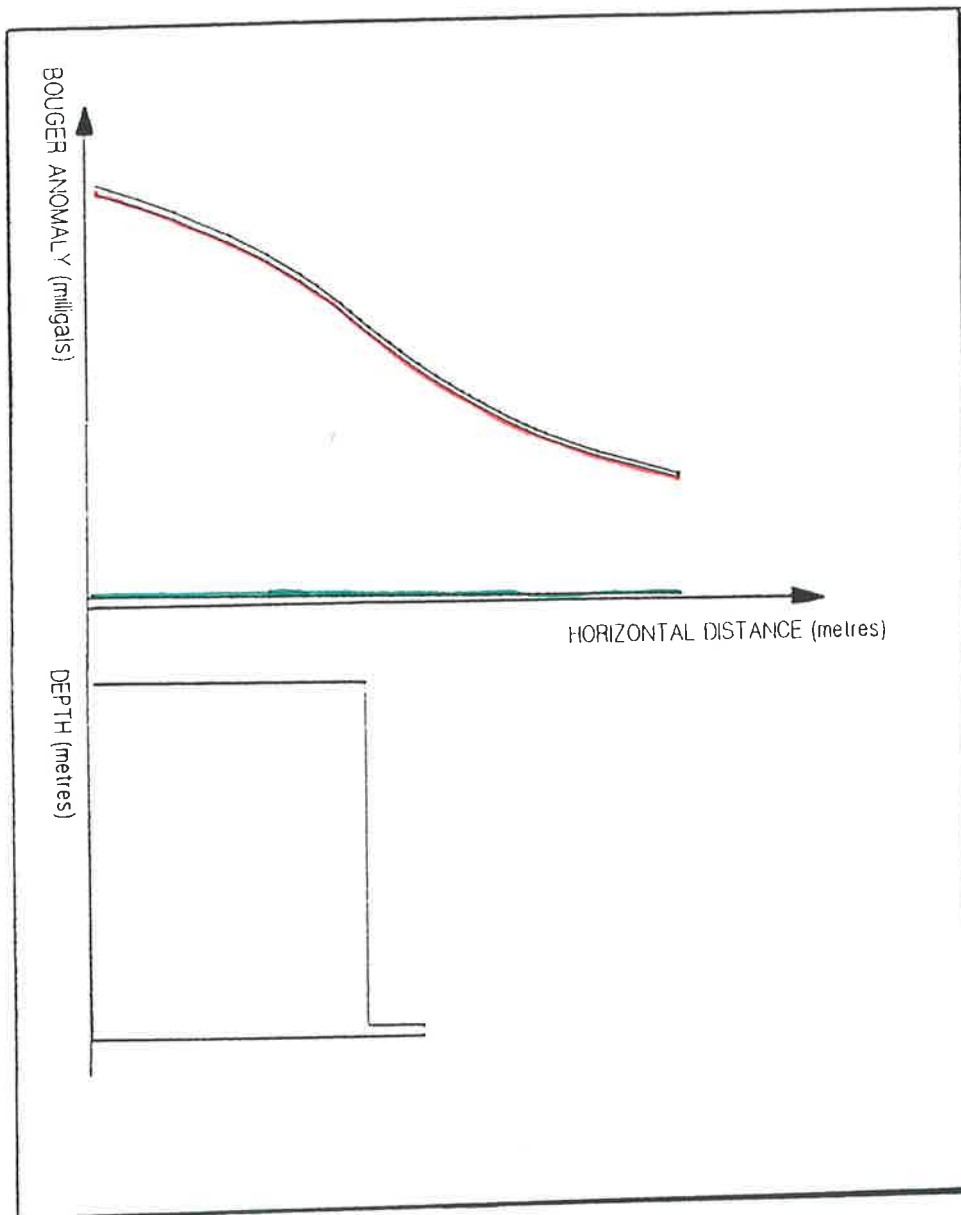


Figure 3.10: Gravity effect of two vertical faults (big difference between the depth).

The green line is the gravity effect due to the lower block. The difference of gravity between the first and last points is very small. The red line is the gravity effect for the upper block. If we add the gravity effect for both blocks we obtain a very similar gravity effect to the upper block. As can be observed from figure 3.10, sometimes the profile gives information about one fault but it must be remembered that essentially an identical gravity effect is given by two faults where the difference of depths is big.

Figure 3.11 represents the example for the normal faults if thickness of blocks is very different.

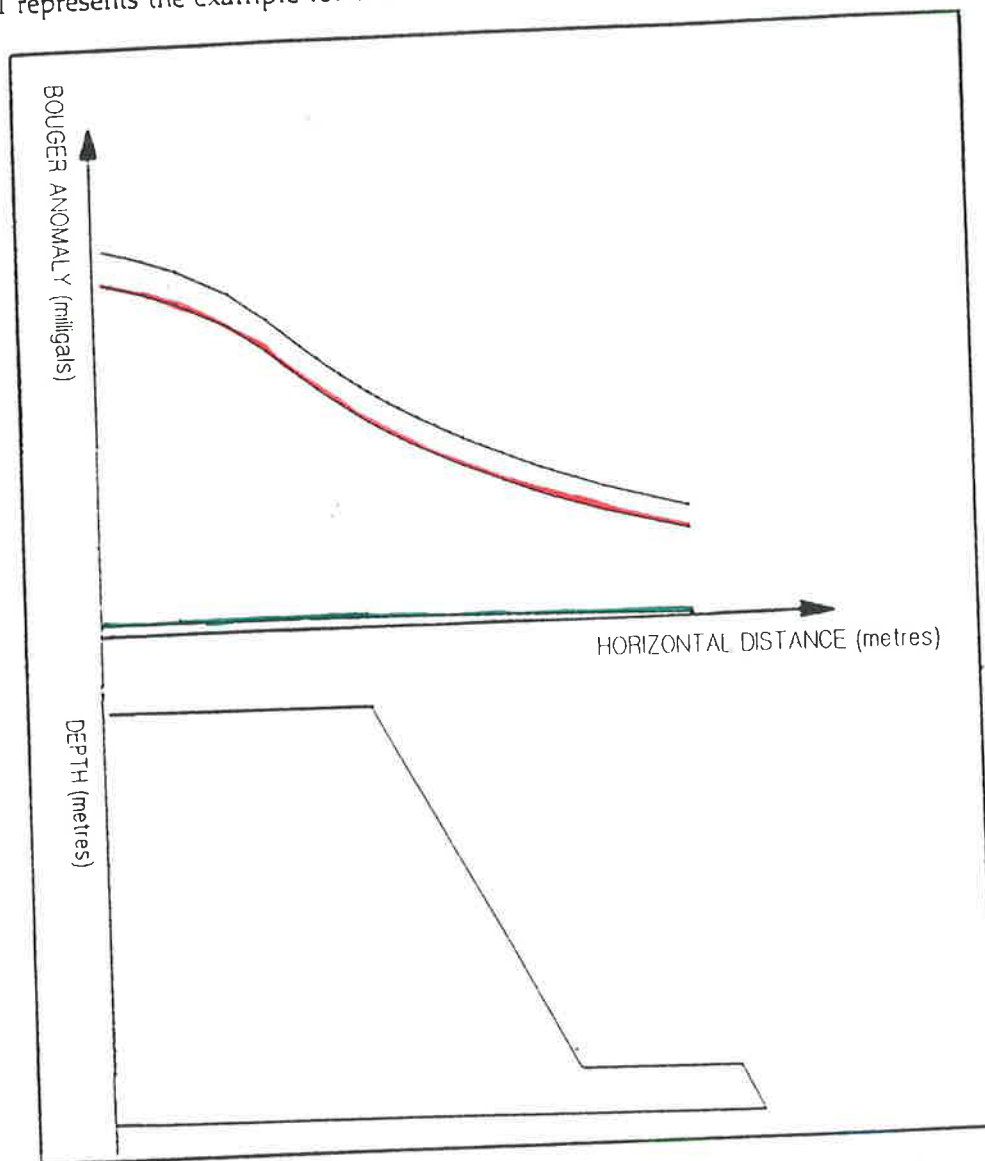


Figure 3.11: Gravity effect of two normal faults (big difference between the depth).

The green line is the gravity effect due to the lower block. The difference of gravity between the first and last points is very small. The red line is the gravity effect for the upper block. If we add the gravity effect for both blocks we obtain very similar gravity effect as for the upper block. As can be observed from figure 3.11 sometimes the profile gives information about one fault but it must be remembered that an identical gravity effect is given by two faults where the difference of depths is big. As we can see from last two figures if the thickness of blocks is very different the gravity effect of the thin block is nearly the same for vertical and normal fault. In this case it will certainly not be possible to define the dip of the smaller fault.

## 3.2 Fault\_Structure Program

The fault structure with the large throw can be approximated by the semi-infinite horizontal slab using a computer program, which has been written by the author and called FAULT\_STRUCTURE. This program calculates the gravity effect of one or two faults and compares this effect with observed gravity. The initial data entered into the program are the values :  $h_1$ ,  $x_{m1}$ ,  $x_{m2}$ ,  $\alpha_1$ ,  $\alpha_2$ ,  $\sigma$ .

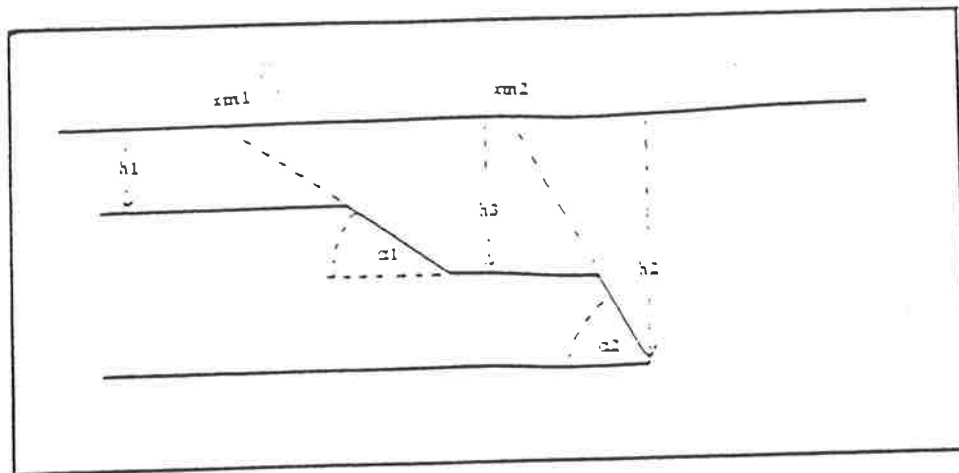


Figure 3.12: Theoretical model.

The initial data is entered not only as one value for each parameter, but as a range of values. The depth  $h_1$  is entered as a range of values from minimum of  $h_1$  to maximum of  $h_1$  with the step  $sh_1$ . The values for  $x_{m1}$ ,  $x_{m2}$ ,  $\alpha_1$ ,  $\alpha_2$ ,  $\sigma$ , are also entered in this manner. Using this method, the data has been entered into the program for many faults with different parameters within a specified range.

The value of  $h_2$  is calculated by the program from the following equation ( see Appendix A ):

$$h_2 = \frac{g_{\max}}{2 \times 1000 \times 6.67E-6 \times \pi \times \sigma} + h_1 \quad (3.1)$$

where

- $\pi$  = 3.14159
- $g_{\max}$  =  $T(2,n) - T(2,1)$
- $\sigma$  - density contrast
- $T(2,n)$  - observed gravity for last point
- $T(2,1)$  - observed gravity for first point

The architecture of the program is as follows:

- a. The program increases the value of  $g_{\max}$  by addition of 'step for  $g_{\max}$ ' ( five times ). This means that the program calculates the gravity effect for the five models with five different depths  $h_2$ .  
The value of  $h_3$  is calculated by addition of steps for depth to  $h_1$ . The maximum value of  $h_3$  must be smaller than the depth  $h_2$ .
- b. The FAULT\_STRUCTURE program calculates the gravity effect for each model, compares this effect with observed gravity and gives the parameters for faults which have the smallest difference between observed and calculated gravity.
- c. Finally, the FAULT\_STRUCTURE program gives the parameters for the fault and creates two plots which show :
  - the observed and computed gravity effect
  - the horizontal gravity gradient
  - the difference between observed and computed gravity effect for every point
  - the theoretical model

The plots have been drawn using a Zeta plotter.

The way in which the program functions is described in the following sections:

### 3.2.1 Input Data

### 3.2.2 Calculating Data

Note: limitation exists on detectability of individual parameters such as  $\alpha_2$ , if  $h_3$  is large but  $\alpha_2$  will be detectable if  $h_1$  and  $h_3$  are small.

## 3.2.1 Input Data

The initial data comprises the observed gravity and the set of values obtained from a range of faults with different parameters.

### 3.2.1.1 Observed gravity

The observed gravity data may come from a single line of gravity observation or be taken from the Bouguer anomaly map, and represents the set of points consisting of the gravity value and the horizontal distance defining the position of the point at which the observation has been made and gravity values.

This data is stored separately from the FAULT\_STRUCTURE program as the data file OBS\_GRAV.DAT. Each line in the file OBS\_GRAV.DAT contains the horizontal distance value and the gravity value separated by blanks or commas for one point. The user has to build the data file once, and use the editing capabilities of the computer system to correct and update that file.

The maximum number of lines in the file OBS\_GRAV.DAT is 200.

### 3.2.1.2 Parameter for the fault structure

When the program is run, the user is queried for the set of data which describes the theoretical model with which this observed data will be compared.

Firstly, on the terminal screen a question appears regarding the number of the faults for the model. If the user is looking only for the model of one fault, type 1. If the user is looking for the model of two faults, type 2.

Next, the terminal will prompt for the initial data of the first fault (see Figure 3.12): easting ( $xm1$ ), depth ( $h1$ ), angle ( $\alpha1$ ). All these parameters are entered as a range of values from minimum to maximum and for each parameter is entered the value of the increment.

The next item is the initial data of the second fault : easting ( $xm2$ ) and angle ( $\alpha2$ ). These parameters are also entered as a range of value from minimum to maximum but the values of the increment are the same as for the first fault.

The last initial data is the density contrast which is entered with the same format (minimum, maximum, increment) and the value of increment for  $G_{max}$ .

The following example shows how to enter the data for the model of two faults where:

- easting ( $x_{m1}$ ) is between 150 to 350 metres and the user wants to calculate the gravity for easting 150, 200, 250, 300, 350 (the value of increment or step for  $x_{m1}$  is 50 metres).
- depth ( $h_1$ ) is between 50 to 250 metres and the user wants to calculate the gravity for depths 50, 60, 70, 80, ..., 250 (the value of step for  $h_1$  is 10 metres).
- angle ( $\alpha_1$ ) is between  $45^\circ$  to  $75^\circ$  metres and the user wants to calculate the gravity for angles  $45^\circ$ ,  $55^\circ$ ,  $65^\circ$ ,  $75^\circ$  (the value of step for  $\alpha_1$  is 10 degrees).
- easting ( $x_{m2}$ ) is between 650 to 1050 metres, the value of step is 50 metres as for ( $x_{m1}$ ).
- angle ( $\alpha_2$ ) is between  $65^\circ$  to  $85^\circ$  degrees, the value of step for is 10 degrees as for ( $\alpha_1$ ).
- density contrast is between 0.5 to 0.65 and the user wants to calculate the gravity for density contrast 0.5, 0.55, 0.6, 0.65 (the value of step is 0.05).

Example:

THE MODEL FOR ONE OR TWO FAULTS ?

ONE FAULT --> 1

TWO FAULTS --> 2

2

THE INITIAL DATA FOR FIRST FAULT

EASTING

minimum value: 150

maximum value: 350

step for easting: 50

DEPTH

minimum value: 50  
maximum value: 250  
step for easting: 10

ANGLE

minimum value: 45  
maximum value: 75  
step for easting: 10

THE INITIAL DATA FOR SECOND FAULT

EASTING

minimum value: 650  
maximum value: 1050

ANGLE

minimum value: 65  
maximum value: 85

DENSITY CONTRAST

minimum value: 0.5  
maximum value: 0.65  
step for den.: 0.05

step for Gmax: 1

### 3.2.3 Minimalization of the Difference between Observed and Calculated Gravity Data

The FAULT\_STRUCTURE program is able to choose the fault structure which gives the most similar gravity effect to the gravity observed. As a method of comparison such two lines are used a sum of differences between observed and calculated gravity for all points where the horizontal distance values have been entered as initial data into the file OBS\_GRAV.DAT.

The difference of the value for one n point is given by :

$$Z(n) = GC2(n) + GC3(n) + RR - T(2,n)$$

$$RR = T(2,1) - GC2(1) - GC3(1)$$

where

GC2(n) - value of gravity effect given by the first fault for (n)th point

GC3(n) - value of gravity effect given by the second fault for (n)th point

T(2,n) - observed gravity for (n)th point. This value comes from OBS\_GRAV.DAT file

RR - difference between calculated and observed gravity for first point

The difference of the values for the whole gravity line is given by :

$$Z = Z(1) * Z(1) + Z(2) * Z(2) + \dots + Z(n) * Z(n)$$

where

Z(n) - difference between observed and calculated gravity for n point

n - point number

The program selects the fault structure from the initial range for which the Z value is the smallest.



### 3.2.4 Output Data

The output data consists of two files with information about the best chosen model and two plots. One plot ( file PLOT2.PLT ) contains drawings of the model, the other ( file PLOT1.PLT ) portrays the calculated and observed gravity, gravity gradient and the difference between calculated and observed gravity, as lines.

The output data file OUT\_INF.DAT contains the initial data for the range of faults and the information about the ten best faults structures. This information is :

Z - the difference of the value for all gravity line

h1 - the depth to the top of the first fault

h2 - the depth to the bottom of the second fault

h3 - the depth to the top of the second fault

rm - density contrast

tk1 - the angle of dip of the first fault

tk2 - the angle of the of dip of the second fault

xm1 - easting for the projection of the plane of the first fault at the surface

xm2 - easting for the projection of the plane of the second fault at the surface

The output data file OUT\_GR.DAT contains the parameters and the calculated gravity, observed gravity and horizontal distance values only for the best fault structures.

### 3.2.5 Relevant Subroutines Called by FAULT\_STRUCTURE Program

This section of the chapter provides a detailed description of numerous subroutines which are called up by the FAULT\_STRUCTURE program. Some of the subroutines considered calculate the gravity effect for the different fault structure and some draw plots.

#### 3.2.5.1 The subroutine: GRAVITY\_OUT0

This subroutine calculates the gravity effect for an outcropping fault structure where the dip ( angle between horizontal surface and the plane of the fault ) is 90°. The gravity for this structure is given by the following equation ( see Appendix A for derivation ):

$$g = 2 \times 6.67 \text{ E-6} \times 1000 \times \sigma \left[ \frac{x}{2} \log \left( \frac{D^2 + x^2}{x^2} \right) + D \left\{ \frac{\pi}{2} + \tan^{-1} \left( \frac{x}{D} \right) \right\} \right] \quad (3.2)$$

where

$$\pi = 3.14159$$

$\sigma$  - density contrast

D - value of depth

x - distance from top of fault to easting point

By using the following relation:

$$V1 = 2 \times 6.67 \text{ E-6} \times \rho \times 1000$$

$$B1 = \frac{x}{2} \times \log \left( \frac{D^2 + x^2}{x^2} \right)$$

$$B2 = D \times \left( \frac{\pi}{2} + \tan^{-1} \left( \frac{x}{D} \right) \right)$$

The expression can be simplified to give

$$g = V1 * ( B1 + B2 )$$

### 3.2.5.2 The subroutine: GRAVITY\_OUT1

This subroutine calculates the gravity effect for the outcrops fault structure where the dip ( angle between horizontal surface and the plane of the fault ) is not 90°. The gravity for this structure is given by the following equation ( see Appendix A for derivation ):

$$\begin{aligned}
 g = & 2 \times 6.67E-6 \times 1000 \sigma \left[ \frac{x}{2} \sin^2 \alpha \log \left\{ \frac{D^2 + (x + D \cot \alpha)^2}{x^2} \right\} \right. \\
 & - x \sin \alpha \cos \alpha \left\{ \frac{\pi}{2} - \tan^{-1} \left( \frac{x}{D} + \cot \alpha \right) \right\} \\
 & \left. + D \left\{ \frac{\pi}{2} + \tan^{-1} \left( \frac{x}{D} + \cot \alpha \right) \right\} \right] \quad (3.3)
 \end{aligned}$$

where

$$\pi = 3.14159$$

$\sigma$  - density contrast

D - value of depth

x - distance from top of fault to easting point

$\alpha$  - dip (  $0^\circ < \alpha < 90^\circ$  &  $90^\circ < \alpha < 180^\circ$  )

By using the following relation:

$$V1 = 2 \times 6.67E-6 \times \sigma \times 1000$$

$$a2 = \frac{D}{\tan(\alpha)}$$

$$\cot \alpha = \frac{a2}{D}$$

$$B3 = x \times \left( \tan^{-1} \left( \frac{x+a2}{D} \right) - \frac{\pi}{2} \right) \times \sin \alpha \times \cos \alpha$$

$$B2 = x \times \sin \alpha \times \sin \alpha \times \log \left( \frac{\sqrt{(D^2 + (x + a2)^2)}}{x} \right)$$

$$B1 = D \times \left( \frac{\pi}{2} + \tan^{-1} \left( \frac{x + a2}{D} \right) \right)$$

The expression can be simplified to give

$$g = V1 * ( B1 + B2 + B3 )$$

### 3.2.5.3 The subroutine: GRAVITY\_0

This subroutine calculates the gravity effect for the fault structure where the dip ( angle between horizontal surface and the plane of the fault ) is  $90^\circ$  and the first depth is not zero. The gravity for this structure is given by the following equation ( see Appendix A for derivation ):

$$g = 2 \times 6.67E-6 \times 1000 \sigma \left[ \frac{x}{2} \log \left( \frac{D^2 + x^2}{d^2 + x^2} \right) + D \left\{ \frac{\pi}{2} + \tan^{-1} \left( \frac{x}{D} \right) \right\} - d \left\{ \frac{\pi}{2} + \tan^{-1} \left( \frac{x}{d} \right) \right\} \right] \quad (3.4)$$

where

$$\pi = 3.14159$$

$\sigma$  - density contrast

d - value of first depth

D - value of second depth

x - distance from top of fault to easting point

$\alpha$  - dip (  $0^\circ < \alpha < 90^\circ$  &  $90^\circ < \alpha < 180^\circ$  )

By using the following relation:

$$V1 = 2 \times 6.67E-6 \times \sigma \times 1000$$

$$B3 = d \times \left( \tan^{-1} \left( \frac{x}{d} \right) + \frac{\pi}{2} \right)$$

$$B1 = \frac{x}{2} \times \log \left( \frac{D^2 + x^2}{d^2 + x^2} \right)$$

$$B2 = D \times \left( \frac{\pi}{2} + \tan^{-1} \left( \frac{x}{D} \right) \right)$$

The expression can be simplified to give

$$g = V1 * ( B1 + B2 - B3 )$$

### 3.2.5.4 The subroutine: GRAVITY\_1

This subroutine calculates the gravity effect for the fault structure where the dip ( angle between horizontal surface and the plane of the fault ) is not 90° and the first depth is not zero. The gravity for this structure is given by the following equation ( see Appendix A for derivation):

$$g = 2 \times 6.67E-6 \times 1000 \sigma \{ x \sin^2\alpha \log (r_2/r_1) + x (\theta_2 - \theta_1) \sin\alpha \cos\alpha + D (\pi/2 + \theta_2) - d (\pi/2 + \theta_1) \} \quad (3.5)$$

where

x - distance from top of fault to easting point

d - value of first depth

D - value of second depth

$\sigma$  - density contrast

$$\pi = 3.14159$$

$$r_1 = \sqrt{d^2 + (x + d \cot\alpha)^2}$$

$$r_2 = \sqrt{D^2 + (x + D \cot\alpha)^2}$$

$$\tan\theta_1 = (x + d \cot\alpha)/d$$

$$\tan\theta_2 = (x + D \cot\alpha)/D$$

$$\alpha - \text{dip } (0^\circ < \alpha < 90^\circ \wedge 90^\circ < \alpha < 180^\circ)$$

By using the following relation:

$$V1 = 2 \times 6.67E-6 \times \sigma \times 1000$$

$$a1 = \frac{d}{\tan(\alpha)}$$

$$a2 = \frac{D}{\tan(\alpha)}$$

$$B3 = x \times \left( \tan^{-1} \left( \frac{x+a2}{D} \right) - \tan^{-1} \left( \frac{x+a1}{d} \right) \right) \times \sin \alpha \times \cos \alpha$$

$$B2 = x \times \sin \alpha \times \sin \alpha + \log \left( \frac{r_2}{r_1} \right)$$

$$B1 = D \times \left( \frac{\pi}{2} + \tan^{-1} \left( \frac{x+a2}{D} \right) \right) - d \times \left( \frac{\pi}{2} + \tan^{-1} \left( \frac{x+a1}{d} \right) \right)$$

The expression can be simplified to give

$$g = V1 * ( B1 + B2 + B3 )$$



### 3.2.5.5 The subroutine: GRADIENT\_0

This subroutine calculates the horizontal gravity gradient for the fault structure where the dip ( angle between horizontal surface and the plane of the fault ) is  $90^\circ$ . The gravity gradient for this structure is given by the following equation:

$$HG = 2 \times 6.67E-6 \times 1000 \times \sigma \times \left[ \log \sqrt{\frac{D^2 + x^2}{d^2 + x^2}} \right] \quad (3.6)$$

where

$$\pi = 3.14159$$

$\sigma$  - density contrast

d - value of first depth

D - value of second depth

x - distance from top of fault to easting point

By using the following relation:

$$V1 = 2 \times 6.67E-6 \times \sigma \times 1000$$

$$RLO = \log \sqrt{\frac{D^2 + x^2}{d^2 + x^2}}$$

The expression can be simplified to give

$$HG = V1 * RLO$$



### 3.2.5.6 The subroutine: GRADIENT\_1

This subroutine calculates the horizontal gravity gradient for the fault structure where the dip ( angle between horizontal surface and the plane of the fault ) is not 90°. The gravity gradient for this structure is given by the following equation :

$$HG = 2 \times 6.67E-6 \times 1000 \times \sigma \times \{ \sin^2\alpha \times \log (r_2/r_1) + (\theta_2 - \theta_1) \sin\alpha \cos\alpha \} \quad (3.7)$$

where

x - distance from top of fault to easting point

$\sigma$  - density contrast

d - value of first depth

D - value of second depth

$$\begin{aligned} \pi &= 3.14159 \\ r_1 &= \sqrt{d^2 + (x + d \cot\alpha)^2} \\ r_2 &= \sqrt{D^2 + (x + D \cot\alpha)^2} \\ \tan\theta_1 &= (x + d \cot\alpha)/d \\ \tan\theta_2 &= (x + D \cot\alpha)/D \end{aligned}$$

By using the following relation:

$$\begin{aligned} V1 &= 2 \times 6.67E-6 \times \sigma \times 1000 \\ a1 &= \frac{d}{\tan(\alpha)} \\ a2 &= \frac{D}{\tan(\alpha)} \\ B3 &= \left( \tan^{-1} \left( \frac{x+a2}{D} \right) - \tan^{-1} \left( \frac{x+a1}{d} \right) \right) \times \sin \alpha \times \cos \alpha \\ B2 &= \sin \alpha \times \sin \alpha + \log \left( \frac{r_2}{r_1} \right) \end{aligned}$$

The expression can be simplified to give

$$HG = V1 * ( B2 + B3 )$$

### 3.2.5.7 The subroutine: MODEL

This subroutine draws the theoretical model of the fault structure. The FAULT\_STRUCTURE program calls the MODEL subroutine as the last one after finding the parameters for the fault or faults which have the smallest difference between observed and calculated gravity. The parameters of the fault are stored as variables in the FAULT common block. The scale for both axes: horizontal distance and depth is the same. This subprogram consists of many ZETA PLOTTER statements which are used to create the plot.



## Chapter 4

# Adelaide City Area as the Example of Using the Fault\_Structure Program

### 4.1 Introduction

Testing the gravity interpretation method turned out to be much more difficult than expected because geology is rarely known with adequate accuracy.

One of the few places in South Australia when geology is sufficiently well known is the City of Adelaide.

The importance of engineering geology has been emphasised since the 1950s, when construction commenced in the city of a new generation of multistorey buildings. Foundation drilling along with geological and geophysical services provided by the Department of Mines and Energy has resulted in the accumulation of a large store of detailed knowledge concerning the characteristics of the complex geological sequence under the Adelaide City Area (see figure 4.5 and 4.6). This data provided an example for testing the FAULT\_STRUCTURE program.

## 4.2 Regional Geology

This section has been taken with minor modifications from "Engineering Geology of the Adelaide City Area" by J.Selby and J.Lindsay.

Early in the Tertiary Period, the Adelaide area was dry land with a subdued relief. The land surface consisted of deeply weathered Precambrian rocks. At about this time Australia finally separated from Antarctica and began to drift northwards. This event set up stresses in the earth's crust which were

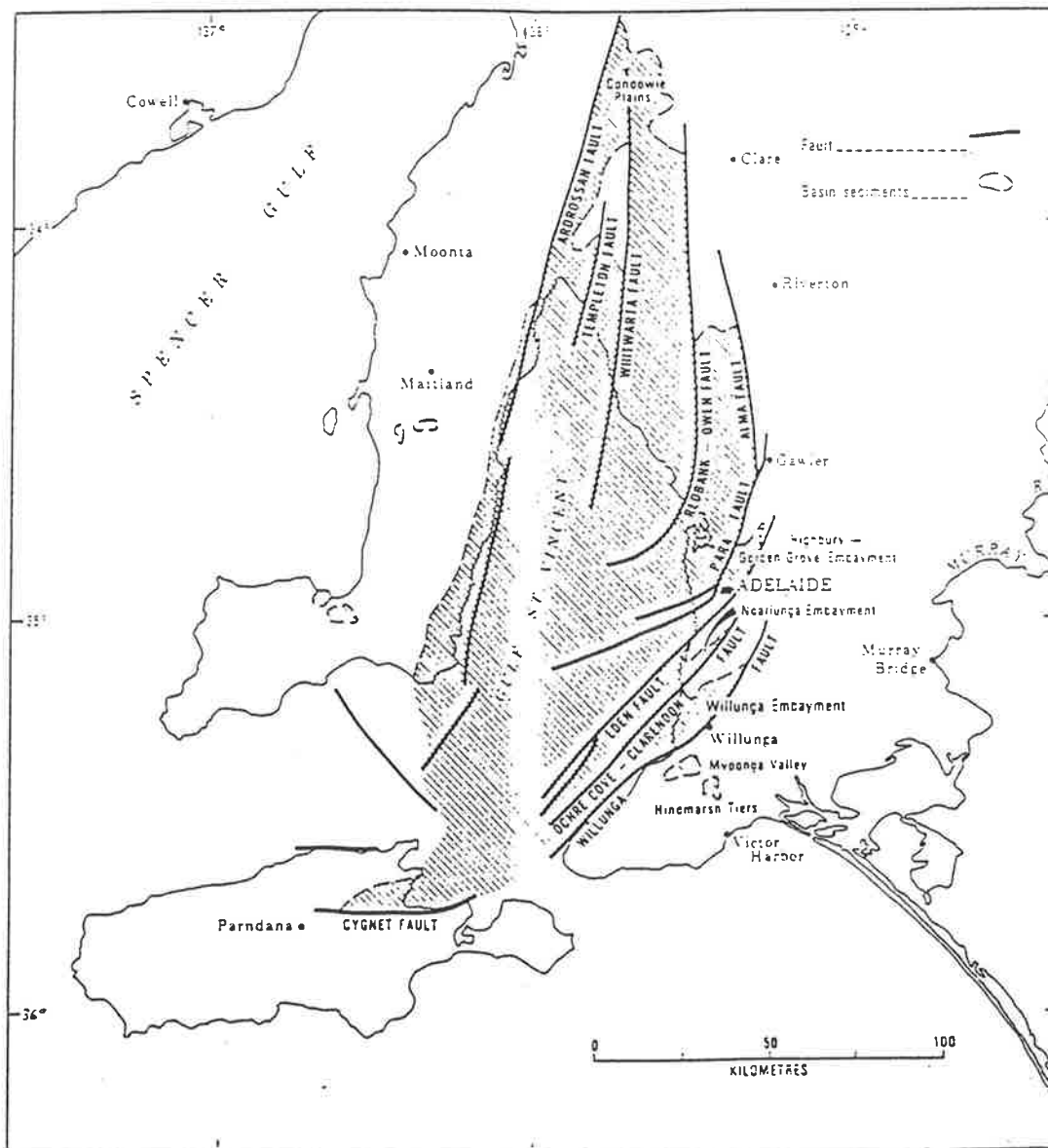


Figure 4.1: The St Vincent Basin, (J.Selby and J.Lindsay).



relieved by faulting, and the downfaulted St Vincent Basin, which stretches from Condowie to Kangaroo Island, was formed (see figure 4.1). The eastern edge of the St Vincent Basin is bounded by a series of major faults, which have formed small embayments on the edge of the main basin. Adelaide is located within one of these embayments and the two fault zones bounding it, the Para and Eden-Burnside Fault, have determined the main features of the present day landscape around the city of Adelaide (see figure 4.2). Sediments which began to fill the faulted embayments were first deposited in swamps and from streams draining the highlands, followed by various cycles of marine deposition as the sea advanced and retreated over the land surface. Movement along the faults persisted throughout this period causing variations in thickness of the strata. Figure 4.3 shows the contrast in thickness of sediments on either side of the Para Fault.

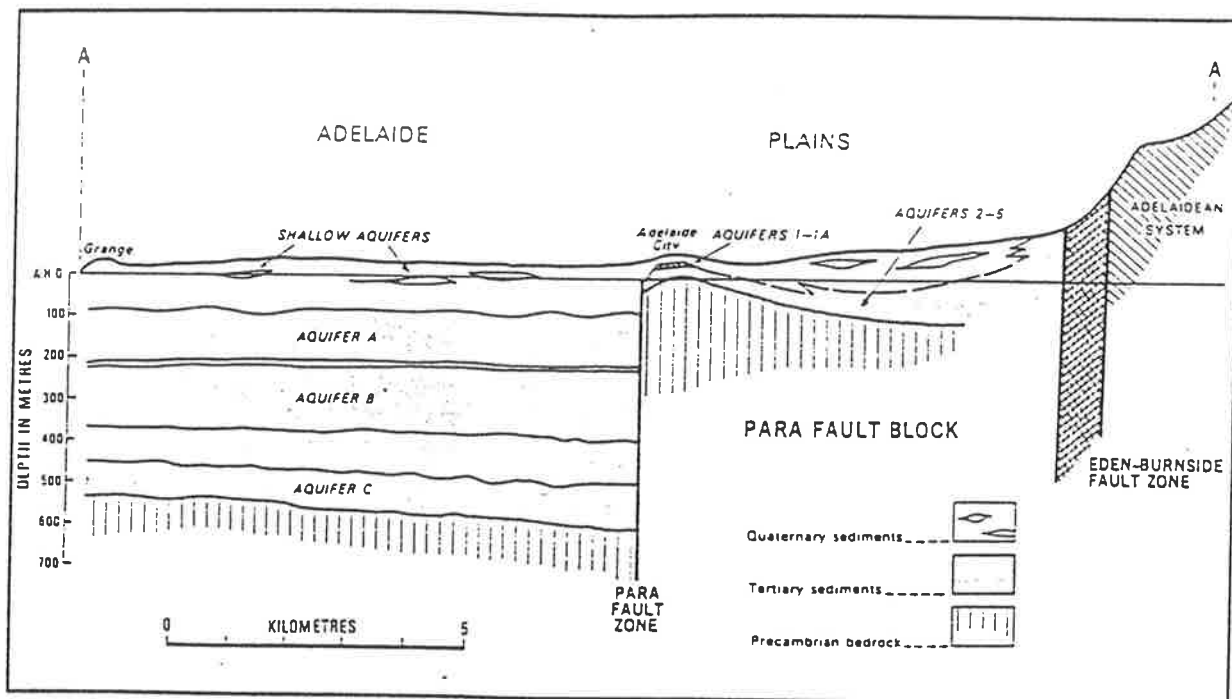


Figure 4.3: Geological section across Adelaide region, (J.Selby and J.Lindsay).

During the Quaternary Period there have been major cyclic climatic changes causing waxing and waning of the polar ice-sheets, with related large world-wide shifts in sea level. Uplift early in the Quaternary Period involved reactivation of the Eden and Para Faults. This led to the deposits of riverine sand and gravel overlain by a thick sequence of alluvial clays with lenses of sand and gravel on the downthrow side of the faults. In the Tertiary Period were deposited the marginally marine South Maslin Sand and Clinton Formation at approximately the same time (about 40 million years ago). Marine microfossils have been found in these sediments confirming that they were laid down in estuaries close to the sea. The richly fossiliferous deposits of the transgression commence with the thin Tortachilla Limestone, well developed near the present coast but only recognised in patches at the base of thicker Blanche Point Formation beneath Adelaide.

AGE	GEOLOGICAL CLASSIFICATION NAME		MAXIMUM THICKNESS (m)	MATERIAL DESCRIPTION	NOTES
QUATERNARY	Recent	1. Alluvium of the Torrens 2. CALLABONNAI CLAY 3. POORAKA FORMATION	21	1. Red brown silty CLAY (CH), grades downwards to SAND and GRAVEL (SP-GP) 2. Red brown CLAY (CH) 3. Light brown silty CLAY (CL-ML), calcareous with layers of calcrete GRAVEL (GM)	1. Gravel used locally for ground water supply 2. Soil 3-horizon 3. The Coleragus Member with older RYON CALCRETE at base in North Adelaide
		HINDMARSH CLAY	22	Red brown mottled CLAY (CH), stiff to hard and fissured; with a middle CLAYEY SAND unit (SC).	Also known informally as the Adelaide or mottled clay Locally sand unit contains small amounts of groundwater
	Pleistocene	CARISBROOKE SAND	13	Yellow, orange brown and grey fine to medium clayey and silty SAND (SC-SM)	AQUIFER 1A
		BURNHAM LIMESTONE	1-2	White clayey, sandy and rubbly LIMESTONE	The Transgression Zone
TERTIARY		HALLETT COVE SANDSTONE	12	Pale grey to yellow brown calcareous SANDSTONE with layers of SAND (SP)	Contains cavities and irregularities lined with clay AQUIFER 1
		PORT WILLUNGA FORMATION Ruwurung Member	112	Sandy SILT and CLAY with strong CHERT nodules (GC-GP)	Removed by erosion north of Wright Barrington Street
		Aldinga Member	27	Green/grey clayey SILT (ML) Fine silty SAND (SM)	Removed by erosion north of Hindley Green St Street AQUIFER 2
		CHINAMAN GULLY FORMATION Tandanya Sand Member	12	Dark grey to black SILT and CLAY (ML-CL) Gravelly, clayey, SAND (SC-GW)	Formerly identified as UPPER BLANCHE POINT FORMATION in City area
		BLANCHE POINT FORMATION Gull Rock Member	20	Alternating bands of cherty siltstone and grey SILT (ML)	Formerly Blanche Point Banded Marls Member
		BASAL BLANCHE PT FMN and TORTACHILLA LIMESTONE	(5)	Green to dark grey clayey SAND (SC) with LIMESTONE	Formerly Blanche Point Transgression Marls Member TORTACHILLA LIMESTONE only in patches
		SOUTH MASLIN SAND	12	Dark grey brown at depth, but weathering to red brown or yellow, silty SAND (SM) with pyrite lumps.	AQUIFER 4
		CLINTON FORMATION	27	Dark grey CLAY (CL) with LIGNITE, irregular clayey SAND zones (SC).	Referred to as the lignite by drillers Sand is AQUIFER 5
PRE-CAMBRIAN	ADELAIDEAN SYSTEM			Brown, pink, grey to white, weathered SILTSTONE with quartz veinlets.	Referred to as pipe clay by early drillers



Uncertainty indicating an erosional break  Unified Soil Classification System symbol:  (CH)

Figure 4.4: Summary of geology, (J.Selby and J.Lindsay).

A regressive, marginally marine interval, represented by the Chinaman Gully Formation separates the upper Blanche Point Formation from the Port Willunga Formation, the lower beds of which were deposited in the city area by further marine transgression, about 38 to 30 million years ago. Late in the Tertiary, about 3 million years ago, a warm and shallow marine bay occupied the present city area. During this transgression, the Hallett Cove Sandstone was deposited, a calcareous sandy formation with many fossil shells, especially near the base. There are no exposures of Precambrian bedrock in the Adelaide city area but it has been intersected in several borehole (see figure 4.6) beneath the Tertiary sedimentary succession. The main rock type is a slaty siltstone which has been deeply and thoroughly weathered.

### **4.3 The Para Fault Zone**

The Para Fault is seen on the ADELAIDE 1:250000 geological map sheet to be inferred to extend to the west of the city of Adelaide as a two branch fault in the western suburbs (see figure 4.6). However, a gravity survey by Finlayson (1978) indicates that the zone consists of three faults which have an echelon relationship and do not join (see figure 4.5). According to Finlayson, all of the faults are assumed to be normal. In this thesis, it is shown (figure 4.7) that the fault has a very steep dip similar to figure 4.3.

### **4.4 Gravity data**

A gravity survey of the Adelaide area was conducted as an east-west traverse from Dew St. to Torrens River along Light Terrace across Port Road to Bonython Park (see figure 4.6). Survey stations were more densely concentrated in the central region where the gravity gradient is steepest.

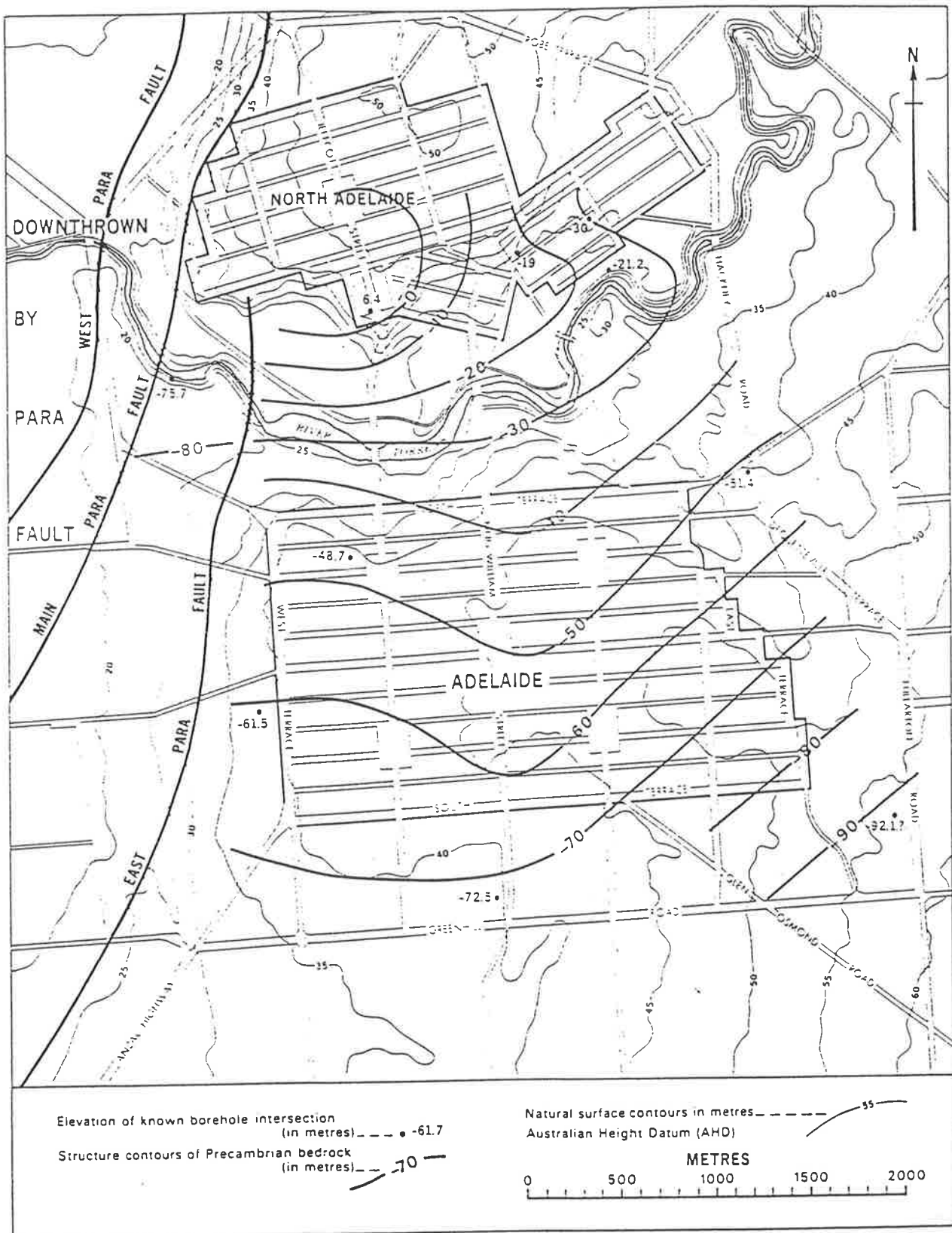


Figure 4.5: Intersections and structure contours of Precambrian bedrock, (J.Selby and J.Lindsay).





## 4.5 Profiles

The results of a gravity survey conducted over the Para Fault of Adelaide indicated the presence of two faults, one being much more prominent than the other (see figure 4.8).

## 4.6 Theoretical Model of Underground Structure Based on Gravity Survey

The figure 4.7 demonstrates the theoretical model which was found by FAULT\_STRUCTURE program. It was found that there are two normal faults with angle of  $85^\circ$ . The distance between these faults is 480m. The first fault is at a depth of 85m and the throw is about 480m. The second fault has a throw of 223m.

Figure 4.8 is a result of comparison of the observed data and the calculated data using a FAULT\_STRUCTURE program. From this picture it may be speculated that the theoretical model gives gravity data which is similar to the observed gravity data.

## 4.7 Previous Work Based on Drilling

The Department of Mines and Energy has provided drilling, geological and geophysical services since 1950s to the architects and civil engineers involved in the erection of many of the city's multistorey buildings. Details of several hundred site investigation bores are stored within the Department's record system, together with depths and yields of all known water and drainage wells. In 1974, a major drilling program was carried out for consultants engaged by the Department of Transport to study

possible routes for a Metropolitan Subway; this provided valuable subsurface information in areas where little had been available previously.

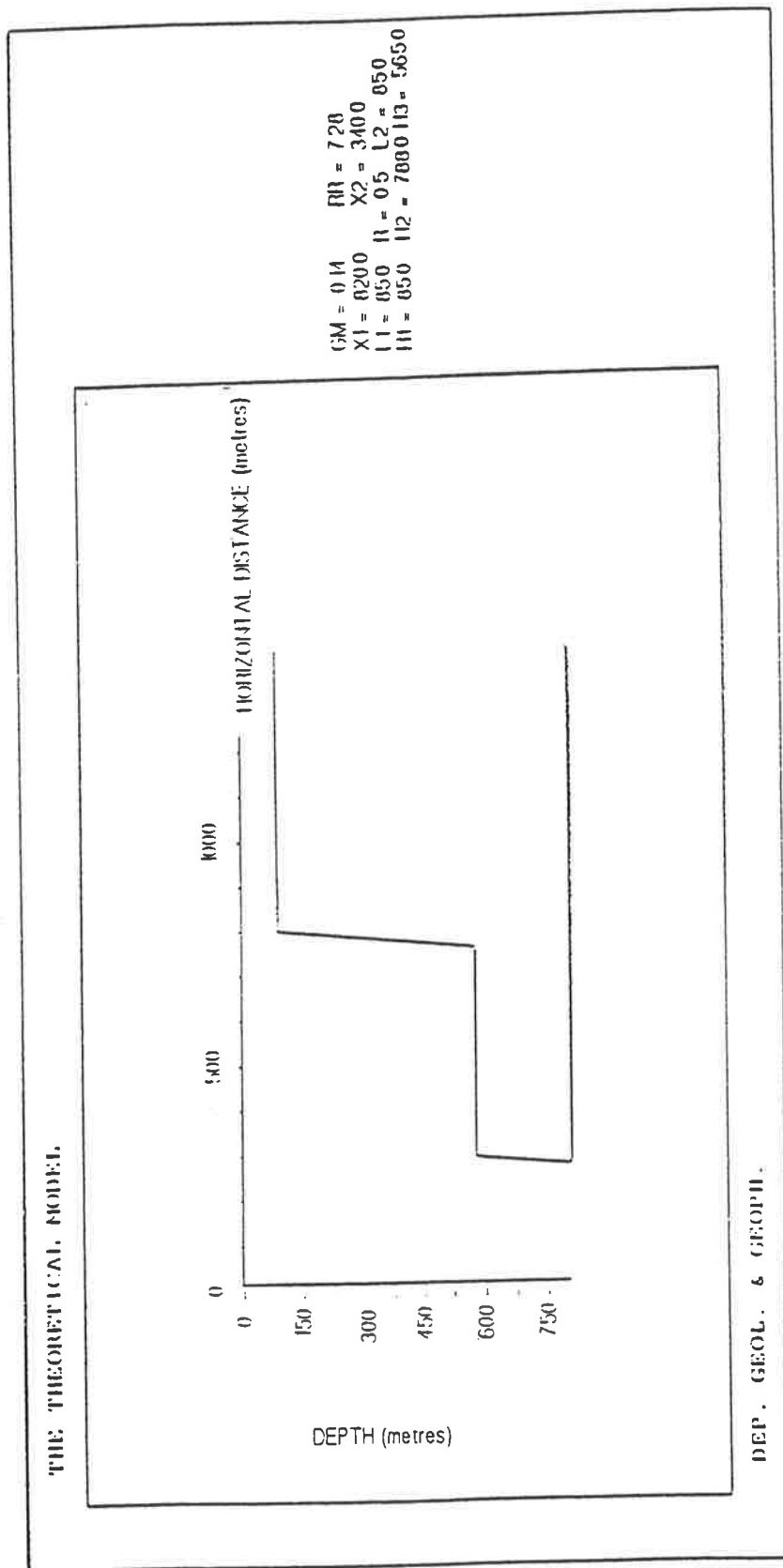


Figure 4.7: Theoretical model.

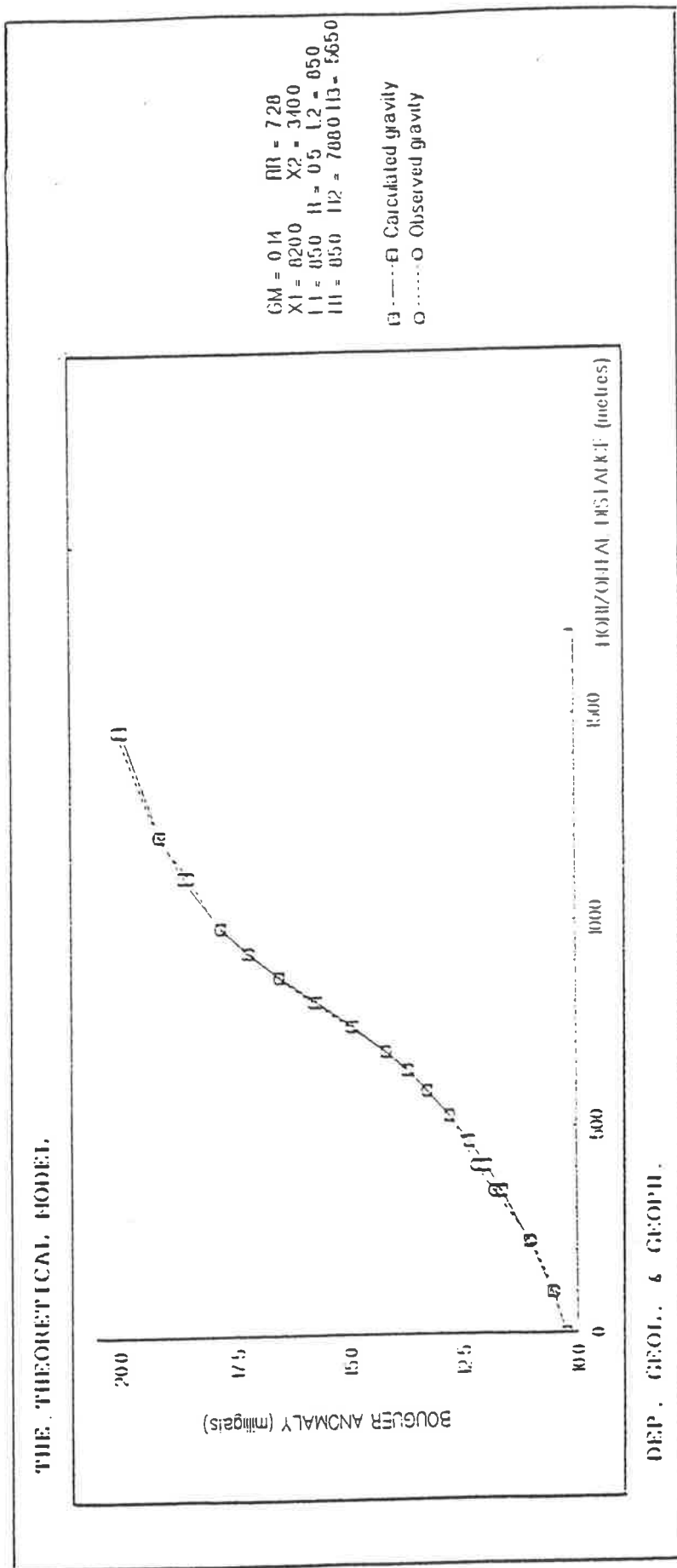


Figure 4.8: The observed and calculated gravity data for the theoretical model.

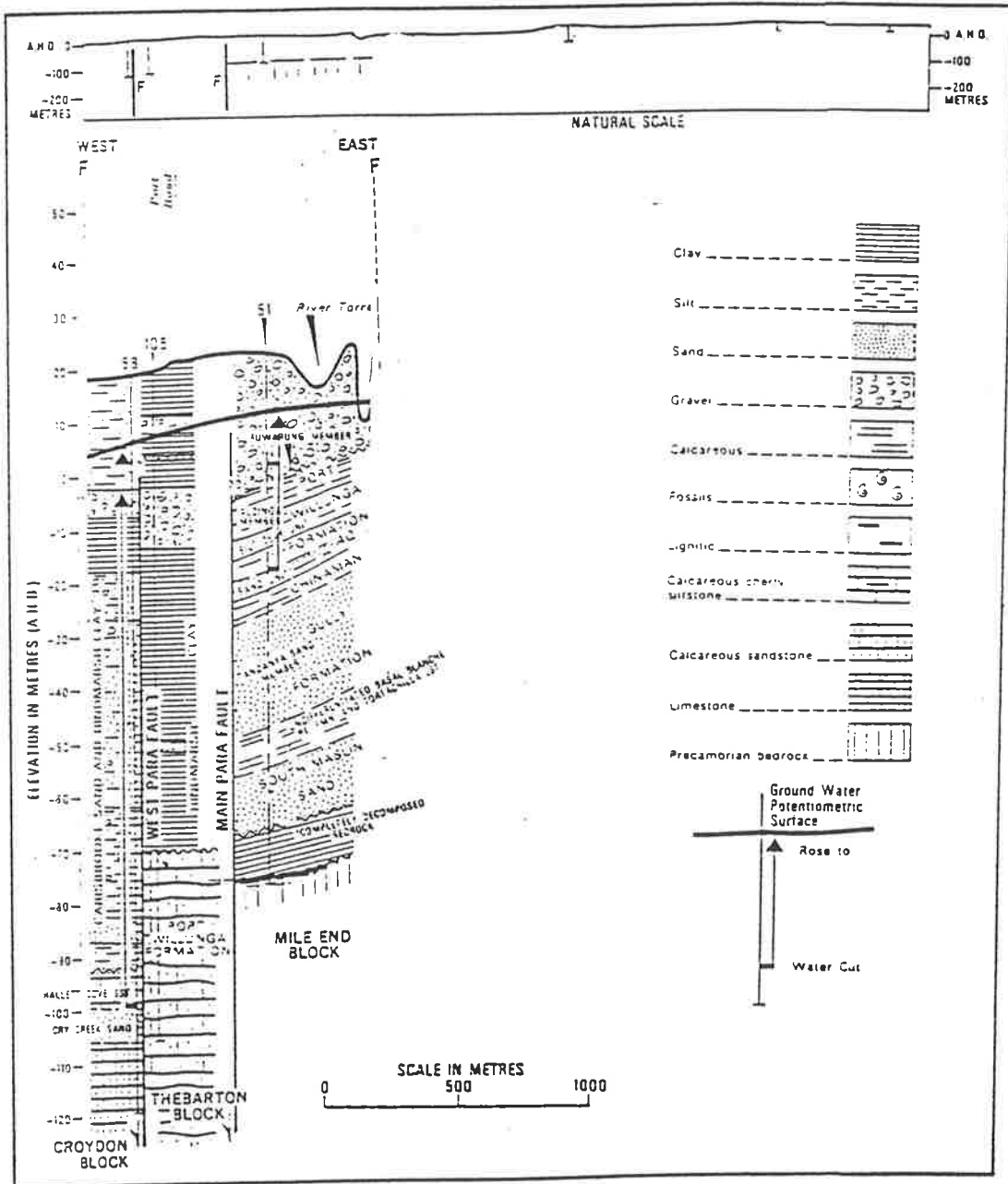


Figure 4.9: Geological section, (J.Selby and J. Lindsay).

The figure 4.9 shows the geological section across the Adelaide city area ( see line FF on figure 4.10). This geological section is only about 100m above the area where the gravity survey was conducted. The table 4.1 shows some stratigraphic information from a few drilling.

Bore No.	El (m)	A	C	K	Total Depth (m)
51	21.2	(22.9)	=	96.9 (0.6+)	97.5
58	19.2	(110.9)	110.9 (26.9+)	-	137.8
68	19.2	(109.7)	109.7 (35.1)	-	155.4
69	19.1	(108.8)	108.8 (43.9)	=	169.2

A - Quaternary alluvium  
C - Burnham Limestone and Hallett Cove Sandstone  
K - Precambrian bedrock

Note: For each stratigraphic unit, its depth below surface is followed by its thickness (in brackets).

Table 4.1: Stratigraphic intersections.

## 4.8 Commentaries

The section is based on drill holes: 51, 58, 68, 69 and 108. These holes establish the depth of basement on the upthrow side of the Para Fault and the throw of the main Para Fault of the West Para Fault but they do not show the exact position of the fault nor do they provide evidence of the depth of basement to the west of the West Para Fault.



The figure 4.9 shows the model of geological structure, which was made as a result of the bores. This picture shows two faults. The basement on the upthrow side of this first fault is at a depth of 95m. The figure 4.7 is a result of computation using the FAULT\_STRUCTURE program. It was found that there are two normal faults with angle 85°. The distance between these faults is 480m (+10m or -10m). The basement on the east side of this first fault is at a depth of 85m and the throw is about 480m. The second fault has a throw of 223m. The FAULT\_STRUCTURE program also gives the information about the ten best fault structures. Compilation of this data allows estimates of parameters as the range of the value. Finally, the theoretical model has parameters:

h1 - from 85m to 105m

h3 - from 565m to 605m

h3 - from 744m to 788m

x1 - from 300m to 360m

x2 - from 820m to 840m

These parameters are similar to the results of the drilling. The bores number 58, 68, 69 give information about the same stratigraphic units but bore number 105 shows different stratigraphic units. It allows to assume that between bore number 68 and bore number 105 exists the fault (see figure 4.10). Bore number 51 intersected Precambrian bedrock at about 97m. It means that the first depth of the theoretical model is very similar to the depth of Precambrian basement as established by drilling in this area. Unfortunately, any drilling in the Adelaide city area has not intersected the second depth of Precambrian bedrock. Bore number 69 has greatest total depth (169m) with Burman Limestone and Hallett Cove Sandstone. It means that the Precambrian rocks lay deeper than 200m. The FAULT\_STRUCTURE program gives this depth as 565m consistent with the drilling.

## **Chapter 5**

# **New Information about Faults in the Frome Embayment in South Australia Section of the Eromanga Basin**

### **5.1 Introduction**

Faults are an important component of the structures in the Frome Embayment, the south west corner of the Eromanga Basin. The fault which forms the western margin of the Frome Embayment is large and is likely to be an important factor in the control of sedimentation, and possibly the migration and the trapping of oil in the Eromanga Basin. There are also smaller faults which may also be important. As outcrops in the basin are poor, additional information provided by gravity surveys are important in exploration of the region.

Knowledge about the faults is also important for another reason. There are conflicting theories about the forces which have produced the structures in the Eromanga Basin. According to the theories the types of faults which occur will differ in inclination depending on what stresses produced the faults.



Information about the inclination of the faults is not readily obtained as they do not outcrop, they are not intersected by drill holes and they are not resolved on the seismic sections. Under favourable circumstances, information about the inclination of the faults can be obtained from the gravity data and this was one of the reasons for developing the computer analyses of fault anomalies.

The Eromanga and Cooper's Basins are the most prosperous regions in South Australia in the production and exploration of oil and natural gas. The availability of surveyed data for the region prompted me to undertake my research in this direction.

The foundation of this part of my research is the gravity data obtained from DELHI.LTD and the South Australia Department of Mining and Energy made 30 years ago for this part of South Australia: the area lies between  $25^{\circ}\text{S}$  -  $32^{\circ}\text{S}$  and  $132^{\circ}\text{E}$  -  $142^{\circ}\text{E}$  boundaries.

The data had been stored on magnetic tapes by the S.A.D.M.E. contained 65.000 pieces of data.

During verification of the data, it appeared there were a number of observations which were wrong or had too big an error margin. As I did not have access to the source of the data these points have been omitted. It was originally intended that the research should focus on the Eromanga Basin and much work was done on both the gravity data and the geology before it was established that the data was not suited to the way in which the problem was studied.

### 5.1.1 Historical Note - Eromanga Basin in South Australia

Studies prior to the current era of geological mapping in the Great Artesian Basin in South Australia were all related to the search for groundwater. These include geological reconnaissance, palaeontology and investigation of groundwater. Rawlinson (1878) quoted by Ward (1946) appears to have made the earliest prediction of large supplies of underground water in an interior basin. Between 1894 and 1895 Mesozoic molluscs and foraminifera from the Lake Eyre region were collected during reconnaissance survey and drilling by the South Australian Government. The fossils were described by Hudleston (1884,1890) and Howchin (1886,1895). A collection of geological specimens, including Mesozoic fossils, from South Australia was exhibited at the Colonial Exhibition in London in 1886. In 1887 Scouler made general geological observations and collected fossils north west of Marree. Brown (1892) reported on his wide-ranging reconnaissance around the northern edge of the Flinders Ranges and the Lake Eyre region during which he made extensive collections of fossils material and noted mound springs, and anomalous boulders of quartzite and porphyry within the Cretaceous shales. The first to describe the stratigraphy and structure of the Great Artesian Basin was Lockhard Jack (1930). In 1955 Woodard and Glaessner and Rao published details of the lithology and fossils plant remains of the sandy sequence below the marine Cretaceous in the northern Flinders Ranges.

The present era of exploration for oil and gas was ushered in by R.C. Sprigg and his colleagues of Geosurveys of Australia Limited who in their summary of the geology of the Great Artesian Basin in South Australia (Sprigg, 1958) noted that traces of oil and gas were present throughout the basin and the petroleum potential was being investigated.

Geological mapping of the margin of the Eromanga Basin began with the production in 1961 of the Gardiner, Moolawatana and Paralana one-mile geological maps showing the edge of the north eastern Flinders Ranges.

The first use of local stratigraphic nomenclature on Survey maps of the Eromanga Basin appeared on the 1:250 000 geological maps MARREE (1965) and OODNATTA (1967). The more recent Survey maps and reports are summarised in figure 5.1.

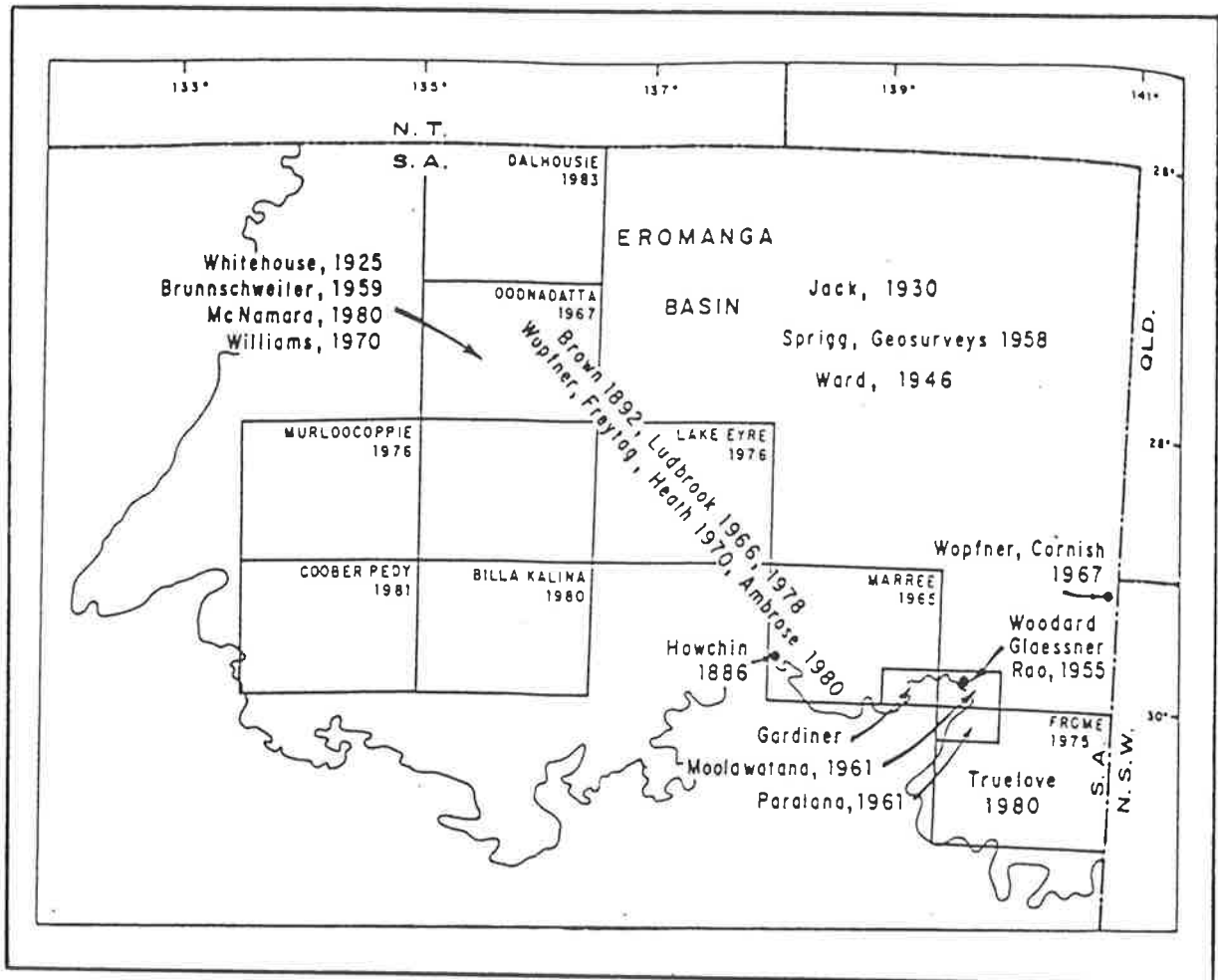


Figure 5.1: Locations of geological contributions.

## 5.2 The Study Area

The area of study is Lake Frome in the South Western part of the Great Artesian Basin (see figure 5.2). This area is bounded on the West by the Northern Flinders Ranges where the high density rocks outcrop.

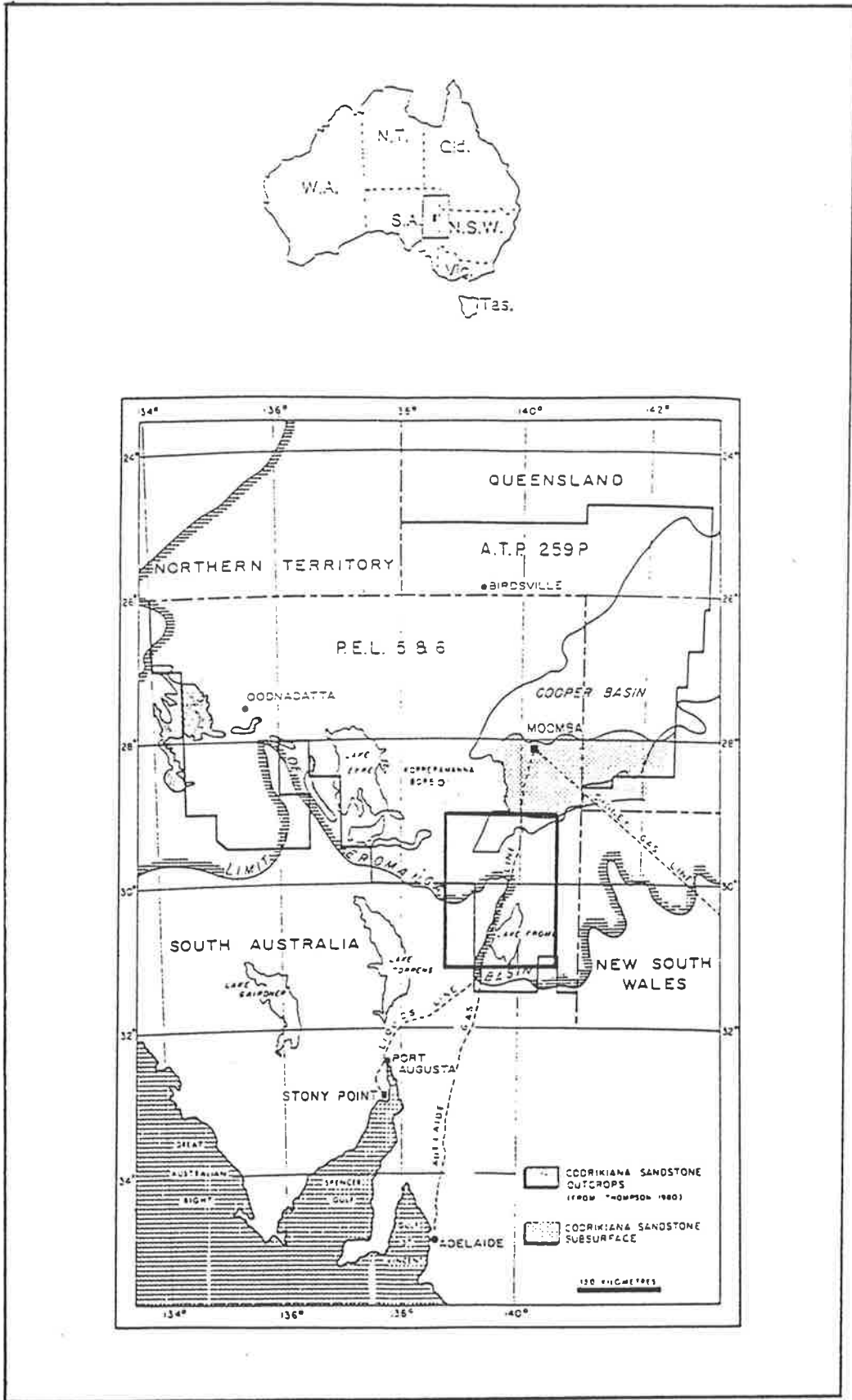


Figure 5.2: Study Area Location.

Extensive areas of outcrop of very thick 20000 feet lower and middle Cambrian marine sediments occur along the eastern flank of the Northern Flinders Ranges.

In some places Proterozoic sediments are overlaid by 200 to 300 feet of limestone and a very thick middle Cambrian section of sands. On the East, the sediments are younger, and Mesozoic and Cainozoic overlies Cambrian sediments, which on account of the high density are regarded as the "basement" rocks in this study.

This area was chosen as a starting point because the structure is well defined on the gravity map (see figure 5.3). Something is already known about the fault which produces this anomaly.

### 5.3 Gravity Data

A model for the contact at the edge of the Precambrian outcrop is required as a first step in interpreting the gravity data from The Lake Frome Basin. A gravity survey of this area was conducted by Geophysical Service for Delhi Petroleum over the period April to October 1963.

The steep gradients of the contours on the Bouguer anomaly map for the Lake Frome area show clearly the approximate positions of faults (see figure 5.3).

### 5.4 Profiles

Three profiles are presented to illustrate the fault structure. Interpretation is only possible where data is available. Any interpretation made between these lines is meaning less because the contours are the result of interpolation and are not based on observation (see figure 5.3).

Line no. 3 demonstrates that this region has a structure with probably one fault with a very large throw (see figure 5.4).

The next profile, no. 12a, indicates that the region, which is only 11 km away from previous place, has a structure with two faults (see Figure 5.5).

The following profile no. 13a also indicates a structure with two faults ( see figure 5.6 ). The distance between line no. 13a and no. 12a is 13 km.

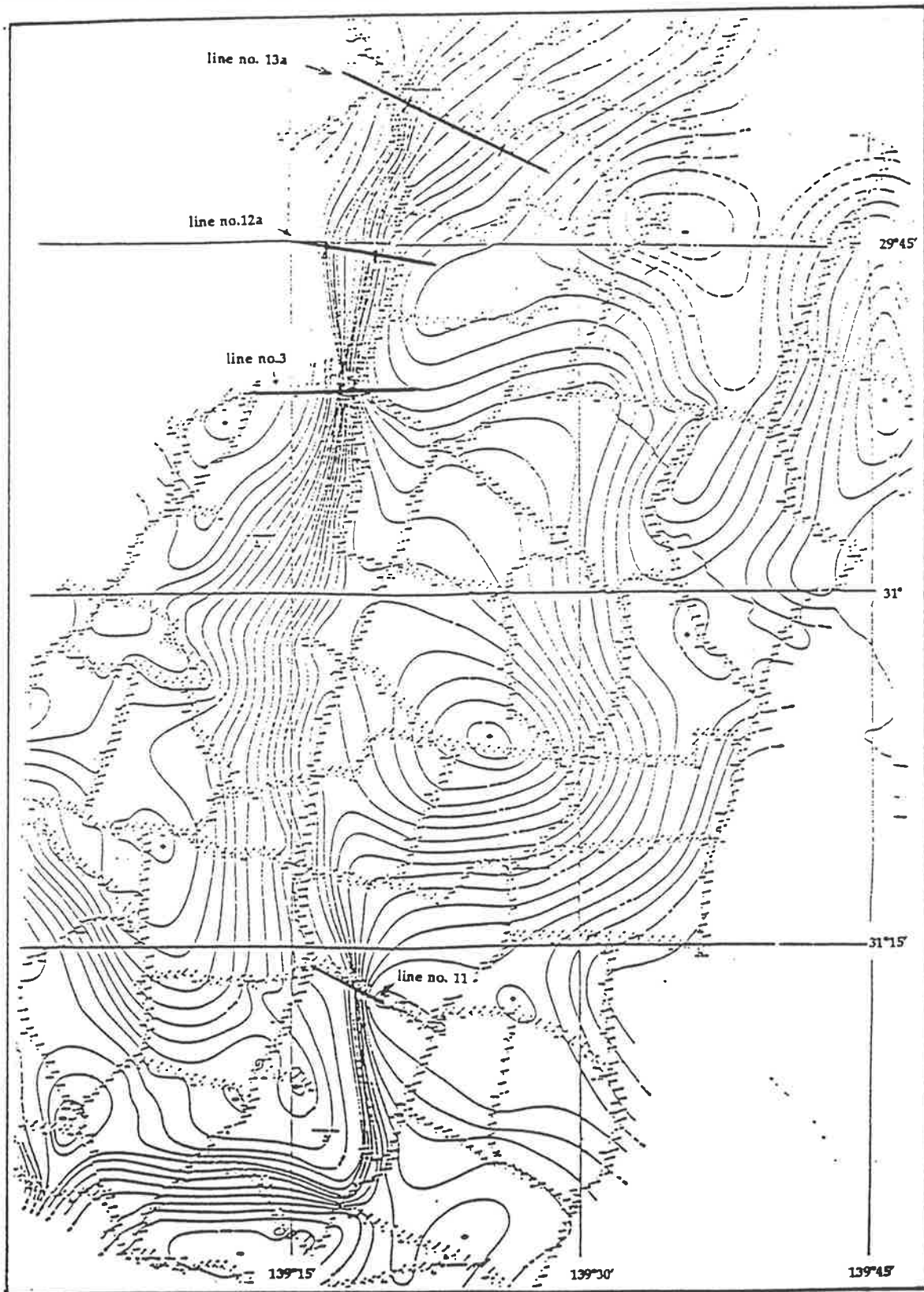


Figure 5.3: The Bouguer anomaly map for Lake Frome area.

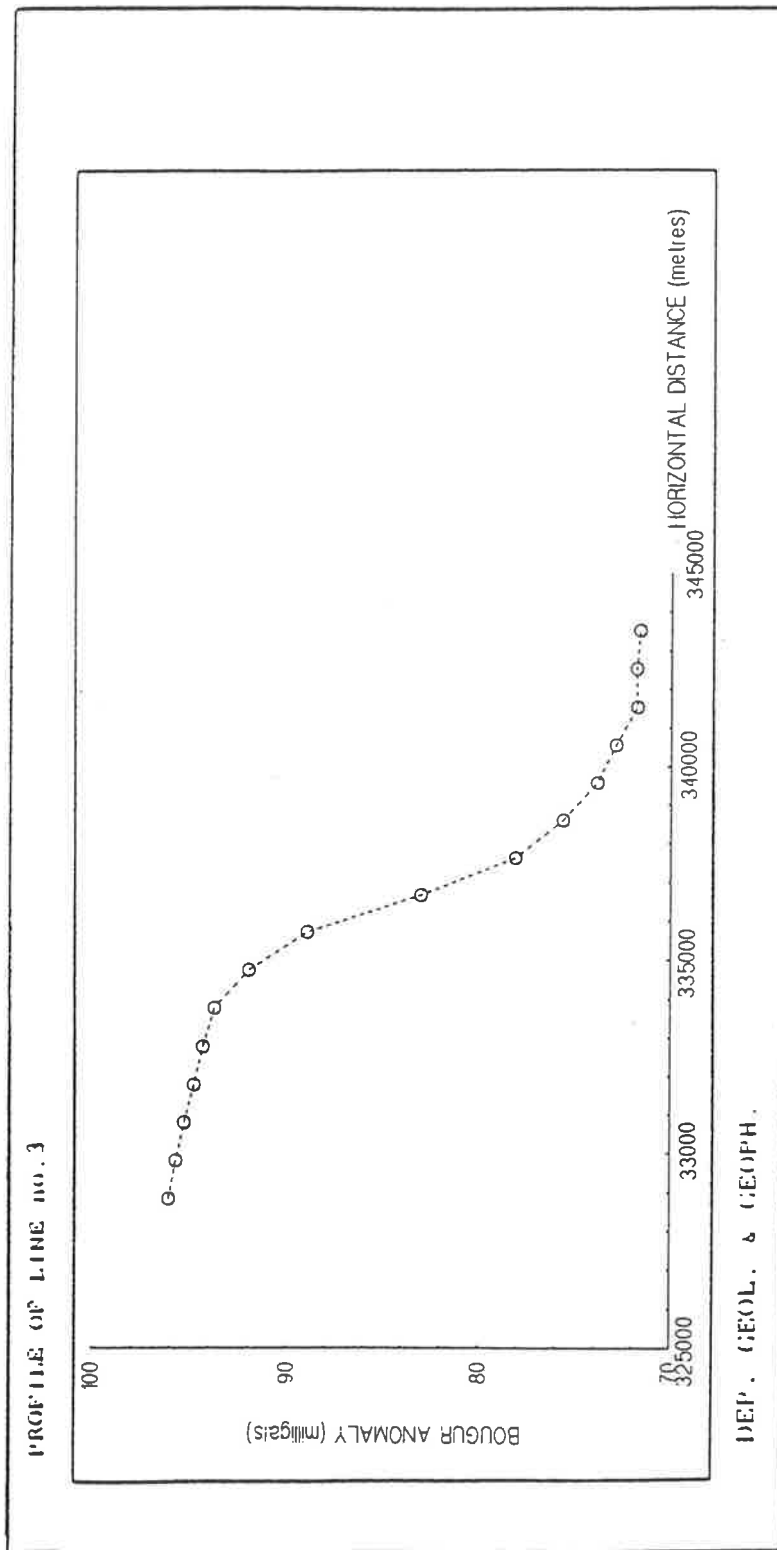


Figure 5.4: The profile of line no. 3.

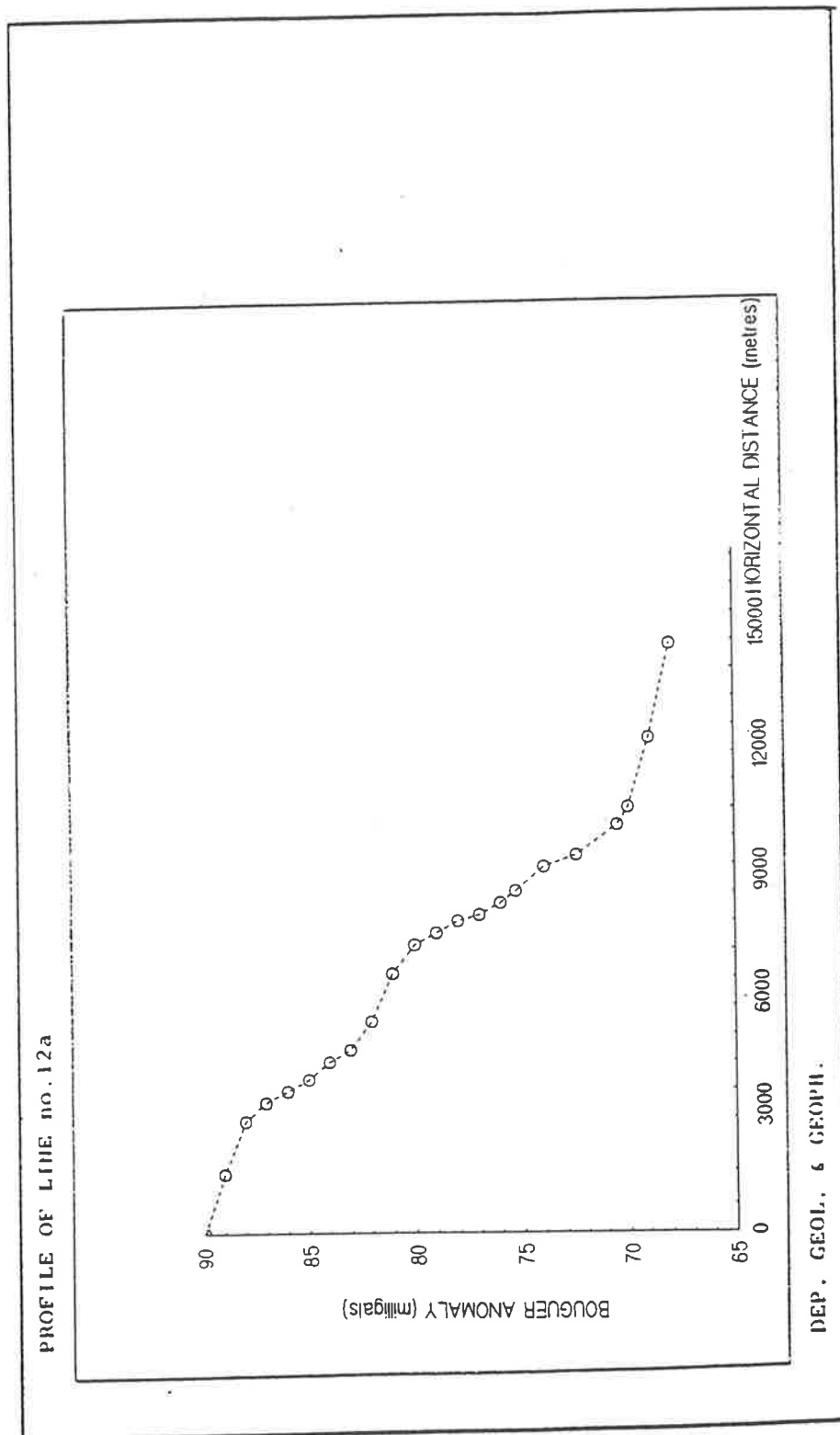


Figure 5.5: The profile of line no. 12a.



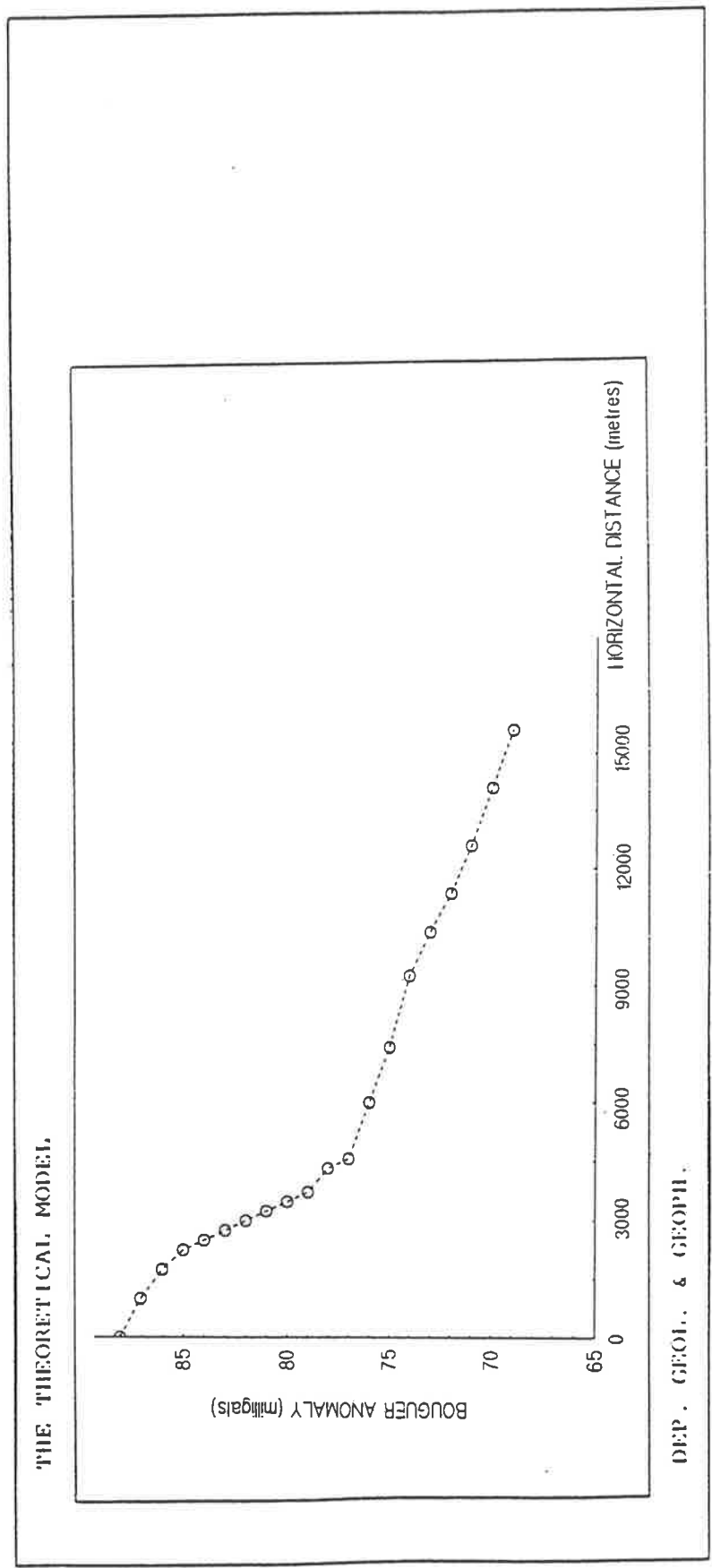


Figure 5.6: The profile of line no. 13a.

## 5.5 Theoretical Model of Underground Structure

A special computer program for a model of a two-fault structure (see Appendix A) was developed and applied to the interpretation of lines no. 12a and no. 13a.

Figure 5.7 demonstrates the theoretical model which matches the observed curves for line no. 13a. Using the computer program, it was found that there are probably two faults. The distance between these faults is 8.3 km. The top of this first fault is at a depth of 700m and the throw is about 1300m. The second fault has a throw of 400m.

Figure 5.9 demonstrates the theoretical model for line no. 12a. There are also two vertical faults. The distance between them is 4.2 km. One is at a depth of 380m and has 500m throw. The second fault has a throw of about 1040m.

By considering line no. 3 (figure 5.12), it can be observed that this line probably represents one fault (see figure 5.14). It is a normal fault with the angle of  $80^\circ$  and the throw is 1700m to the East.

As the previous lines had the gravity profiles for two faults, it can be suggested that line no. 3 also demonstrates the gravity effect for two faults (see figure 5.13). It is indicated that the gravity effect of two vertical faults is similar to the gravity effect of one fault, so it may be said that the distance between these faults is also proportionally smaller. Figure 5.13 is a result of computation using a special program. This theoretical model gives the parameters for two vertical faults. The distance between them is smaller than in the previous model and approximates 1230m. One fault is at a depth of 700m and has a throw 1400m. The second fault has a throw of 300m. This improved resolution comes from using the FAULT\_STRUCTURE program.

It can be concluded that the gravity effect for this region is produced by more than one fault (see figure 5.3). From this picture, one can speculate that this part of Lake Frome is cut by at least two steeply dipping normal faults. The possibilities exist, however, that this is just one fault or many faults with small distances between each other. Comparing line no. 12a with line no. 13a reveals a decrease in distance between the two faults, suggesting that this area is cut by more than one fault, with smaller distances between each fault.

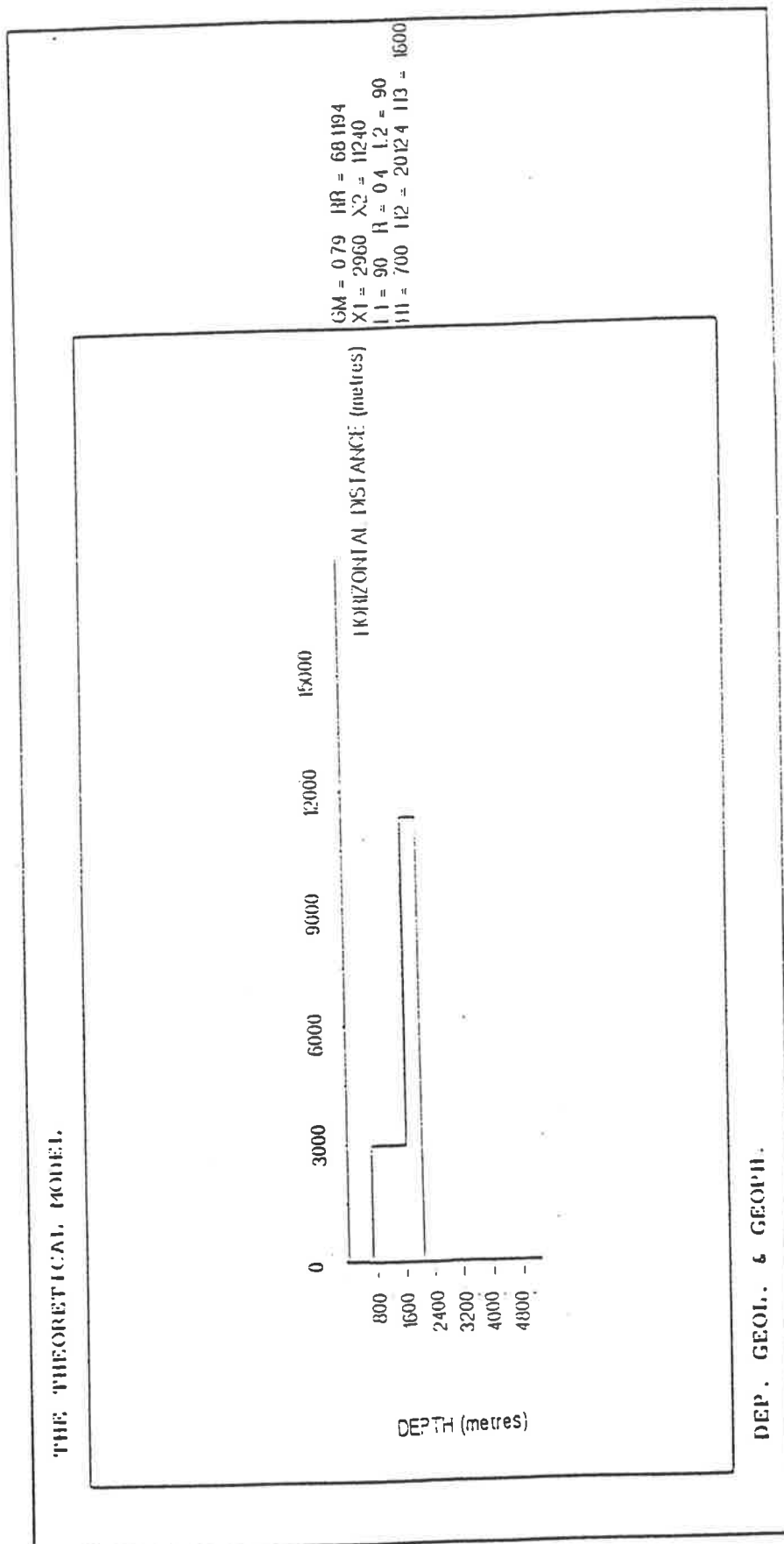


Figure 5.7: The theoretical model for line no. 13a.

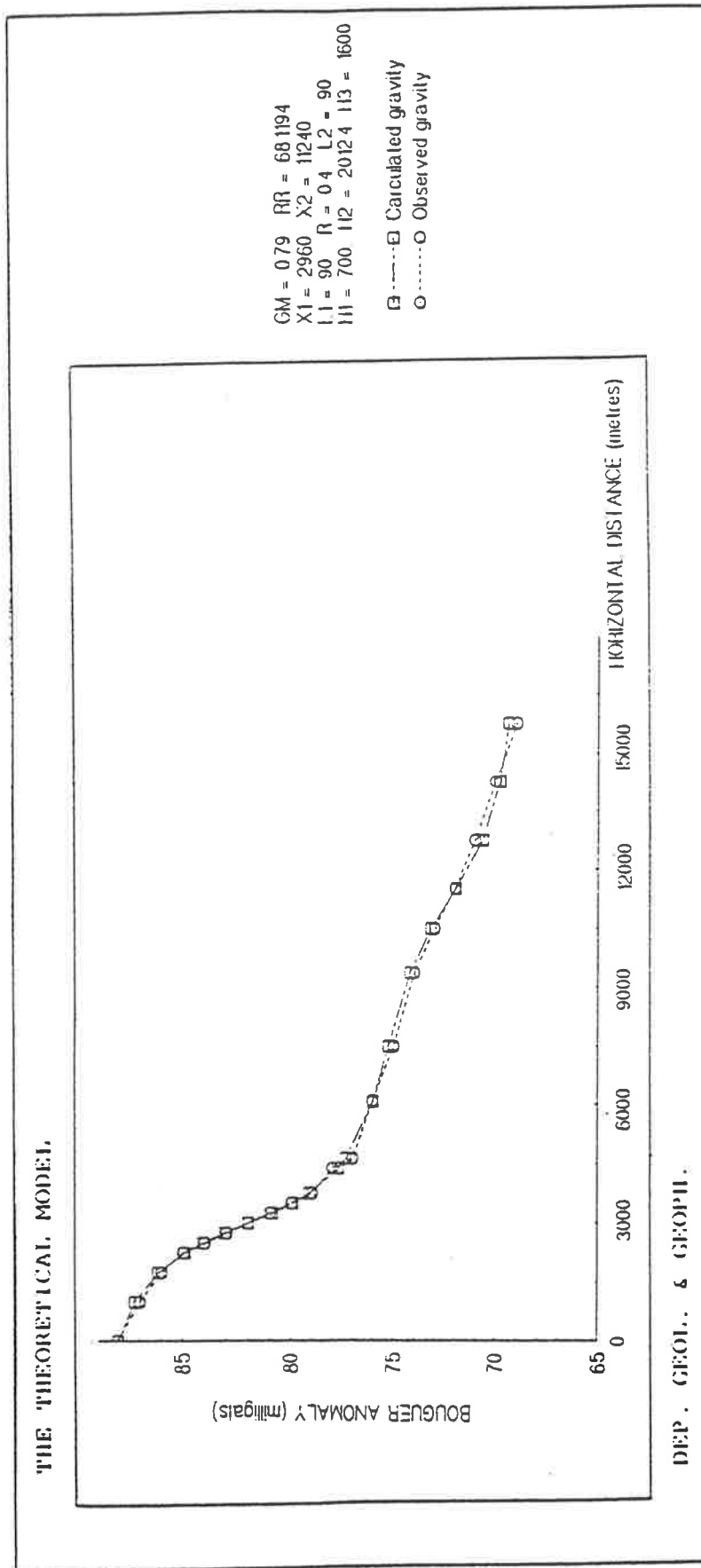


Figure 5.8: Observed and calculated gravity for line no. 13a.

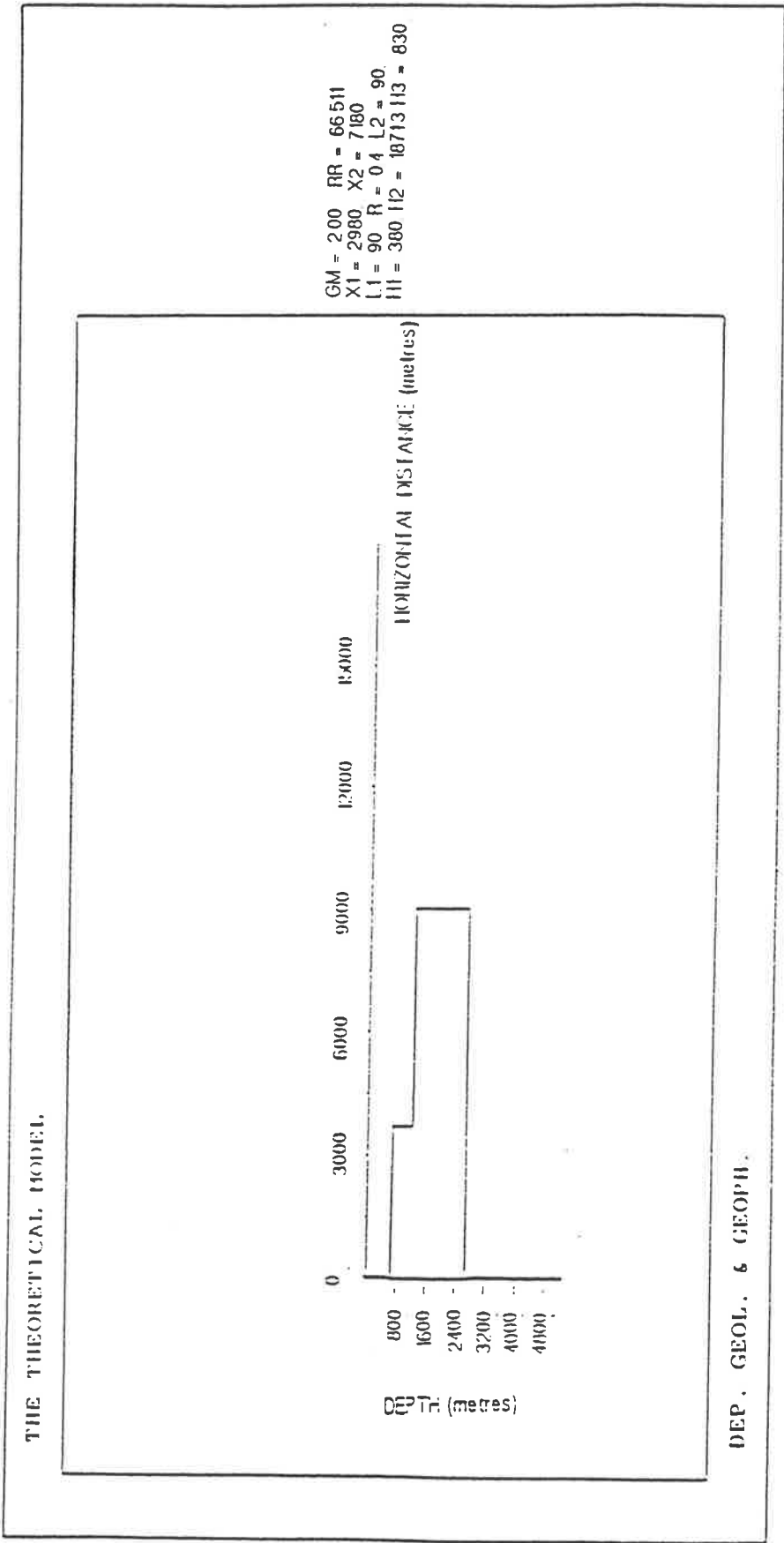


Figure 5.9: The theoretical model for line no. 12a.

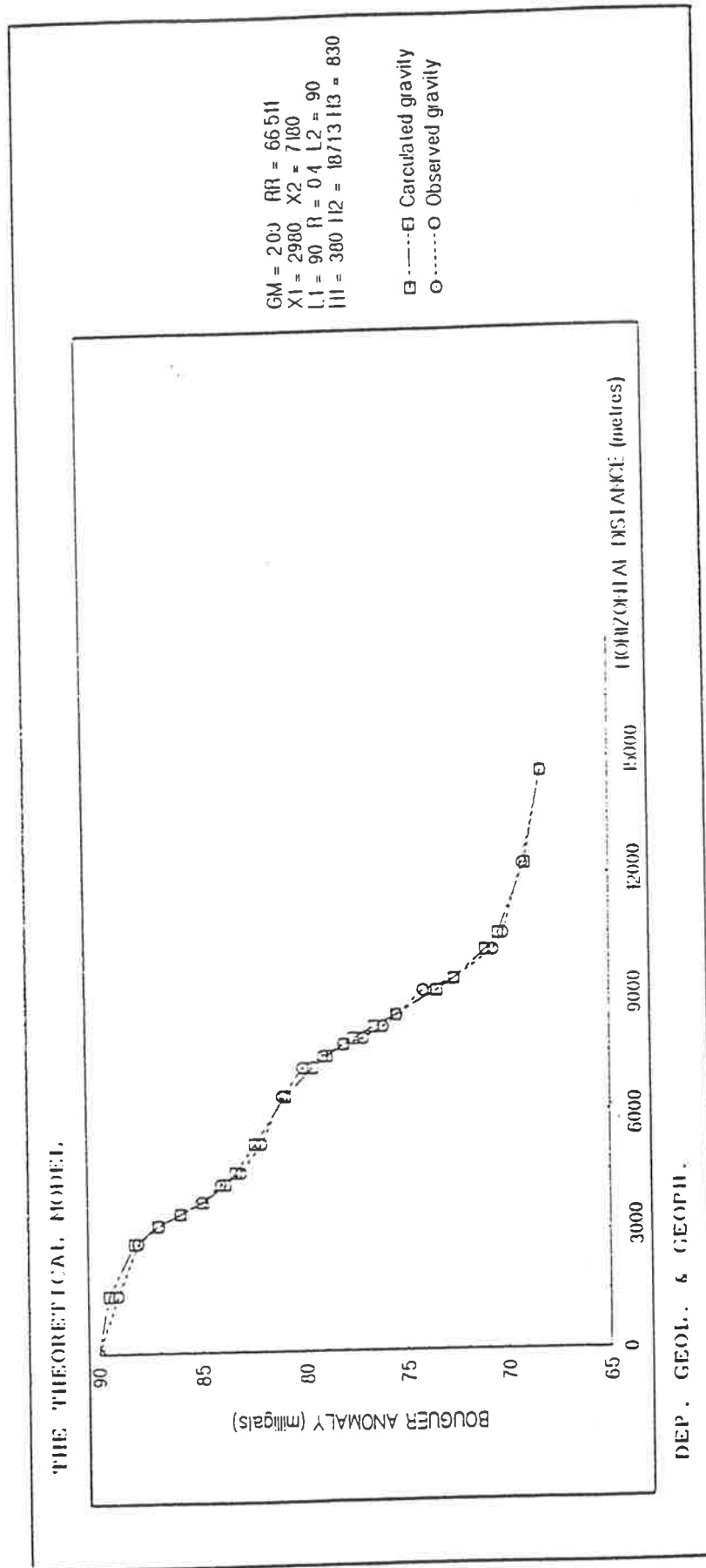


Figure 5.10: Observed and calculated gravity for line no. 12a.

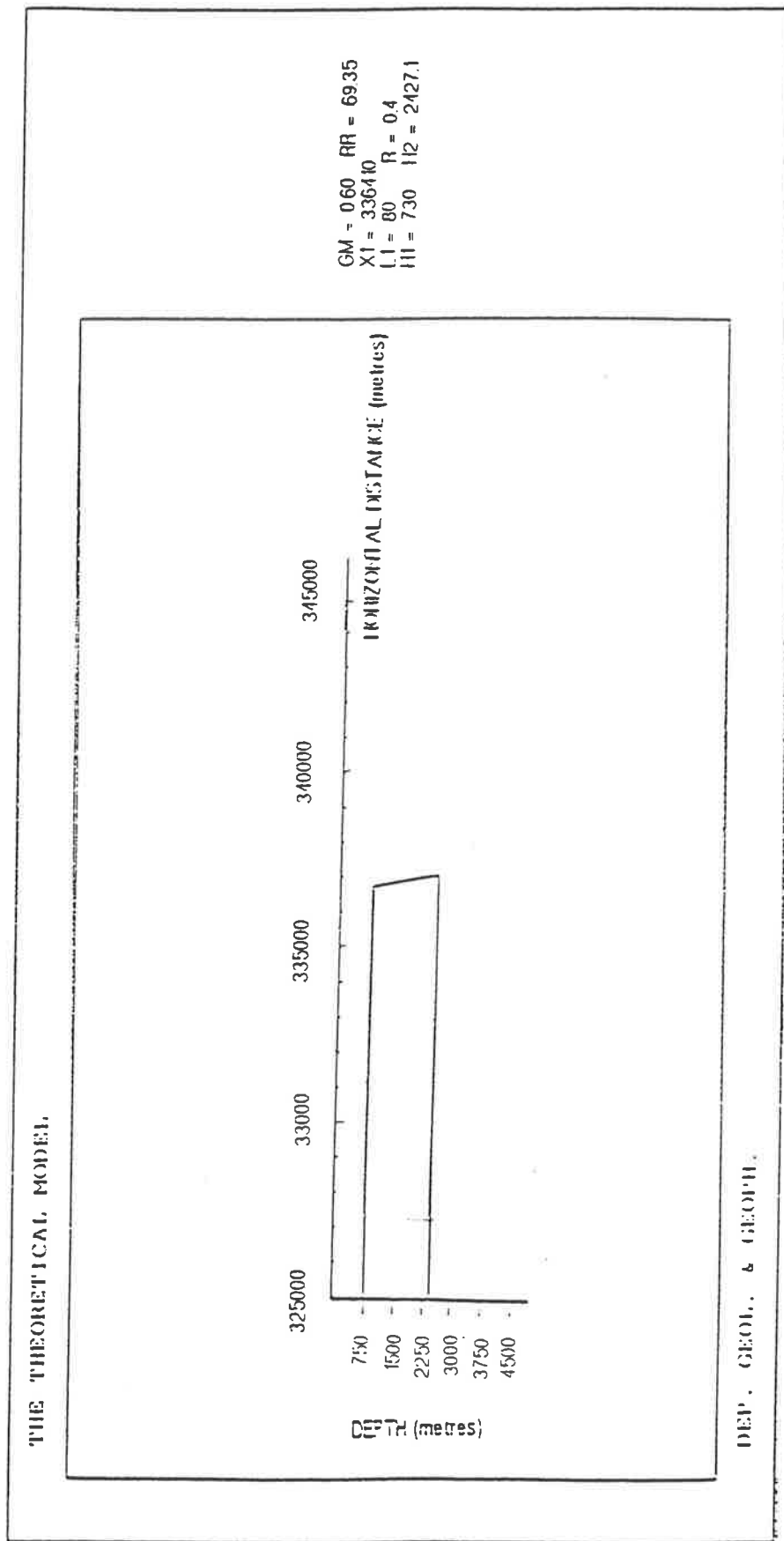


Figure 5.11: First theoretical model for line no. 3.

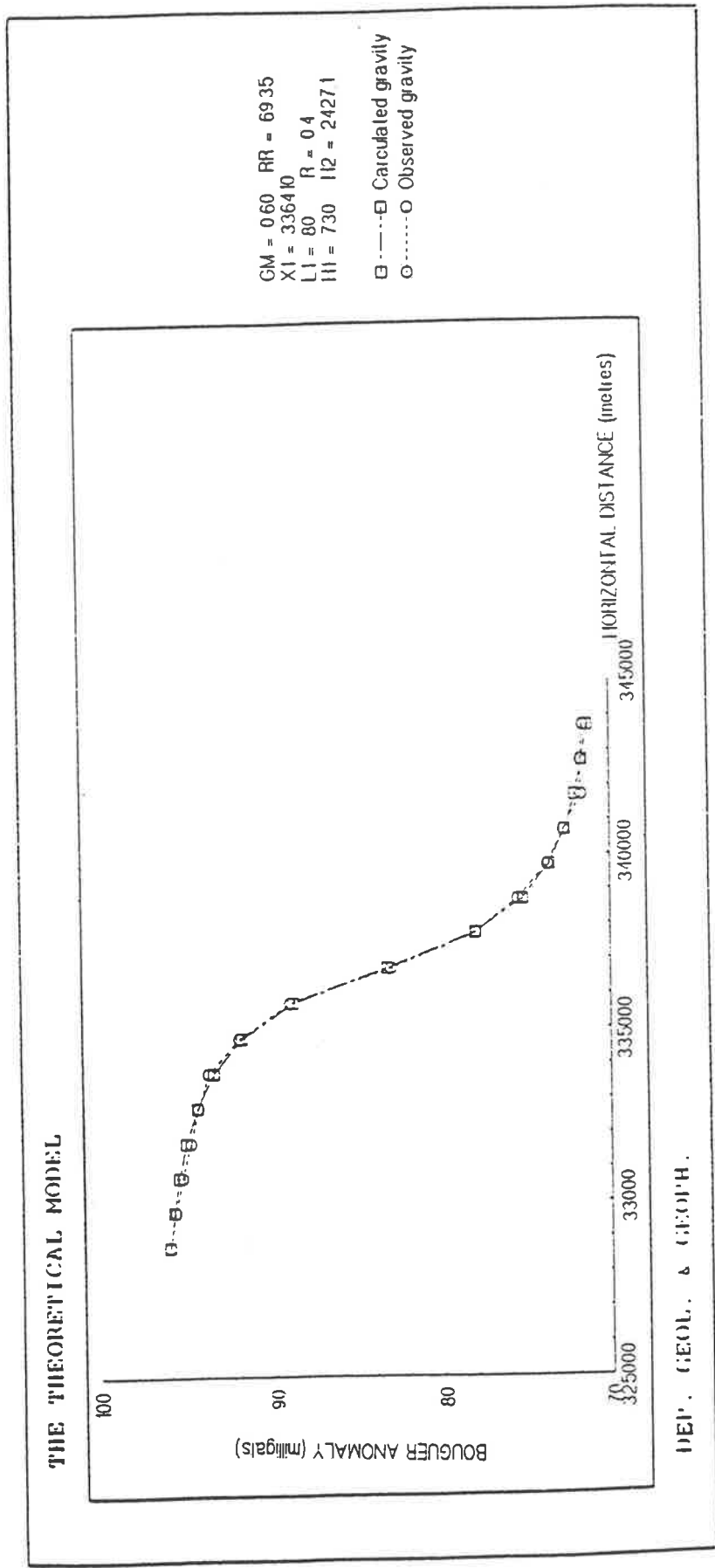


Figure 5.12: Observed and calculated gravity for line no. 3 (one fault).



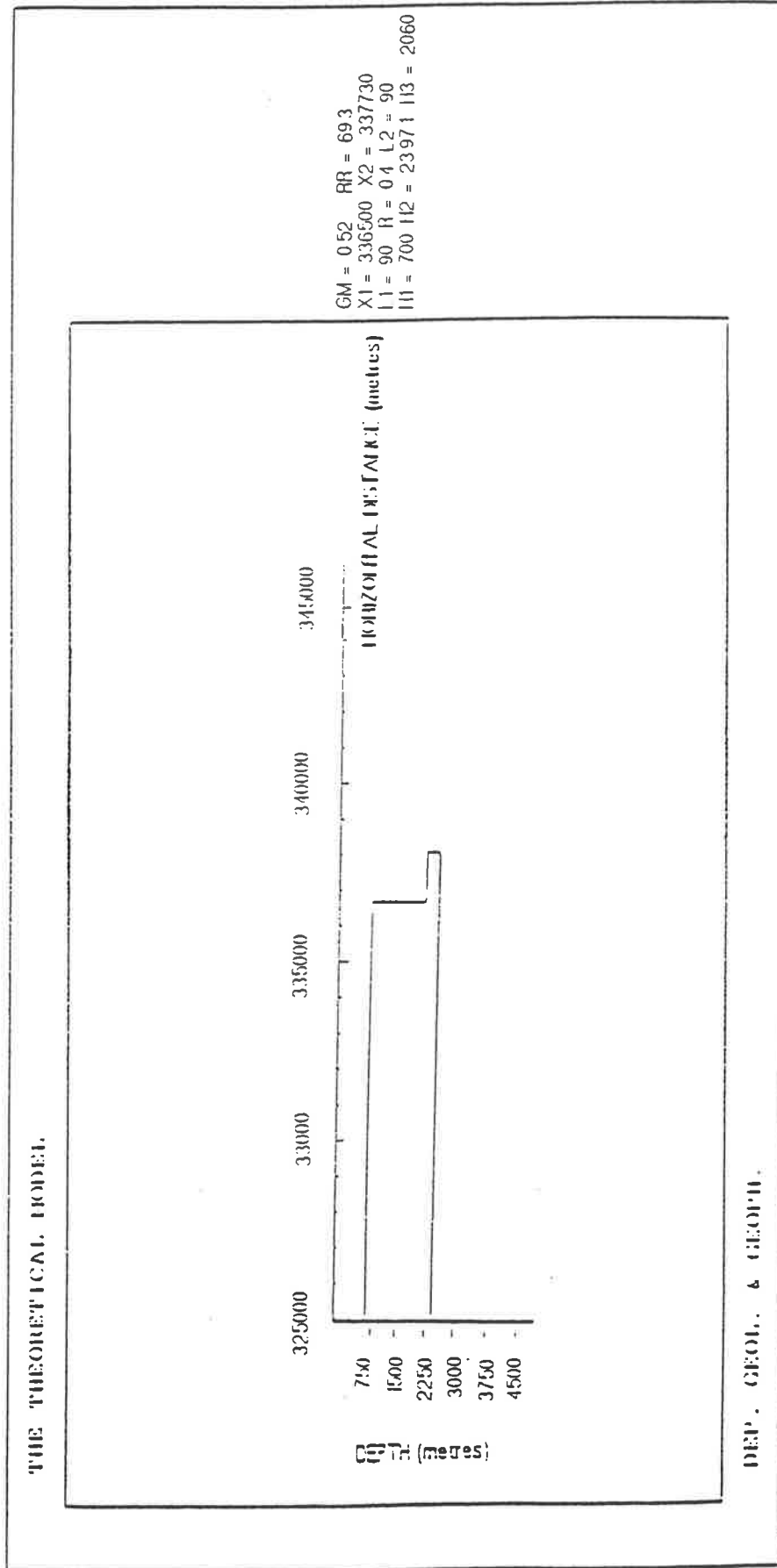


Figure 5.13: Second theoretical model for line no. 3.

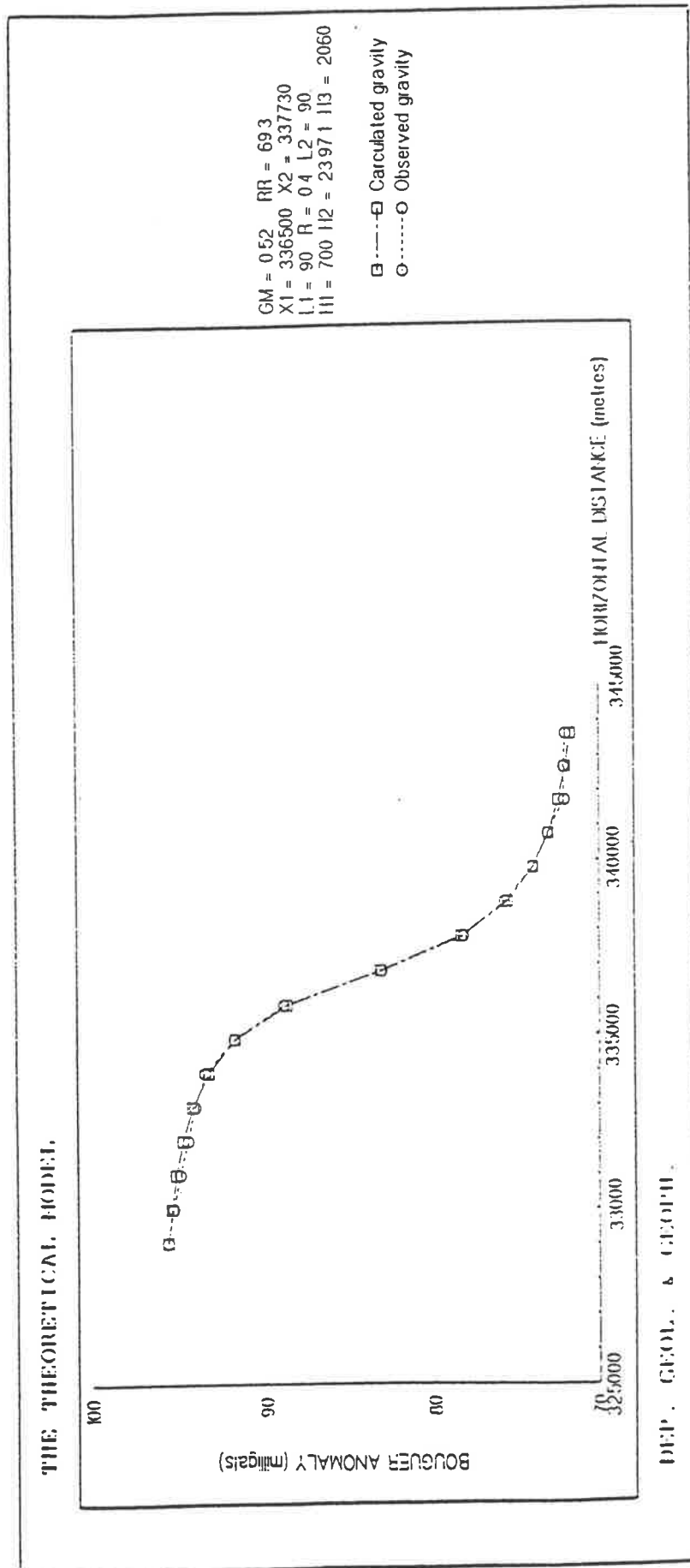


Figure 5.14: Observed and calculated gravity for line no. 3 (two faults).

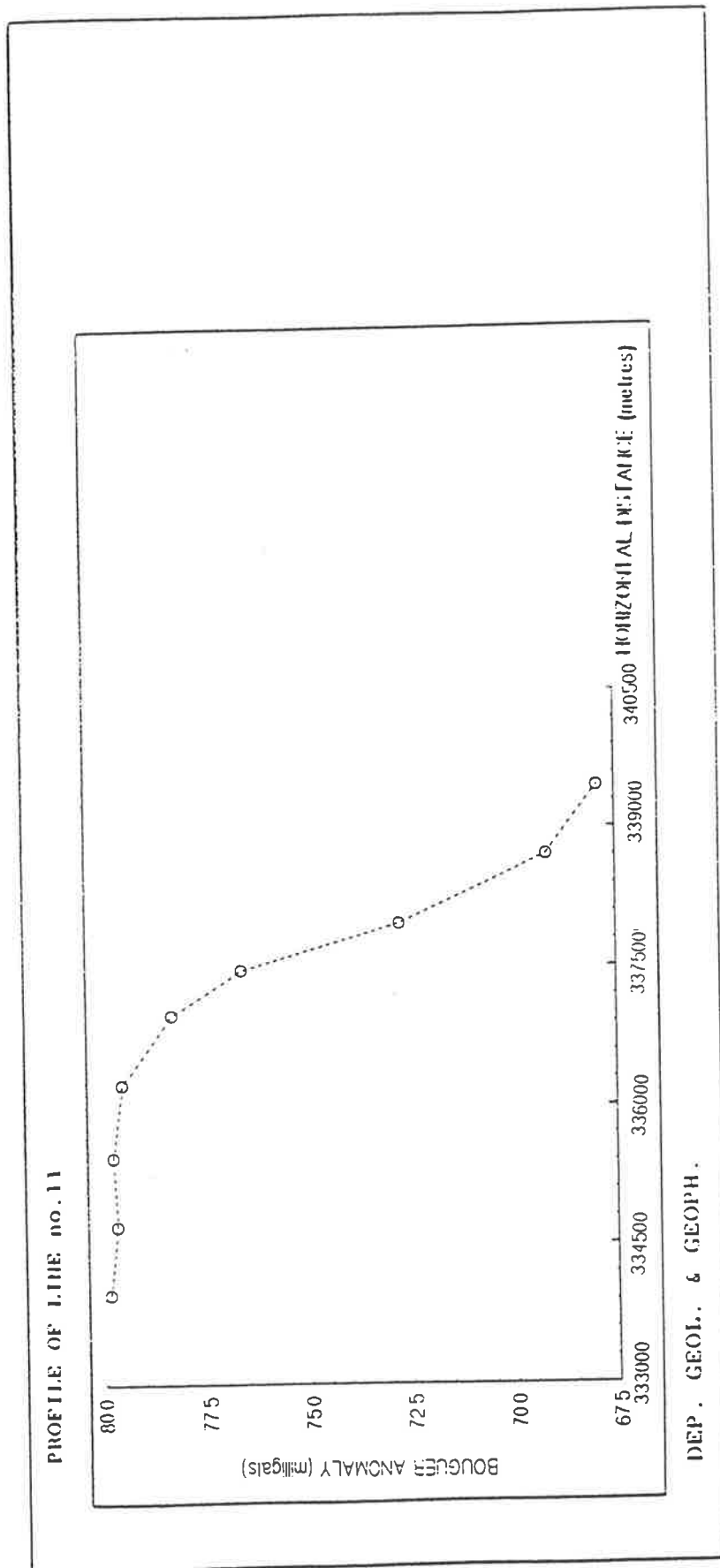


Figure 5.15: The profile of line no. 11.

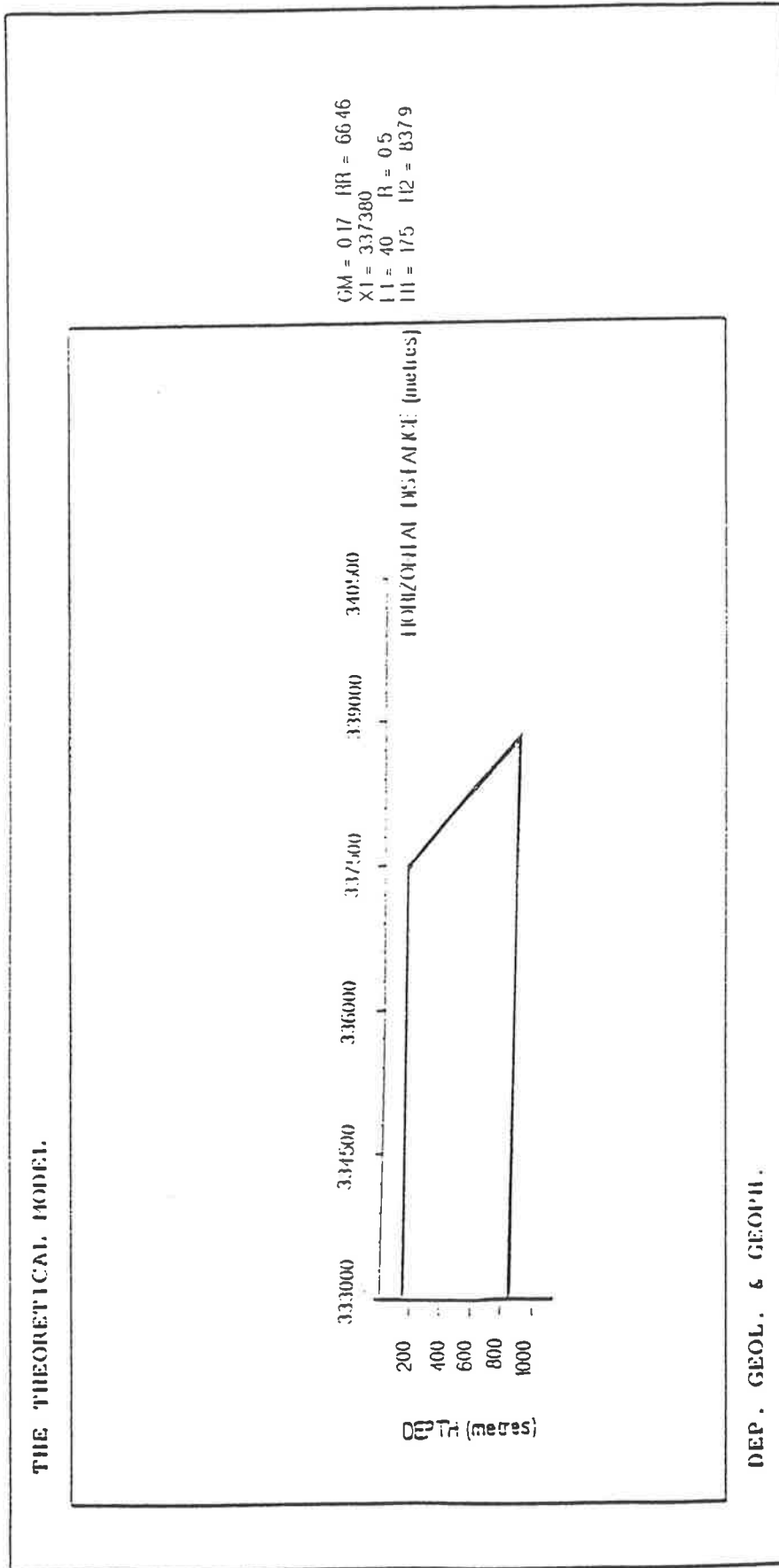


Figure 5.16: The theoretical model for line no. 11.

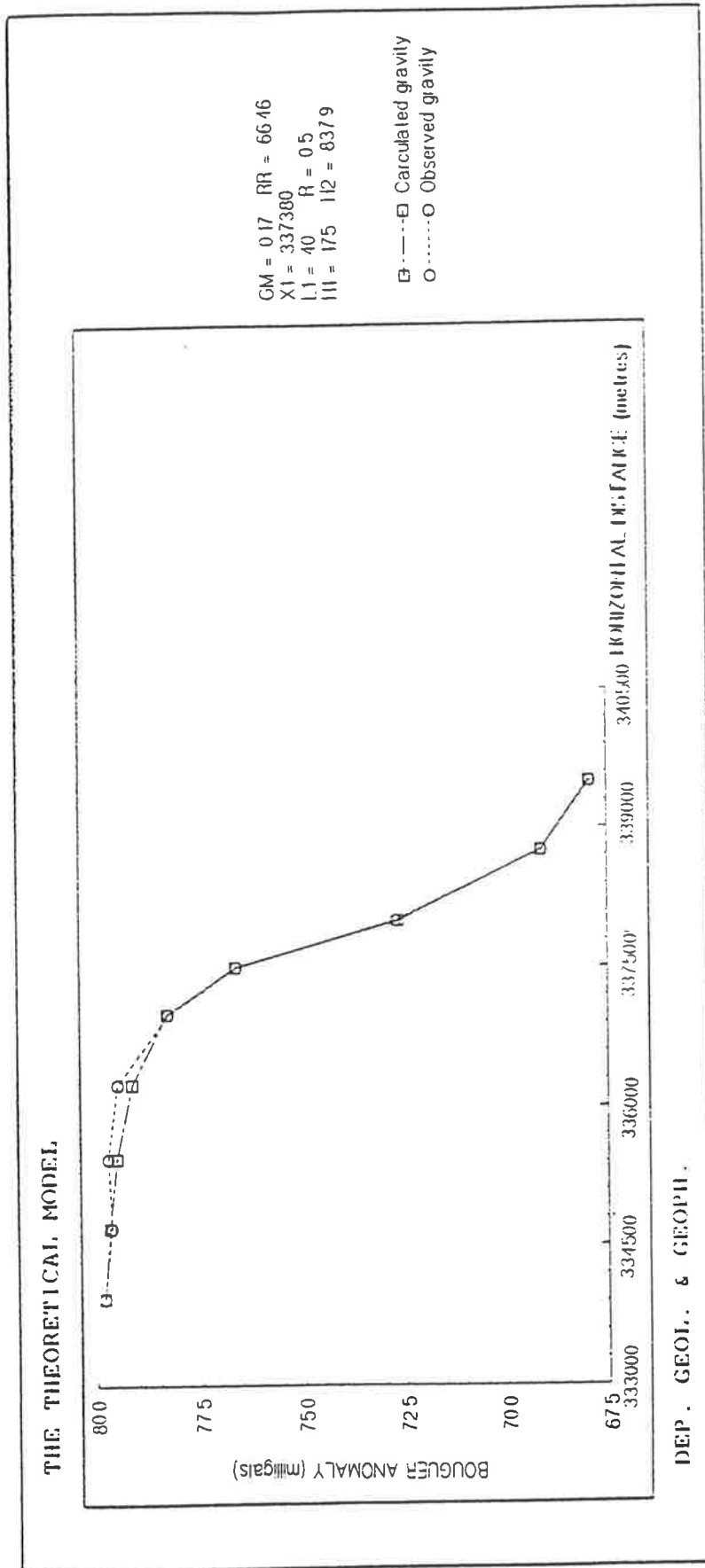


Figure 5.17: Observed and calculated gravity for line no. 11.

Figure 5.15 is another example where the Bouguer anomaly demonstrates the next geological structure with faulting. From this graph, it might be assumed that there is a structure with one fault.

Figure 5.16 shows the theoretical model for the same area and gives the closest gravity effect to the observed gravity from the map. This is the normal fault with angle of  $40^\circ$  and the down throw about 700m to the east. The top of the fault is at a depth of 200m. Because this line is so short the model matching is not satisfactory.

## 5.6 Commentaries

Preparation of the Bouguer anomaly map for this part of South Australia has been very difficult and time consuming task, because much of the information on the magnetic tape was incorrect. There was an incorrect listing of the many station positions from the gravity survey. These gravity values were produced by incorrect reading from the survey instruments or by a wrong entry on to magnetic tape. The anomaly ( line 3, figure 5.11 and figure 5.13 ) where the cross-section gives the picture of one fault and the identical gravity effect appears to be given by two faults with a small distance between each other, is most likely caused by inaccurate surveying. For one line, the survey has been done at a different time in comparison with another for the second line and has used different gravity meters and the different instrument constant may not have been properly compared.

Experience with use of the method using data from the Para Faults in Adelaide and from other areas showed the importance of having very closely spaced stations and exact information about the position of the faults in obtaining a more exact solution. If this sort of information had been available for the Paralana Faults, a more reliable solution of the dip of the faults could have been obtained. As no detailed information of this kind was available for the Frome Embayment, no further work was done it would have required field work which was outside the scope of this research.

## Chapter 6

### Conclusions

The method developed in this thesis to interpret gravity data over a step fault uses the simple formula for an infinite fault and matches the calculated anomaly due to the model with the observed data.

The method has been tested with ideal data in which there is no noise, ideal data to which noise has been added and with real data.

The procedures to obtain results are simple so that they can be learned and applied quickly and easily.

The accuracy of the interpretation obtained from this program depends on a number of factors the significance of which must be understood by the interpreter to obtain reliable results; this is true with all methods used in the interpretation of geophysical surveys. These factors are:

- quality of data
- control provided by additional data

The quality of gravity data covers the accuracy with which the observations have been made, the accuracy with which the position of the observation points have been observed, this includes the eastings and northings as well as the elevations, and the care with which corrections have been made in processing the data. The quality of the gravity data also includes the spacing between the station

and the length of the traverse lines; it is important that the anomaly should be adequately sampled in those parts of the anomaly where the field changes rapidly, it is also important that the background values are reasonably well defined by having readings made some considerable distance from the position of the faults.

While ideally the information about the quality of the data should be contained within the number of the data set, in practice, information about the quality of the data is often partly based on knowledge of the organisation who carried out the work, the type of equipment used and the history of the collection of the data.

The accuracy of the interpretation depends to some extent on what additional information is available. In the problem considered there are seven unknowns; the position of the two faults; the dip of the two faults and the depths of the horizontal interface at the top of the fault, at the step and at the base of the fault. If some of these values are known, it may be possible to obtain results where it would not have been possible otherwise. For example, if the position of the faults is known at the surface from geological mapping, it is then possible to obtain a more accurate estimate of the dips of the faults. Additional information may come from field geological observation and drilling which provide information about the position of the boundaries and the density contrast between the rocks involved; from magnetic surveys which may delineate precisely the position of the edge of the basement rocks if they are magnetic and from seismic surveys, which locate the position of the main faults at depth but may not clearly distinguish the basement from the sediments.

A further matter which must always be considered in interpretation is the basic assumption usually made about the uniformity of the densities of the rocks involved. This assumption may not be justified. It is known that the density and thickness of the soil and weathered rocks may vary appreciable and this may be a significant source of noise and cause of error.

It is known that the density of sedimentary rocks usually increases with depth due to compaction and it is also possible the density of sediments in the basin may vary laterally due to facies changes close to an active fault. There are also many cases where there are large high density or low density bodies within the basement rocks and these too can have a serious effect on the accuracy of the interpretation.



These matters, however are not within the scope of this thesis.

To be useful this method should be applied to the type of problem it was designed to solve, the examination of the faulted edge of a sedimentary basin.

Initially, the method was designed to examine faults at the edge of the Eromanga Basin but it was found that there was no geological information with which to check the accuracy of the use of the method; it was also discovered that the gravity data was limited on the western side of the Paralana Fault which made it difficult to interpret the data.

The method was found to be much effective for faults which were on the edge of smaller Telford, Adelaide and Wilunga sedimentary basins; it can be used with similar basins in South Australia and elsewhere.

The method has also been applied to gravity data over faults in basins in South Eastern Australia, where the position of the faults and total basement depth were defined by seismic surveys but where the depth of the basement on the upthrow side of the faults was uncertain.

The method has also been applied to the Darling Fault in Western Australia and to the Rift Valley Faults in East Africa but here the positions of the faults are not known with enough precision to test the method.

The method can be used with more complex systems of faults provided the faults are well separated but application becomes more difficult.

The only even moderately satisfactory place in which the method could be tested using real data was over the Para Fault west of Adelaide City, where holes drilled as part of an engineering geology study provided the most precise evidence of the position and throws of faults. Even here the information about the faults was just enough to test the accuracy of the gravity interpretation method.

The program used in this research was written for a VAX main frame computer and the diagrams produced on a ZETA-plotter as these were the facilities available when the research started (1985). These programs could be rewritten and run on a modern fast personal computer.

The program which are written for normal, vertical and reverse of infinite strike extent could be extended to include cases where the faults have a limited strike extent, where the basement is not

horizontal and allowance could be made for more than two faults although there is a limit to the complexity of the structures that can be dealt with.

The speed with which results can be obtained using this method is increased if the interpretation is done in stages. This involves selecting relatively large step sizes for an initial interpretation and then repeating the procedures using a small step size.

To get the best results from using the method the following points should be observed:

- the anomaly should be well sampled with a high density of stations in the parts of the curve where gravity changes rapidly and adequate information about the regional background
- care should go into obtaining the best possible estimates of the position and depth of the faults and boundaries
- the contrast in density between the rock groups and the variations of the density within the rock groups should be established from drill holes surface samples and by any other appropriate methods.

# Appendix A

## Mathematical Formula for Simple Shapes

### A.1 Fundamental Theory

This section has been taken with minor modification from "Applied Geophysics" by W.Telford, L.Geldart, R.Sheriff and D.Keys.

#### A.1.1 Force of Gravitation

The expression for the force of gravitation is given by Newton's law which is the basis for gravity work. This law states that the force between two particles of mass  $m_1$  and  $m_2$  is directly proportional to the product of the masses and inversely proportional to the square of the distance between the centres of mass. This force is given by the equation

$$F = -\gamma \frac{m_1 m_2}{r^2} r_1 \quad (\text{A.1})$$

where  $F$  is the force on  $m_2$ ,  $r_1$  is a unit vector directed from  $m_1$  towards  $m_2$ ,  $r$  is the distance between  $m_1$  and  $m_2$  and  $\gamma$  is the universal gravitational constant.

The minus sign arises because the force is always attractive.  $F$  is in dynes,  $m_1$  and  $m_2$  in grams,  $r$  in centimetres. The value of  $\gamma$  is then  $6.67 \times 10^{-8}$  which is equal to the force in dynes between two small uniform spheres, each of mass 1g, placed so that the centres are 1cm apart.

Obviously the gravitational force is one of so-called weak forces existing in nature. recently it has been suggested that the quantity  $\gamma$  is not constant, but is decreasing slowly with time.

There are many possible consequences of such a variation, one of which would be an increase in the earth radius with time. This in turn would have a profound effect on the geophysical history of the earth. However, the postulated rate of change of  $\gamma$ , if it exists at all, is so small (about 1% in the earth's life time of several billion years) that it has no significance whatever in gravity prospecting.

## A.1.2 Acceleration of Gravity

The acceleration of  $m_2$  due to the presence of  $m_1$  can be found by dividing  $F$  by  $m_2$ . In particular, if  $m_1$  is the mass of the earth  $M_e$  the acceleration of the mass  $m_2$  at the surface of the earth is

$$g = \frac{F}{m_2} = -\gamma \frac{M_e}{R_e^2} r_1 \quad (\text{A.2})$$

$R_e$  is the radius of the earth and  $r_1$  extending outward from the centre of the earth along the radius. This acceleration, which is called acceleration of gravity was first measured by Gallileo . The value at the earth surface is about  $980 \text{ cm/sec}^2$ . (  $1 \text{ cm/sec}^2$  is called the gal.)

Modern gravity meters which measured extremely small variations in this acceleration, have a sensitivity of about  $10^{-5}$  gals. As a result they are capable of distinguishing changes in the absolute value of  $g$  with a precision of one part in  $10^8$  .

## A.1.3 Gravitational Potential

Gravitational fields are conservative, that is to say, the work done moving a mass in a gravitational

field is independent of the path traversed and depends only on the end points. In fact if the mass is eventually returned to its original position the net energy expenditure is zero, regardless of the path followed. Another way of expressing this is to say that the sum of kinetic and potential energy is constant within a closed system. The gravitational force is a vector whose direction is along the line joining the centres of the two masses. The force giving rise to a conservative field may be derived from a scalar potential function:

$$\nabla U(r) = F(r)/m_2 = g(r) \tag{A.3}$$

Alternatively we can solve this equation for the gravity potential in the form

$$U(r) = \int_{\infty}^R g \cdot dr = -\gamma M \int_{\infty}^R \frac{dr}{r^2} = \gamma \frac{M}{R} \tag{A.4}$$

which is a statement of the work done in moving unit mass from a very distant point (mathematically from infinity) by any path at all to a point distant R from the centre of gravity of M.

It is often simpler to solve gravity problems by calculating scalar potential U, rather than the vector g. It is then relatively easy to obtain g from eq. (A.3).

### A.1.4 Three-Dimensional Potential

Considering a three-dimensional mass of arbitrary shape, the potential and the acceleration of gravity at a point some distance away can be calculated by dividing the mass into small elements and integrating to get the total effect. Clearly it is easier to use the potential if the problem can be solved at all.

The potential due to an element of mass dm at a distance r from P is

$$dU = \gamma dm/r = \gamma \sigma dx dy dz/r \tag{A.5}$$

where  $\sigma$  is the density and  $r^2 = x^2 + y^2 + z^2$ .

Then the potential of the total mass m will be

$$U = \gamma\sigma \int_x \int_y \int_z \frac{1}{r} dx dy dz \quad (\text{A.6})$$

### A.1.5 Two Dimensional Potential

If the mass is very long in the gamma direction and has a uniform cross-section of arbitrary shape in the xz-plane, the gravity attraction derives from a logarithmic rather than Newtonian potential. Then becomes

$$U = \gamma\sigma \int_x \int_z dx dz \int_{-\infty}^{+\infty} \frac{dy}{r} \quad (\text{A.7})$$

In order to keep the last integral finite, we replace the limits of  $\pm\infty$  by  $\pm L$ , where L is finite. Later we shall let L approach infinity.

Then writing  $U_L$  for the value of this integral we have

$$U_L = \int_{-L}^L \frac{dy}{r} = \int_{-L}^L \frac{dy}{\sqrt{(x^2+z^2+y^2)}} = \int_{-L}^L \frac{dy}{\sqrt{(a^2+y^2)}} \quad (\text{A.8})$$

where  $a^2 = x^2 + z^2$ . And

$$U_L = \log \left\{ \frac{L + \sqrt{(L^2+a^2)}}{-L + \sqrt{(L^2+a^2)}} \right\} \quad (\text{A.9})$$

Now we change the potential of the two-dimensional cross-section by subtracting a constant, say the potential  $a^2 = 1$ . This is necessary to maintain  $U_L$  finite.

The expression is then modified to

$$\begin{aligned}
 U_L &= \log \left\{ \frac{L + \sqrt{(L^2+a^2)}}{-L + \sqrt{(L^2+a^2)}} \right\} - \log \left\{ \frac{L + \sqrt{(L^2+1)}}{-L + \sqrt{(L^2+1)}} \right\} \\
 &= \log \left[ \left\{ \frac{L + \sqrt{(L^2+a^2)}}{-L + \sqrt{(L^2+a^2)}} \right\} \left\{ \frac{-L + \sqrt{(L^2+1)}}{L + \sqrt{(L^2+1)}} \right\} \right] \\
 &\approx \log \left[ \left\{ \frac{1 + (1 + a^2/2L^2)}{a^2/2L^2} \right\} \left\{ \frac{1/2L^2}{2 + 1/2L^2} \right\} \right]
 \end{aligned} \tag{A.10}$$

(since  $L \gg a$ )

Now we allow  $L$  to go to infinity and obtain

$$U_L = \log \frac{2}{a^2} \times \frac{1}{2} = -\log(x^2+z^2) = -2 \log r \tag{A.11}$$

where now  $r^2 = x^2 + z^2$

The resulting logarithmic potential expression becomes

$$U = 2\gamma\sigma \int_x \int_z \log\left(\frac{1}{r}\right) dx dz \tag{A.12}$$

The gravity effect for the two-dimensional body is

$$g_z = \frac{\partial U}{\partial z} = -2\gamma\sigma \int_x \int_z \frac{z}{r^2} dx dz \tag{A.13}$$

We have assumed the density to be constant throughout the volume. This is not generally the situation in the field. If density is a function of the coordinates, the potential can be calculated only for a few simple shapes.

## A.2 Gravity Effects of Simple Two-dimensional Bodies

### A.2.1 Thin Dipping Sheet

In general, a body can be considered two-dimensional when its strike length is about twenty times all the other dimensions, including the depth below the surface, and the cross-section is the same at all

points along the strike. Considering the gravity effect of a thin sheet of infinite strike length, we have the following geometrical relations:

$$\begin{aligned}
 p &= (x-h \cot\alpha)\sin\alpha = x \sin\alpha - h \cos\alpha \\
 r_1 &= \sqrt{x^2 + h^2} \\
 z &= r \sin\left(\alpha + \theta - \frac{\pi}{2}\right) = p(\sin\alpha \tan\theta - \cos\alpha) \\
 r &= p \sec\theta \\
 dz &= p \sin\alpha \sec^2\theta d\theta \\
 r_2 &= \sqrt{(x + \delta \cos\alpha)^2 + (h + \delta \sin\alpha)^2} \\
 dx &= \text{cosec}\alpha d\tau \\
 \tan\theta_1 &= \sqrt{(r_1^2 - p^2)} / p = (x \cos\alpha + h \sin\alpha) / p \\
 \tan\theta_2 &= \sqrt{(r_2^2 - p^2)} / p = (x \cos\alpha + \delta + h \sin\alpha) / p
 \end{aligned}$$

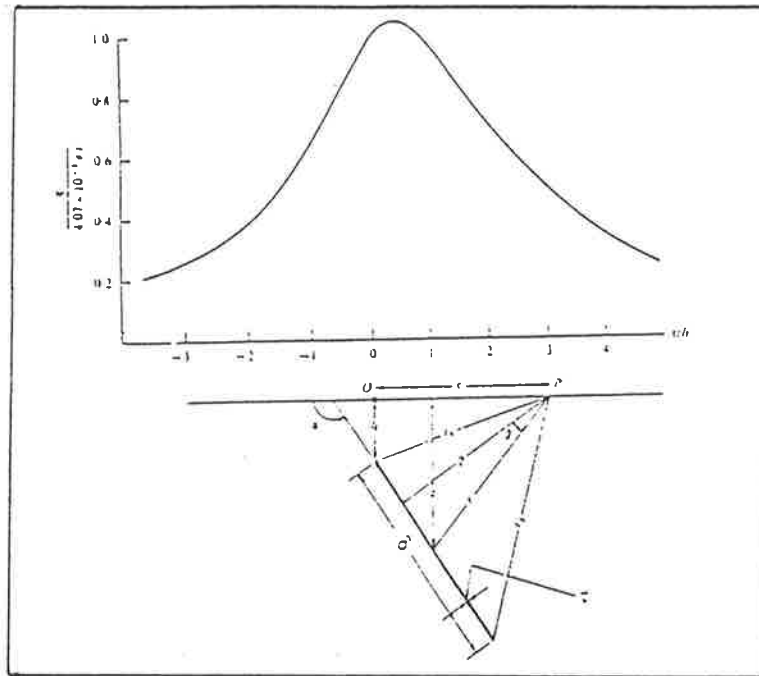


Figure A.1: Gravity effect of a thin sheet of infinite strike length.

For a two dimensional structure we get

$$\begin{aligned}
 g &= 2\gamma\sigma \int_x \int_z \frac{z}{r^2} dx dz \\
 &= 2\gamma\sigma \int_x \int_0^{\theta_2} \frac{(\sin\alpha \tan\theta - \cos\alpha)\text{cosec}\alpha \sin\alpha \sec^2\theta}{\sec^2\theta} d\tau d\theta \\
 &= 2\gamma\sigma \int_{\theta_1}^{\theta_2} (\sin\alpha \tan\theta - \cos\alpha) d\theta \\
 &= 2\gamma\sigma \left[ \sin\alpha \log \sec\theta - \theta \cos\alpha \right]_{\theta_1}^{\theta_2}
 \end{aligned} \tag{A.14}$$



Inserting the appropriate values of  $\theta_1$  and  $\theta_2$  this becomes

$$g = 2\gamma\sigma\tau \left[ \frac{1}{2} \sin\alpha \log \left\{ \frac{(h + \delta\sin\alpha)^2 + (x + \delta\cos\alpha)^2}{(x^2 + h^2)} \right\} - \cos\alpha \left\{ \tan^{-1} \left( \frac{h \sin\alpha + \delta + x \cos\alpha}{x \sin\alpha - h \cos\alpha} \right) - \tan^{-1} \left( \frac{h \sin\alpha + x \cos\alpha}{x \sin\alpha - h \cos\alpha} \right) \right\} \right] \quad (\text{A.15})$$

When the sheet lies horizontal we have

$$g = 2 \times 6.67E-6 \times 1000 \sigma \tau \left\{ \tan^{-1} \left( \frac{\delta - x}{h} \right) + \tan^{-1} \left( \frac{x}{h} \right) \right\} \quad (\text{A.16})$$

### A.2.2 Thick Prism

The thin sheet approximation breaks down when the depth to the top is small compared to the sheet thickness, for such bodies we must consider a true prism shape. The geometry is illustrated below

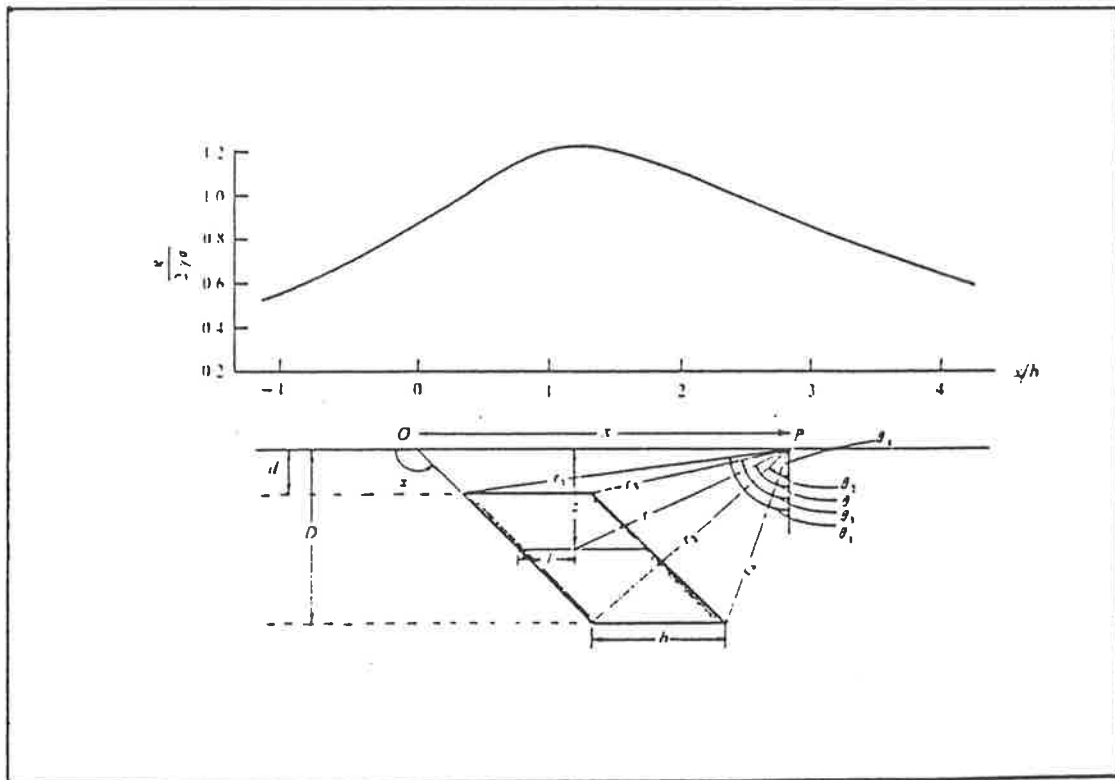


Figure A.2: Gravity effect of thick prism of infinite strike length.

We can use an expression similar to eq. (A.15) for the horizontal thin sheet at depth  $z$ , provided the origin 0 in figure A.2 is moved to point 0 in figure A.3, the width in figure A.2 is changed to  $b$ , and  $h$  and  $t$  are replaced by  $z$  and  $dz$ . So

$$\delta g = 2\gamma\sigma dz \left\{ \cot^{-1}\left(\frac{x - b + z \cot\alpha}{z}\right) - \cot^{-1}\left(\frac{x + z \cot\alpha}{z}\right) \right\} \quad (\text{A.17})$$

The gravity for the complete prism is given by

$$g = 2\gamma\sigma \int_d^D \left\{ \cot^{-1}\left(\frac{x - b + z \cot\alpha}{z}\right) - \cot^{-1}\left(\frac{x + z \cot\alpha}{z}\right) \right\} dz \quad (\text{A.18})$$

The integration can be carried out by making a change of variable and integrating by parts.

The result is

$$\begin{aligned} g = 2\gamma\sigma & \left[ \frac{1}{2}x \sin^2\alpha \log \left\{ \frac{D^2 + (x + D \cot\alpha)^2}{D^2 + (x - b + D \cot\alpha)^2} \times \frac{d^2 + (x - b + d \cot\alpha)^2}{d^2 + (x + d \cot\alpha)^2} \right\} \right. \\ & + \frac{1}{2}b \sin^2\alpha \times \log \left\{ \frac{D^2 + (x - b + D \cot\alpha)^2}{d^2 + (x - b + d \cot\alpha)^2} \right\} \\ & - x \sin\alpha \cos\alpha \left\{ \tan^{-1}\left(\frac{x - b}{D} + \cot\alpha\right) - \tan^{-1}\left(\frac{x}{D} + \cot\alpha\right) - \tan^{-1}\left(\frac{x - b}{d} + \cot\alpha\right) + \tan^{-1}\left(\frac{x}{d} + \cot\alpha\right) \right\} \\ & + b \sin\alpha \cos\alpha \left\{ \tan^{-1}\left(\frac{x - b}{D} + \cot\alpha\right) - \tan^{-1}\left(\frac{x - b}{d} + \cot\alpha\right) \right\} \\ & \left. - D \left\{ \tan^{-1}\left(\frac{x - b}{D} + \cot\alpha\right) - \tan^{-1}\left(\frac{x}{D} + \cot\alpha\right) \right\} - d \left\{ \tan^{-1}\left(\frac{x - b}{d} + \cot\alpha\right) - \tan^{-1}\left(\frac{x}{d} + \cot\alpha\right) \right\} \right] \end{aligned} \quad (\text{A.19})$$

By using the following relations

$$\begin{aligned} r_1 &= \sqrt{d^2 + (x + d \cot\alpha)^2} \\ r_2 &= \sqrt{D^2 + (x + D \cot\alpha)^2} \\ r_3 &= \sqrt{d^2 + (x - b + d \cot\alpha)^2} \\ r_4 &= \sqrt{D^2 + (x - b + D \cot\alpha)^2} \\ \tan\theta_1 &= (x + d \cot\alpha)/d \\ \tan\theta_2 &= (x + D \cot\alpha)/D \\ \tan\theta_3 &= (x - b + d \cot\alpha)/d \\ \tan\theta_4 &= (x - b + D \cot\alpha)/D \end{aligned}$$

the expression can be simplified to give

$$\begin{aligned}
 g = 2\gamma\sigma [ & \sin^2\alpha \{ x \log \frac{(r_2 r_3)}{(r_1 r_4)} + b \log \frac{r_4}{r_3} \} \\
 & - \sin\alpha \cos\alpha \{ x (\theta_4 - \theta_3 - \theta_2 - \theta_1) - b (\theta_4 - \theta_3) \} \\
 & - D (\theta_4 - \theta_2) + d (\theta_3 - \theta_1) ] \quad (A.20)
 \end{aligned}$$

In the metric system when  $g$  is named in milligal ( 1 gal = 1 cm/sec<sup>2</sup> ) the constant  $2\gamma$  is numerically equal to  $(0.04191/3.14154 = 2 * 6.67 * 10^{-6} * 1000)$  with distance  $x$  named in metres.

In the imperial system where distance  $x$  is named in feet the constant  $2\gamma$  is equal  $4.07*10^{-3}$ .

### A.2.3 Semi-Infinite Horizontal Slab

If the width  $b$ , of the prism is very great,

$$r_3 \approx r_4 \approx \infty \qquad \theta_3 \approx \theta_4 \approx -\pi/2$$

the equation (A.20) now becomes

$$\begin{aligned}
 g = 2 \times 6.67E-6 \times 1000 \sigma \{ & x \sin^2\alpha \log \frac{r_2}{r_1} + x (\theta_2 - \theta_1) \sin\alpha \cos\alpha \\
 & + D (\frac{\pi}{2} + \theta_2) - d (\frac{\pi}{2} + \theta_1) \} \quad (A.21)
 \end{aligned}$$

If, in addition,  $\alpha = 90^\circ$ , this can be written

$$g = 2 \times 6.67E-6 \times 1000 \sigma [ \frac{x}{2} \log \frac{D^2 + x^2}{d^2 + x^2} + D \{ \frac{\pi}{2} + \tan^{-1} (\frac{x}{D}) \} - d \{ \frac{\pi}{2} + \tan^{-1} (\frac{x}{d}) \} ] \quad (A.22)$$

If the slab outcrops,

$$d = 0 \qquad r_1 = x \qquad \theta_1 = \pi/2$$

and equation (A.21) becomes

$$g = 2 \times 6.67E-6 \times 1000 \sigma \left[ \frac{x}{2} \sin^2 \alpha \log \left\{ \frac{D^2 + (x + D \cot \alpha)^2}{x^2} \right\} \right. \\ \left. - x \sin \alpha \cos \alpha \left\{ \frac{\pi}{2} - \tan^{-1} \left( \frac{x}{D} + \cot \alpha \right) \right\} + D \left\{ \frac{\pi}{2} + \tan^{-1} \left( \frac{x}{D} + \cot \alpha \right) \right\} \right] \quad (\text{A.23})$$

If  $\alpha = 90^\circ$  the equation is further simplified to

$$g = 2 \times 6.67E-6 \times 1000 \sigma \left[ \frac{x}{2} \log \left( \frac{D^2 + x^2}{x^2} \right) + D \left\{ \frac{\pi}{2} + \tan^{-1} \left( \frac{x}{D} \right) \right\} \right] \quad (\text{A.24})$$

When thick structures are not truly two-dimensional, the formula can be modified exactly as for the thin sheet. Also, it is possible to calculate values of depth and thickness. For example, from (A.22) we have

$$\Delta g_{\max} = g_{+} - g_{-} = 2 \times 6.67E-6 \times 1000 \sigma \pi (D - d) \\ \left( \frac{dg}{dx} \right)_{x=0} = 2 \times 6.67E-6 \times 1000 \sigma \log (D/d) \quad (\text{A.25})$$

From these relations we obtain the following:

$$\sigma (D - d) = \frac{\Delta g_{\max}}{2 \times 20.94E-6 \times 1000} \\ \log (D/d) = \frac{1}{2 \times 6.67E-6 \times 1000 \sigma} \left( \frac{dg}{dx} \right)_{x=0} \quad (\text{A.26})$$

By assuming a value for  $\sigma$ , we can solve D and d.

# Appendix B

## Computer Programs

### B.1 FAULT\_STRUCTURE Program

```
c      PROGRAM FAULT_STRUCTURE.FOR
C      this program looks for the best parameters for two faults,
c      compares the calculated gravity with observed gravity.
C      THIS PROGRAM GIVES H1,H2,R,TK,X=0 AND GRAVITY EFFECT
C      FOR THE FAULT.
c
      IMPLICIT DOUBLE PRECISION (A-H,O-Z)
      INTEGER IE1, IE2, IB1, IB2
c
      COMMON H1, H2, R, TK, X, GC1
      common /FAULT/ M, S1, s2, s3, d1, d2, e1, e2, b1, b2, AA, XF1, XF2,
+         TK1, TK2, GM, H3, RM, RM1
      COMMON /MAXIM/ GGMAX, Z, NUM, X2, X4, H0, K
c
      dimension t(3,200),gcm(200),gc2(200),gc3(200),ad(4,200),
+         GGMAX(10,10)
      INTEGER NUM
c
      CHARACTER*(*) MES1,MES2,MES3,MES4,MES5,MES6,MES15,
+         MES9,mes10,mes11,mes12,MES13,MES14
      PARAMETER (MES2='THE THEORETICAL MODEL          ')
      PARAMETER (MES1='DEP. GEOL. & GEOPH.')
      PARAMETER (MES3='DEPTH')
      PARAMETER (MES4='Easting (metres)')
      PARAMETER (MES5='Bouguer anomaly (milligals)')
      PARAMETER (MES10='Bouguer anomaly - observed')
      PARAMETER (MES11='Bouguer anomaly - calculated')
      PARAMETER (MES6='X1=          X2=')
      PARAMETER (MES9='L1=          R=          L2=')
      PARAMETER (MES15='H1=          H2=          H3=')
```

```

parameter (mes12='GM=      RR=')
parameter (mes13='Horiz. gravity gradient ')
PARAMETER (MES14='(metres)')

C
C
C
C
M=how many lines has the file bb3.dat
C
d2 = step of the depth for the y-lower axis
C
d1 max. of depth
C
DATA d1,d2/1200.0,50.0/

C
OPEN (UNIT=11,FILE='PLOT1.PLT',STATUS='NEW',
+     CARRIAGECONTROL='LIST')
CALL PLOTS (53,0,11)

C
C----- read data from the terminal
C
WRITE(6,*) 'THE MODEL FOR ONE OR TWO FAULTS ? '
WRITE(6,*) ' ONE FAULT  --> 1'
WRITE(6,*) ' TWO FAULTS --> 2'
READ(6,*) NUMFAULT
WRITE(6,*) ' '
WRITE(6,*) ' '
write(6,*) 'THE INITIAL DATA FOR FIRST FAULT'
WRITE(6,*) ' '
WRITE(6,*) '     EASTING '
WRITE(6,*) 'minimum value: '
READ(6,*) X1
WRITE(6,*) 'maximum value: '
READ(6,*) X3
IF ( X1 .EQ. X3 ) GOTO 1
WRITE(6,*) 'step for easting: '
read(6,*) xS
1 CONTINUE
write(6,*) ' '
WRITE(6,*) '     DEPTH '
WRITE(6,*) 'minimum value: '
READ(6,*) H11
WRITE(6,*) 'maximum value: '
READ(6,*) H12
IF ( H11 .EQ. H12 ) GOTO 2
WRITE(6,*) 'step for depth: '
read(6,*) H1S
2 CONTINUE
write(6,*) ' '
WRITE(6,*) '     ANGLE '
WRITE(6,*) 'minimum value: '
READ(6,*) TK11
WRITE(6,*) 'maximum value: '
READ(6,*) TK12
IF ( TK11 .EQ. TK12 ) GOTO 3
WRITE(6,*) 'step for angle: '
read(6,*) TKS
3 CONTINUE
C
if(numfault.eq.1)goto 5
WRITE(6,*) ' '
WRITE(6,*) ' '
write(6,*) 'THE INITIAL DATA FOR SECOND FAULT'
WRITE(6,*) ' '
WRITE(6,*) '     EASTING '
WRITE(6,*) 'minimum value: '
READ(6,*) X41
WRITE(6,*) 'maximum value: '
READ(6,*) X42
write(6,*) ' '

```

```

WRITE(6,*) '      ANGLE      '
WRITE(6,*) 'minimum value: '
READ(6,*) TK21
WRITE(6,*) 'maximum value: '
READ(6,*) TK22
5  continue
write(6,*) '      '
WRITE(6,*) '      DENSITY CONTRAST      '
WRITE(6,*) 'minimum value: '
READ(6,*) R11
WRITE(6,*) 'maximum value: '
READ(6,*) R12
IF ( R11 .EQ. R12 ) GOTO 7
WRITE(6,*) 'step for density contrast: '
read(6,*) RS
7  continue
data gr,pi/6.67e-6,3.14159/
WRITE(6,*) 'step for Gmax: '
read(6,*) d3
c   data d3/2.0/
c
c----- data for the plots
c
c   S3 = axis X ; S1= axis Y-upper ; s2=axis y-lower
c
c   data s1,s2,s3/17.0,5.0,20.0/
c
c   D=H1S
c   if (numfault.eq.1) d=100000
c   open (unit=2,file='OUT_INF.dat',status='new')
c   open (unit=3,file='OUT_GR.dat',status='new')
c   open (unit=1,file='obs_grav.DAT',status='old')
c
c----- reading data from file OBS_GRAV.DAT
c   T(1,J) --> easting value, T(2,J) --> bouguer anomaly
c
c   do 10 j=1,200
c   read (1,FMT=*,END=11) (T(I,j),I=1,2)
c   M=M+1
10  CONTINUE
11  CONTINUE
c   aa=1
c   if (t(2,1).gt.t(2,m))aa=-1
c
c
c   ib2=t(2,1)
c   if (aa .eq. -1) ib2=t(2,m)
c   b2=ib2 - 1
c   if (ib2 .le. 0) b2=ib2-1
c   ib1=t(2,m)
c   if (aa .eq. -1) ib1=t(2,1)
c   b1=ib1+1
c   if (ib1 .le. 0) b1=ib1-1
c
c
c   iel=t(1,1)
c   e2=iel
c   ie2=t(1,m)
c   e1=ie2
c   if(aa.eq.-1) then
c     b1=ib2
c     b2=ib1
c   endif
c
c
c   eps=0.0001

```

```

x2=x1
gm=100000000.0
DO 20 J1=1,10000
R=r11
do 30 j=1,10000
IF ((r-r12).gt.eps) GOTO 34
H0=h11
do 40 i=1,10000
a1=pi*gr*r*2000
gmax=abs(t(2,1)-t(2,m))
do 50 k=1,7
h4=gmax/a1+h0
TK1=tk11
do 60 l=1,10000
Z=0.0
h3=h0
do 70 il=1,1000000
if(il.eq.1)goto 91
tk2=tk21
do 80 i2=1,1000000
x4=x41
do 90 i3=1,1000000
z=0.0
91 if(il.eq.1) THEN
GOTO 92
ELSE
GOTO 93
ENDIF
92 tk=tk1
x=(t(1,1)-x2)*aa
h1=h0
h2=h4
94 if(abs(tk-90.0).le.eps) goto 95
if(abs(H1-0.0).le.eps) goto 941
CALL gravity_1
GOTO 942
941 Call gravity_out1
942 if (ww) 99,96,100
96 rr=t(2,1)-gcl
goto 97
95 if(abs(h1-0.0).le.eps) goto951
call gravity_0
goto 952
951 call gravity_out0
952 if (ww) 99,98,100
98 rr=t(2,1)-gcl
goto 97
93 h1=h3
h2=h4
x=(t(1,1)-x4)*aa
tk=tk2
ww=-1
goto 94
99 rr=t(2,1)-gcl
tk=tk1
h1=h0
h2=h3
x=(t(1,1)-x2)*aa
ww=1
100 goto 94
97 rr=rr-gcl
do 110 n=1,m
if (il.eq.1) THEN
GOTO 111
ELSE
GOTO 112

```



```

111          ENDIF
            h1=h0
            h2=h4
            tk=tk1
            x=(t(1,n)-x2)*aa
            if(abs(tk-90.) .le. eps) goto 113
            if(abs(H1-0.) .le. eps) goto 1111
            CALL gravity_1
            GOTO 1112
1111         call gravity_out1
1112         goto 114
113         if (abs(h1-0.0) .le. eps) goto 1131
            call gravity_0
            goto 114
1131         call gravity_out0
114         gc2(n)=gc1
            gc3(n)=0.
            goto 115
112         h2=h3
            h1=h0
            X=(T(1,N)-X2)*aa
            tk=tk1
            ss=-1
            if(abs(tk-90.) .le. eps) goto 116
            if(abs(H1-0.) .le. eps) goto 1121
            CALL gravity_1
            GOTO 1122
1121         call gravity_out1
1122         goto 117
116         if(abs(h1-0.0) .le. eps) goto 1161
            call gravity_0
            goto 117
1161         call gravity_out0
117         gc2(n)=gc1
            h1=h3
            x=(t(1,n)-x4)*aa
            h2=h4
            tk=tk2
            if(abs(tk-90.) .le. eps) goto 118
            if(abs(H1-0.) .le. eps) goto 1171
            CALL gravity_1
            GOTO 1172
1171         call gravity_out1
1172         GOTO 119
118         if(abs(h1-0.0) .le. eps) goto 1181
            call gravity_0
            goto 119
1181         call gravity_out0
119         gc3(n)=gc1
115         gc4=gc2(n)+gc3(n)+rr
            Z1=gc4-T(2,N)
            Z=Z+Z1*Z1
110         continue
            NUM=NUM+1
            CALL MAXGR
            if (z.gt.gm) goto 121
            rml=rr
            gm=Z
            h1m=h0
            h2m=h2
            h3m=h3
            rm=r
            Tk1m=Tk1
            tk2m=tk2
            X1M=X2
            x2m=x4

```





```

xf2=x2m
rr=rml
IF (LLL.EQ.0) S2=0.0
call plot (10.0,s2+3.0,-3)
CALL NEWPEN (1)
C the drawing of frames
CALL PLOT (-7.0,-s2-1.0,3)
CALL PLOT (-7.0,S1+0.5,2)
CALL PLOT (S3+10.0,S1+0.5,2)
CALL PLOT (S3+10.0,-s2-1.0,2)
CALL PLOT (-7.0,-s2-1.0,2)
c the drawing of frames
CALL PLOT (-9.0,-s2-3.0,3)
CALL PLOT (-9.0,S1+2.5,2)
CALL PLOT (S3+20.0,S1+2.5,2)
CALL PLOT (S3+20.0,-s2-3.0,2)
CALL PLOT (-9.0,-s2-3.0,2)
c the description of frames
CALL SYMBOL (-6.0,-s2-2.2,0.5,mes1,0.0,19)
CALL SYMBOL (-6.0,s1+1.3,0.5,mes2,0.0,32)
IF (LLL.EQ.1)GOTO 130
call newpen (2)
CALL SYMBOL (s3+11.0,5.1,0.1,5,0.0,-1)
call plot (s3+12.5,5.1,2)
call newpen(1)
CALL symbol (s3+13.0,5.0,0.2,mes11,0.0,28)
CALL symbol (s3+13.0,3.0,0.2,mes10,0.0,26)
CALL symbol (s3+13.0,1.0,0.2,mes13,0.0,26)
call newpen (4)
call symbol(s3+11.0,3.1,0.1,3,0.0,-1)
call plot (s3+12.5,3.1,2)
CALL NEWPEN (3)
CALL symbol (S3+11.,1.1,0.1,3,0.0,-1)
c CALL PLOT (S3+12.5,1.1,2)
call newpen (1)
CALL SYMBOL (S3+11.0,11.0,0.3,MES12,0.0,12)
call number (s3+11.9,11.0,0.3,gm,0.0,2)
call number (s3+14.6,11.0,0.3,rr,0.0,4)
CALL symbol (s3+11.0,10.0,0.3,mes6,0.0,15)
CALL number (s3+11.9,10.0,0.3,XF1,0.0,1)
CALL number (s3+15.5,10.0,0.3,XF2,0.0,1)
CALL symbol (s3+11.0,9.0,0.3,mes9,0.0,19)
CALL number (s3+11.9,9.0,0.3,tk1,0.0,1)
CALL number (s3+14.3,9.0,0.3,r,0.0,2)
CALL number (s3+16.7,9.0,0.3,tk2,0.0,1)
CALL symbol (s3+11.0,8.0,0.3,mes15,0.0,23)
CALL number (s3+11.9,8.0,0.3,h1,0.0,1)
CALL number (s3+14.9,8.0,0.3,H2,0.0,1)
CALL number (s3+17.9,8.0,0.3,H3,0.0,1)
130 CONTINUE
c the axis
call newpen (4)
c the axis x
22 call plot (0.0,0.0,3)
call plot (s3,0.0,2)
CALL SYMBOL (s3+0.5,-0.25,0.5,MES4,0.0,16)
d=e2
x=0.0
do 140 j=1,100
CALL number (X-0.1,-0.7,0.15,d,0.0,-1)
CALL SYMBOL (X,Y-0.25,0.5,13,0.0,-1)
if (x .eq. S3) goto 150
dxx=(e1-e2)/s3
d=d+dxx
x=x+1.0
140 continue

```

```

c      the axis y1-upper
150   call newpen (4)
      call plot (0.0,0.0,3)
      call plot (0.0,s1,2)
      b3=b2
      y=0.0
      do 160 j=1,100
      CALL NUMBER (-1.5,Y-0.075,0.15,b3,0.0,2)
      CALL SYMBOL (-0.5,Y,0.5,15,0.0,-1)
      if (y .eq. s1) goto 170
      dyy=abs(b2-b1)/s1
      b3=b3+dyy
      y=y+1.0
160   continue
170   continue
      CALL SYMBOL (-5.0,s1,0.5,MESS,270.0,28)
      call newpen(4)
c      the drawing of graph for the observed gravity
      ra=e1-e2
      r=s3/ra
      rb=abs(b1-b2)
      r1=s1/rb
      do 220 j=1,m
      x=(t(1,j)-e2)*r
      y=(t(2,j)-b2)*r1
      if(j.eq.1)goto 230
      call plot (x,y,2)
230   call symbol (x,y,0.1,3,0.0,-1)
      LLL=0
      if (LLL.eq.0)goto 220
      call number (x-0.3,y+0.3,0.15,t(2,j),0.0,2)
      call plot (x,y,3)
220   continue
      call newpen (2)
      IF (LLL.EQ.1) GOTO 240
c      the drawing of graph for the calculated gravity
      do 250 j=1,M
      x=(t(1,j)-e2)*r
      y=(t(3,j)-b2+rr)*r1
      if(j.eq.1) goto 251
      call plot (x,y,2)
251   call symbol (x,y,0.1,5,0.0,-1)
      if (LLL.eq.0)goto 250
      call number(x-0.3,y-0.3,0.15,t(1,j),0.0,2)
      call plot (x,y,3)
250   continue
c      the drawing of horiz. gravity gradient
      CALL NEWPEN (3)
      X=0.0
      tk=tk1
      wt=h1
      ws=h2
      h2=h3
      w3=h3
      if(tk.ne.90.)goto204
      call gradient_0
      goto 205
204   CALL gradient_1
205   y1=gcl
      tk=tk2
      h1=h3
      h2=ws
      x=xf2-xf1
      if(tk.ne.90.)goto206
      call gradient_0
      goto207

```

```

206      call gradient_1
207      y1=y1+gc1
          R2=0.5*s1/y1
          x=e1
          ra=e1-e2
          r=s3/ra
          DO 201 K=1,m
          x=(t(1,k)-xf1)*aa
          h1=wt
          h2=h3
          tk=tk1
          if(tk.ne.90.)goto208
          call gradient_0
          goto209
208      call gradient_1
209      continue      ! x2=x
          y2=gc1
          ad(1,k)=gc1
          x=(t(1,k)-xf2)*aa
          h1=h3
          h2=ws
          tk=tk2
          if(tk.ne.90.)goto213
          call gradient_0
          goto 211
213      call gradient_1
211      ad(2,k)=gc1
          ad(3,k)=ad(1,k)+ad(2,k)
          y2=y2+gc1
          x1=(t(1,k)-e2)*R
          y=y2*r2
          CALL SYMBOL (x1,ad(1,k)*r2,0.1,3,0.0,-1)
          CALL SYMBOL (x1,ad(2,k)*r2,0.1,3,0.0,-1)
          call newpen(1)
          CALL SYMBOL (x1,ad(3,k)*r2,0.1,5,0.0,-1)
          call newpen(3)
          ad(4,k)=x1
201      CONTINUE
202      continue
240      CALL PLOT (S2+21.0,0.0,999)
12      CLOSE (UNIT=1)
          CLOSE (UNIT=2)
          CLOSE (UNIT=3)
          CLOSE (UNIT=11)
          h1=wt
          h2=ws
          h3=w3
          s2=20.0
          call model
          STOP
          END

```

## B.2 Subroutine GRAVITY\_0

```
      SUBROUTINE GRAVITY_0
      implicit double precision (a-h,o-z)
C     THIS SUBR. CALCULATES GRAVITY EFFECT FOR FAULT;L=90.0, H1>0.0
      COMMON h1,h2,r,tk,x,gc1
      DATA gr/6.67e-6/
      v1=2*gr*r*1000
      p=3.14159
      t=tand(tk)
      x1=x*x
      h11=h1*h1
      h22=h2*h2
      r1=(h22+x1)/(h11+x1)
      b1=x/2*log(r1)
      f2=atan(x/h2)
      f1=atan(x/h1)
      b2=h2*(p/2+f2)
      b3=h1*(p/2+f1)
      gc1=v1*(b1+b2-b3)
      RETURN
      END
```

## B.3 Subroutine GRAVITY\_1

```

SUBROUTINE GRAVITY_1
implicit double precision (a-h,o-z)
calculates boug. anomaly for the fault; tk=90.0; h1>0.0
COMMON h1,h2,r,tk,x,gc1
DATA gr/6.67e-6/
v1=2*gr*r*1000
p=3.14159
t=tand(tk)
a1=h1/T
a2=h2/t
x1=x+a1
x2=x+a2
f1=atan(x1/h1)
f2=atan(x2/h2)
h11=h1*h1
x11=x1*x1
r1=sqrt(h11+x11)
h22=h2*h2
x22=x2*x2
r2=sqrt(h22+x22)
b1=h2*(p/2+f2)-h1*(p/2+f1)
s=sind(tk)
c=cosd(tk)
r1=r2/r1
rlo=log(r1)
s1=s*s
b2=x*s1*rlo
b3=x*(f2-f1)*s*c
gc1=v1*(b1+b2+b3)
RETURN
END
```



## B.4 Subroutine GRAVITY\_OUT0

```
      SUBROUTINE GRAVITY_OUT0
      implicit double precision (a-h,o-z)
      OBLICZA boug. anomaly dla fault
      THIS SUBR. CALCULATES GRAVITY EFFECT FOR FAULT;L=90.0 , H1=0.0
C
C
C      COMMON h1,h2,r,tk,x,gc1
C
      DATA gr/6.67e-6/
      v1=2*gr*r*1000
      p=3.14159
      x1=x*x
      h22=h2*h2
      r1=(h22+x1)/x1
      b1=x/2*log(r1)
      f2=atan(x/h2)
      b2=h2*(p/2+f2)
      gc1=v1*(b1+b2)
      RETURN
      END
```

## B.5 Subroutine GRAVITY\_OUT1

```

SUBROUTINE GRAVITY_OUT1
implicit double precision (a-h,o-z)
calculates boug. anomaly for the fault (H1=0.0,TK.NE.90.0)
C
C
COMMON h1,h2,r,tk,x,gc1
DATA gr/6.67e-6/
v1=2*gr*r*1000
p=3.14159
C
t=tand(tk)
a2=h2/t
x2=x+a2
f1=p/2
f2=atan(x2/h2)
x11=x1*x1
r1=x
h22=h2*h2
x22=x2*x2
r2=sqrt(h22+x22)
b1=h2*(p/2+f2)
s=sind(tk)
c=cosd(tk)
r1=r2/r1
rlo=log(r1)
s1=s*s
b2=x*s1*rlo
b3=x*(f2-f1)*s*c
gc1=v1*(b1+b2+b3)
RETURN
END
```

## B.6 Subroutine GRADIENT\_0

```
      SUBROUTINE GRADIENT_0
      implicit double precision (a-h,o-z)
      calculates HORIZONTAL GRAVITY GRADIENT for fault
      L=90.0
      COMMON h1,h2,r,tk,x,gc1
      DATA gr/6.67e-6/
      v1=2*gr*r*1000
      h11=h1*h1
      x11=x*x
      r1=sqrt(h11+x11)
      h22=h2*h2
      r2=sqrt(h22+x11)
      r1=r2/r1
      rlo=log(r1)
      gc1=v1*RLO
      RETURN
      END
```

## B.7 Subroutine GRADIENT\_1

```

SUBROUTINE GRADIENT_1
implicit double precision (a-h,o-z)
calculates HORIZONTAL GRAVITY GRADIENT for fault
C COMMON h1,h2,r,tk,x,gc1
DATA gr/6.67e-6/
v1=2*gr*r*1000
p=3.14159
t=tand(tk)
a1=h1/T
a2=h2/t
x1=x+a1
x2=x+a2
f1=atan(x1/h1)
f2=atan(x2/h2)
h11=h1*h1
x11=x1*x1
r1=sqrt(h11+x11)
h22=h2*h2
x22=x2*x2
r2=sqrt(h22+x22)
b1=h2*(p/2+f2)-h1*(p/2+f1)
s=sind(tk)
c=cosd(tk)
r1=r2/r1
rlo=log(r1)
s1=s*s
b2=s1*rlo
b3=(f2-f1)*s*c
gc1=v1*(b2+b3)
RETURN
END
```

## B.8 Subroutine MAXGR

```

SUBROUTINE MAXGR
C
  IMPLICIT DOUBLE PRECISION (A-H,O-Z)
  DIMENSION GGMAX(10,10)
  COMMON /maxim/ GGMAX,z,NUM,x2,x4,h0,kk
  COMMON H1,H2,R,TK,X,GC1
  common /fault/ M,S1,S2,S3,D1,D2,E1,E2,B1,B2,AA,XF1,XF2,
    TK1,TK2,GM,H3,RM,RM1
  INTEGER NUM
C
  IF (NUM .GT. 10) GOTO 15
  DO 13 J=1,NUM
    IF (NUM .EQ.1) GOTO 121
    IF (Z .GT. GGMAX(1,J)) GOTO 13
    DO 11 K=NUM,J+1,-1
      DO 10 L=1,9
        GGMAX(L,K) = GGMAX(L,K-1)
10      CONTINUE
11      CONTINUE
12      CONTINUE
        GGMAX(1,J)=Z
        GGMAX(2,J)=H0
        GGMAX(3,J)=H2
        GGMAX(4,J)=H3
        GGMAX(5,J)=R
        GGMAX(6,J)=TK1
        GGMAX(7,J)=TK2
        GGMAX(8,J)=X2
        GGMAX(9,J)=X4
        GGMAX(10,J)=kk
        GOTO 21
13      CONTINUE
121     CONTINUE
        IF (J .EQ. 11) GOTO 21
        GGMAX(1,J)=Z
        GGMAX(2,J)=H0
        GGMAX(3,J)=H2
        GGMAX(4,J)=H3
        GGMAX(5,J)=R
        GGMAX(6,J)=TK1
        GGMAX(7,J)=TK2
        GGMAX(8,J)=X2
        GGMAX(9,J)=X4
        GGMAX(10,J)=kk
31      CONTINUE
        GOTO 21
15      CONTINUE
        DO 18 J=1,10
          IF (Z .GT. GGMAX(1,J)) GOTO 18
          DO 17 K=10,J+1,-1
            DO 16 L=1,9
              GGMAX(L,K)=GGMAX(L,K-1)
16          CONTINUE

```

```
17      CONTINUE
        GGMAX(1,J)=Z
        GGMAX(2,J)=H0
        GGMAX(3,J)=H2
        GGMAX(4,J)=H3
        GGMAX(5,J)=R
        GGMAX(6,J)=TK1
        GGMAX(7,J)=TK2
        GGMAX(8,J)=X2
        GGMAX(9,J)=X4
        GGMAX(10,J)=kk
        GOTO 21
18      CONTINUE
21      CONTINUE
        RETURN
        END
```

## B.9 Subroutine MODEL

```

subroutine model
implicit double precision (A-H,O-Z)
COMMON /FAULT/ M,S1,s2,s3,d1,d2,e1,e2,b1,b2,AA,XF1,XF2,
+      TK1,TK2,GM,h3,RM,RM1
COMMON H1,H2,R,TK,X,GC1
dimension t(3,21),gcm(21),gc2(21)
CHARACTER*(*) MES1,MES2,MES3,MES4,MES6,MES15,
+      MES9,MES12
PARAMETER (MES2='THE THEORETICAL MODEL' )
c  PARAMETER (MES7='05-07-1991')
PARAMETER (MES1='DEP. GEOL. & GEOPH.')
PARAMETER (MES3='Depth (metres)')
PARAMETER (MES4='Easting (metres)')
PARAMETER (MES6='X1=      X2=')
PARAMETER (MES9='L1=      R=      L2=')
PARAMETER (MES15='H1=      H2=      H3=')
c  parameter (mes12='GM=      RR=')
PARAMETER (MES14='(metres)')
+ OPEN (UNIT=12,FILE='PLOT2.PLT',STATUS='NEW',
CARRIAGECONTROL='LIST')
CALL PLOTS (53,0,12)
CALL DASHDF(0.,0.,0.,0.)
LLL=1
C
S1=0.
rr=rml
call plot (10.0,s2+3.0,-3)
CALL NEWPEN (1)
C  the drawing of frames
CALL PLOT (-7.0,-s2-1.0,3)
CALL PLOT (-7.0,S1+0.5,2)
CALL PLOT (S3+10.0,S1+0.5,2)
CALL PLOT (S3+10.0,-s2-1.0,2)
CALL PLOT (-7.0,-s2-1.0,2)
c  the drawing of frames
CALL PLOT (-9.0,-s2-3.0,3)
CALL PLOT (-9.0,S1+2.5,2)
CALL PLOT (S3+20.0,S1+2.5,2)
CALL PLOT (S3+20.0,-s2-3.0,2)
CALL PLOT (-9.0,-s2-3.0,2)
c  the description of frames
CALL SYMBOL (-6.0,-s2-2.2,0.5,mes1,0.0,19)
CALL SYMBOL (-6.0,s1+1.3,0.5,mes2,0.0,32)
CALL SYMBOL (S3+11.0,-11.0,0.3,MES12,0.0,12)
call number (s3+11.9,-11.0,0.3,gm,0.0,2)
call number (s3+14.6,-11.0,0.3,rr,0.0,4)
CALL symbol (s3+11.0,-10.0,0.3,mes6,0.0,15)
CALL number (s3+11.9,-10.0,0.3,XF1,0.0,1)
CALL number (s3+15.5,-10.0,0.3,XF2,0.0,1)
CALL symbol (s3+11.0,-9.0,0.3,mes9,0.0,19)
CALL number (s3+11.9,-9.0,0.3,tk1,0.0,1)
CALL number (s3+14.3,-9.0,0.3,rm,0.0,2)
CALL number (s3+16.7,-9.0,0.3,tk2,0.0,1)

```

```

CALL symbol (s3+11.0,-8.0,0.3,mes15,0.0,23)
CALL number (s3+11.9,-8.0,0.3,h1,0.0,1)
CALL number (s3+14.9,-8.0,0.3,H2,0.0,1)
CALL number (s3+17.9,-8.0,0.3,H3,0.0,1)
c   the axis
c   call newpen (4)
c   the axis x
    dxx=(e1-e2)/s3
22  call plot (0.0,0.0,3)
    call plot (s3,0.0,2)
    CALL SYMBOL (s3+0.5,-0.25,0.5,MES4,0.0,16)
    d=e2
    x=0.0
    do 140 j=1,100
    CALL number (X-0.1,-0.7,0.15,d,0.0,-1)
    CALL SYMBOL (X,Y-0.25,0.5,13,0.0,-1)
    if (x.eq.S3) goto 150
    d=d+dxx
    x=x+1.0
140  continue
150  CONTINUE
c   the axis y2-lower
    call newpen (2)
    call plot (0.0,0.0,3)
    call plot (0.0,-s2,2)
    RB=D1
    RC=S2/RB
    d3=0.0
    y=0.0
    do 190 j=1,30
    call number (-1.5,y-0.075,0.15,d3,0.0,-1)
    call symbol (-0.5,y,0.5,15,0.0,-1)
    d3=d3+dxx
    y=y-1.0
    if (y.lt.-s2)goto 200
190  continue
200  call symbol (-5.0,0.0,0.5,mes3,270.0,13)
c   call symbol (-5.5,0.0,0.3,mes14,270.0,8)
c   the drawing of the faults
c   the drawing of the faults
    x3=0.0
    RA=E1-E2
    R=S3/RA
    rc=r
    if (tk1.ne.90.0) x3=h1/tand(tk1)
    if (aa .eq. 1.) x3=-x3
    bb=0.0
    if (aa.eq.1) bb=s3
    call plot (bb,-h1*RC,3)
    X=(XF1+X3-E2)*R
    call plot (X,-h1*RC,2)
    x4=0.0
    if (tk1.ne.90.0) x4=h3/tand(tk1)
    if (aa .eq. 1.0) x4=-x4
    call plot ((xf1+x4-E2)*R,-H3*RC,2)
    x51=0.0
    if (tk2.ne.90.)x51=h3/tand(tk2)
    if (aa .eq. 1.) x51=-x51
    call plot ((xf2+x51-e2)*r,-h3*rc,2)
    x61=0.
    if (tk2.ne.90.)x61=h2/tand(tk2)
    if (aa .eq. 1.0) x61=-x61
    call plot ((xf2+x61-e2)*r,-h2*rc,2)

```



```

call plot (bb,-h2*RC,2)
call plot (bb,-h1*RC,3)
if (xf2.ne.xf1) goto 180
x5=0.0
if(tk.ne.90.0) x5=((h2-H1)*tand(tk))*R
c   do 210 j=1,1000
c   call plot (x5,-h2*RC,2)
c   call plot (x5,-h1*RC,3)
c   x5=x5+0.5
c   if (x5.gt.X) goto 180
c210 continue
180 call newpen(4)
call plot(x,y,3)
240 CALL PLOT (S2+21.0,0.0,999)
12  CLOSE (UNIT=12)
RETURN
END

```

# Appendix C

## Initial and Output Data for Theoretical Models

### C.1 Adelaide City Area

#### C.1.1 Gravity Data from File OBS\_GRAV.DAT

0.0	10.25
100.0	10.52
222.0	11.02
343.9	11.81
404.9	12.19
465.9	12.45
526.8	12.75
587.8	13.26
637.8	13.62
682.9	14.11
743.9	14.95
804.9	15.8
865.9	16.55
926.8	17.16
987.8	17.81
1109.8	18.45
1208.5	19.13
1464.6	19.98

## C.1.2 Output Data from File OUT\_INF.DAT

### INITIAL DATA

	Minimum	Maximum	Step
First fault			
Easting :	760.0	900.0	20.0
Depth :	75.0	210.0	10.0
Angle :	70.0	105.0	5.0
Second fault			
Easting :	200.0	400.0	20.0
Angle :	70.0	105.0	5.0
Density :	0.50	0.60	0.05
Step of Gmax:	1.0		
Max of K:	7		

### OUTPUT DATA

DIFF	DEPTH1	DEPTH2	DEPTH3	DENSITY	ANGLE1	ANGLE2	EAST1	EAST2	K
0.14	85.0	788.0	565.0	0.500	85.0	85.0	820.0	340.0	6.
0.15	85.0	788.0	585.0	0.500	85.0	85.0	820.0	320.0	6.
0.15	85.0	788.0	585.0	0.500	85.0	90.0	820.0	300.0	6.
0.15	85.0	788.0	585.0	0.500	85.0	85.0	820.0	360.0	6.
0.15	95.0	845.7	595.0	0.500	90.0	80.0	820.0	300.0	7.
0.15	85.0	788.0	585.0	0.500	85.0	85.0	820.0	300.0	6.
0.15	85.0	788.0	585.0	0.500	85.0	80.0	820.0	360.0	6.
0.16	95.0	845.7	595.0	0.500	90.0	90.0	820.0	280.0	7.
0.16	85.0	788.0	585.0	0.500	80.0	85.0	840.0	300.0	6.
0.16	105.0	744.0	605.0	0.550	80.0	80.0	840.0	280.0	6.

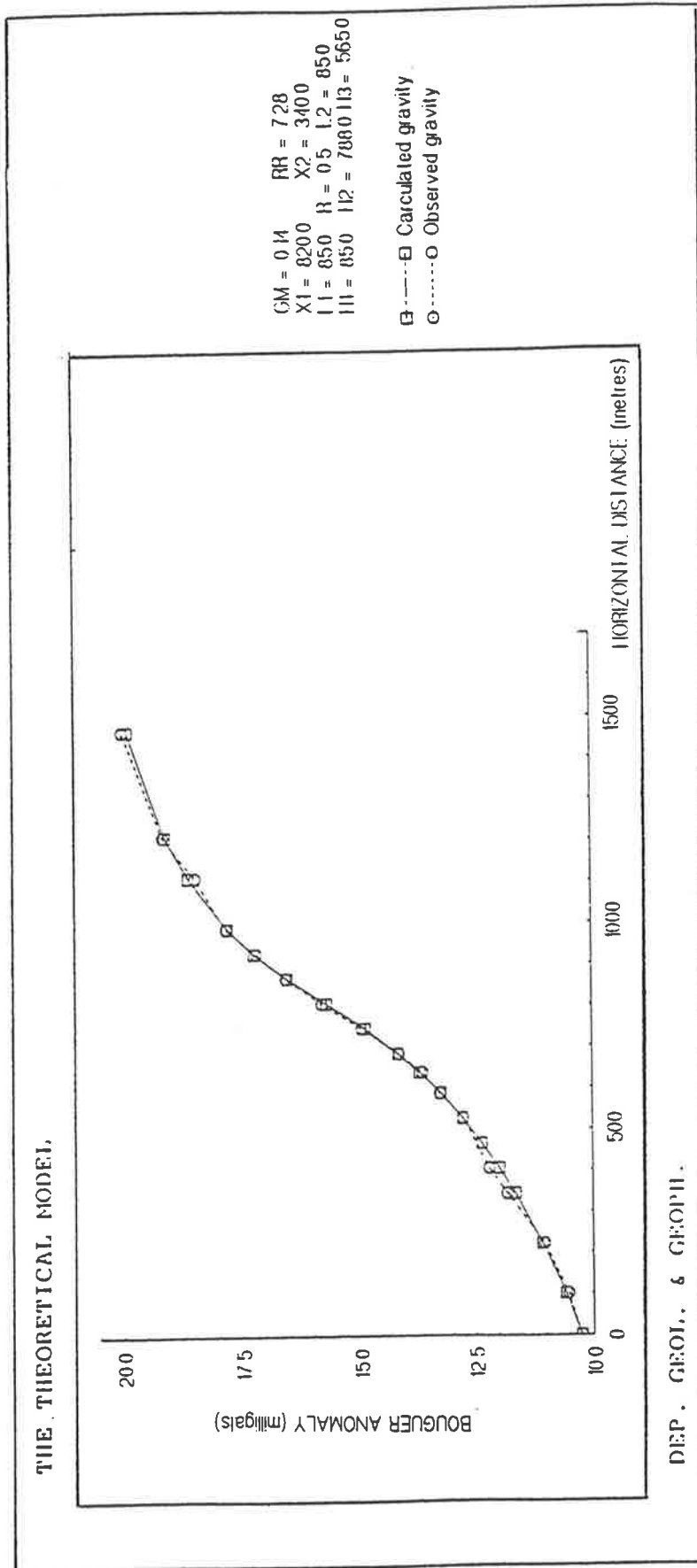
### C.1.3 Output Data from File OUT\_GR.DAT

O U T P U T   D A T A   F O R   T H E O R E T I C A L   M O D E L

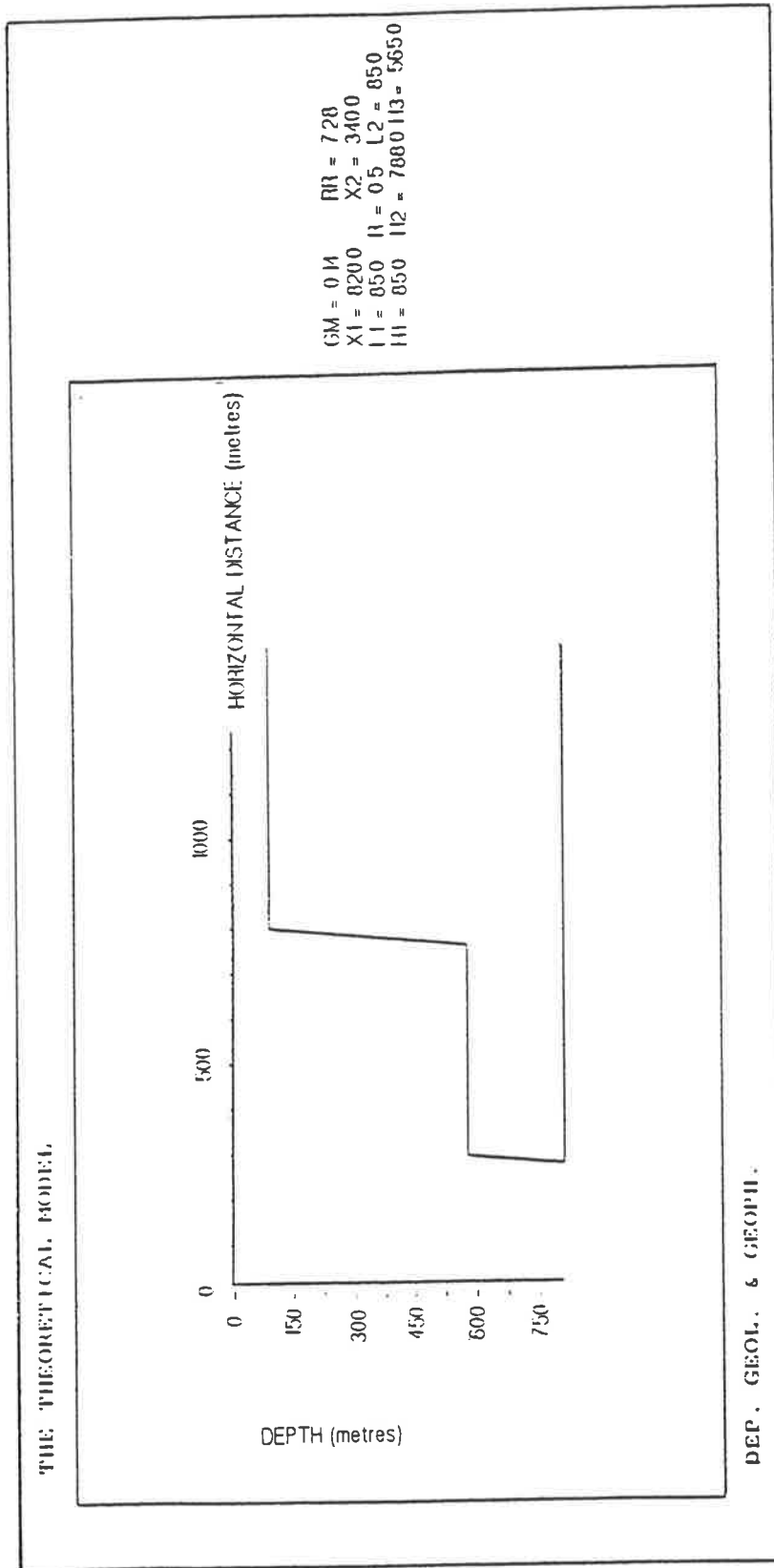
DIFF	DEPTH1	DEPTH2	DEPTH3	DENSITY	ANGLE1	ANGLE2	EAST1	EAST2	K
0.14	85.0	788.0	585.0	0.500	85.0	85.0	820.0	340.0	6.

Calculated gravity	Observed gravity	Easting
2.90851	10.25000	0.0
3.24471	10.52000	100.0
3.72673	11.02000	222.0
4.30266	11.81000	343.9
4.63434	12.19000	404.9
5.00309	12.45000	465.9
5.41821	12.75000	526.8
5.89292	13.26000	587.8
6.33923	13.62000	637.8
6.79744	14.11000	682.9
7.51793	14.95000	743.9
8.34873	15.80000	804.9
9.17683	16.55000	865.9
9.87469	17.16000	926.8
10.43495	17.81000	987.8
11.25979	18.45000	1109.8
11.73661	19.13000	1208.5
12.53511	19.98000	1464.6

# C.1.4 Output Plot from File PLOT1.PLT



# C.1.5 Output Data from file PLOT2.PLT



## C.2 Eromanga Basin - Line no.13a

### C.2.1 Gravity Data from File OBS\_GRAV.DAT

0.	88.
1000.	87.
1750.	86.
2250.	85.
2500.	84.
2750.	83.
3000.	82.
3250.	81.
3500.	80.
3750.	79.
4375.	78.
4625.	77.
6075.	76.
7500.	75.
9375.	74.
10500.	73.
11500.	72.
12750.	71.
14250.	70.
15750.	69.

## C.2.2 Output Data from File OUT\_INF.DAT

### I N I T I A L   D A T A

	Minimum	Maximum	Step
First fault			
Easting :	2900.0	3000.0	20.0
Depth :	600.0	780.0	20.0
Angle :	40.0	120.0	5.0
Second fault			
Easting :	11180.0	11300.0	20.0
Angle :	40.0	120.0	5.0
Density :	0.35	0.50	0.05
Step of Gmax:	1.0		
Max of K:	5		

### O U T P U T   D A T A

DIFF	DEPTH1	DEPTH2	DEPTH3	DENSITY	ANGLE1	ANGLE2	EAST1	EAST2	K
0.79	700.0	2012.4	1600.0	0.400	90.0	90.0	2960.0	11240.0	4.
0.79	700.0	2012.4	1600.0	0.400	90.0	90.0	2960.0	11260.0	4.
0.79	700.0	2012.4	1600.0	0.400	90.0	90.0	2960.0	11220.0	4.
0.80	700.0	2012.4	1600.0	0.400	90.0	90.0	2960.0	11200.0	4.
0.80	700.0	2012.4	1600.0	0.400	90.0	90.0	2960.0	11180.0	4.
0.80	700.0	2012.4	1600.0	0.400	90.0	90.0	2940.0	11240.0	4.
0.80	700.0	2012.4	1600.0	0.400	90.0	90.0	2940.0	11220.0	4.
0.81	700.0	2012.4	1600.0	0.400	90.0	90.0	2940.0	11260.0	4.
0.81	700.0	2012.4	1600.0	0.400	90.0	90.0	2940.0	11200.0	4.
0.81	680.0	1992.4	1580.0	0.400	90.0	90.0	2960.0	11260.0	4.



### C.2.3 Output Data from File OUT\_GR.DAT

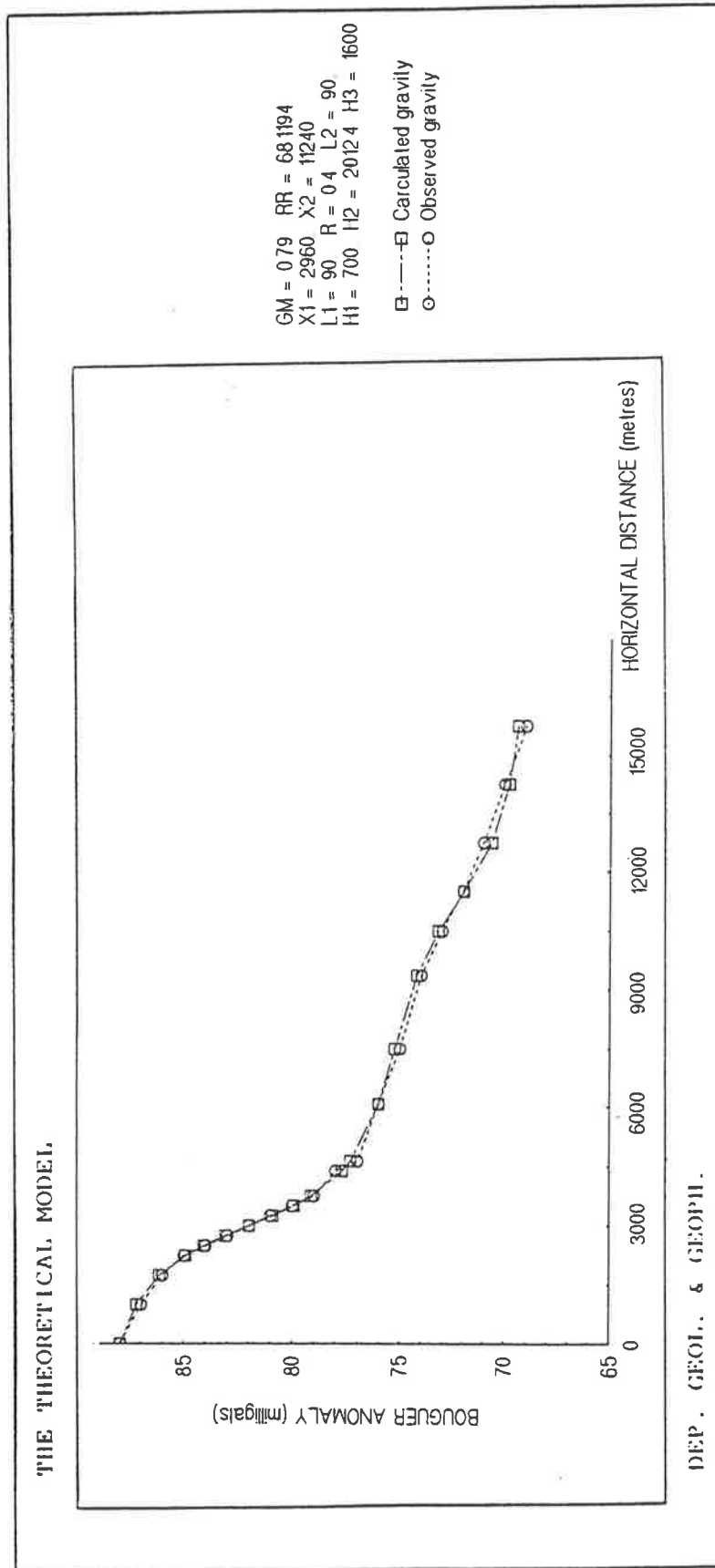
OUTPUT DATA FOR THEORETICAL MODEL

DIFF	DEPTH1	DEPTH2	DEPTH3	DENSITY	ANGLE1	ANGLE2	EAST1	EAST2	K
0.79	700.0	2012.4	1600.0	0.400	90.0	90.0	2960.0	11240.0	4.

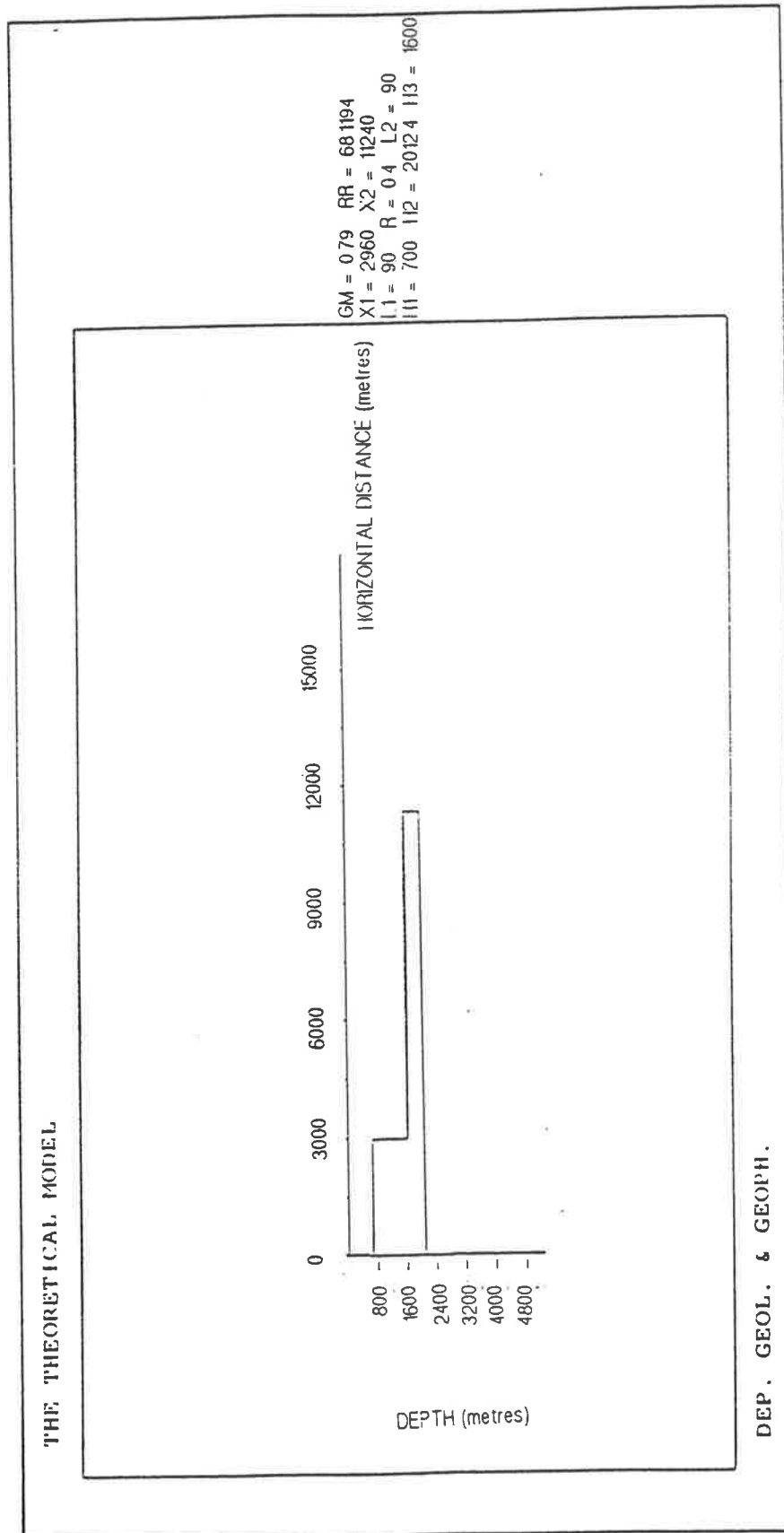
Calculated gravity	Observed gravity	Easting
--------------------	------------------	---------

19.89273	88.00000	0.0
19.11724	87.00000	1000.0
18.03431	86.00000	1750.0
16.81819	85.00000	2250.0
15.98471	84.00000	2500.0
14.99050	83.00000	2750.0
13.89085	82.00000	3000.0
12.80210	81.00000	3250.0
11.83229	80.00000	3500.0
11.02370	79.00000	3750.0
9.61247	78.00000	4375.0
9.22238	77.00000	4625.0
7.87638	76.00000	6075.0
7.12394	75.00000	7500.0
6.09384	74.00000	9375.0
5.07558	73.00000	10500.0
3.82201	72.00000	11500.0
2.50655	71.00000	12750.0
1.68651	70.00000	14250.0
1.27426	69.00000	15750.0

### C.2.4 Output Plot from File PLOT1.PLT



## C.2.5 Output Data from file PLOT2.PLT



## C.3 Eromanga Basin - Line no.12a

### C.3.1 Gravity Data from File OBS\_GRAV.DAT

0.	90.
1250.	89.
2375.	88.
2750.	87.
3000.	86.
3250.	85.
3625.	84.
3875.	83.
4500.	82.
5500.	81.
6125.	80.
6375.	79.
6625.	78.
6750.	77.
7000.	76.
7250.	75.28
7750.	74.
8000.	72.48
8625.	70.51
9000.	70.
10500.	69.
12500.	68.

### C.3.2 Output Data from File OUT\_INF.DAT

#### I N I T I A L   D A T A

	Minimum	Maximum	Step
First fault			
Easting :	2940.0	3100.0	20.0
Depth :	320.0	440.0	20.0
Angle :	70.0	100.0	5.0
Second fault			
Easting :	7040.0	7240.0	20.0
Angle :	70.0	100.0	5.0
Density :	0.35	0.50	0.05
Step of Gmax:	1.0		
Max of K:	5		

#### O U T P U T   D A T A

DIFF	DEPTH1	DEPTH2	DEPTH3	DENSITY	ANGLE1	ANGLE2	EAST1	EAST2	K
2.00	380.0	1871.3	830.0	0.400	90.0	90.0	2980.0	7180.0	4.
2.00	380.0	1871.3	830.0	0.400	90.0	90.0	2980.0	7160.0	4.
2.00	380.0	1871.3	830.0	0.400	90.0	90.0	2960.0	7180.0	4.
2.00	380.0	1871.3	830.0	0.400	90.0	90.0	2960.0	7160.0	4.
2.01	360.0	1851.3	810.0	0.400	90.0	90.0	2980.0	7180.0	4.
2.01	380.0	1871.3	830.0	0.400	90.0	90.0	3000.0	7180.0	4.
2.03	360.0	1851.3	810.0	0.400	90.0	90.0	2960.0	7180.0	4.
2.06	360.0	1851.3	810.0	0.400	90.0	90.0	2980.0	7160.0	4.
2.06	400.0	1891.3	850.0	0.400	90.0	90.0	2980.0	7180.0	4.
2.06	380.0	1871.3	830.0	0.400	90.0	90.0	2980.0	7200.0	4.

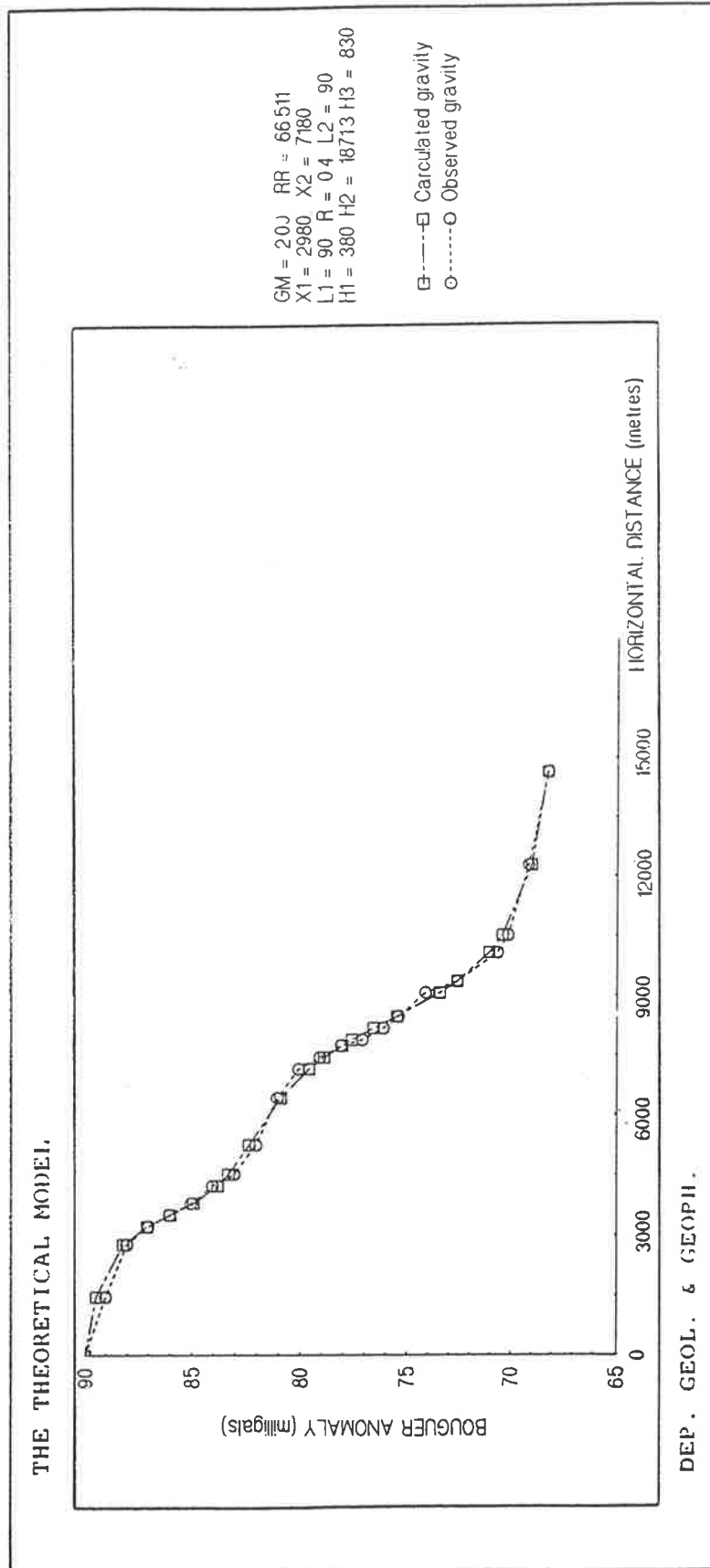
### C.3.3 Output Data from File OUT\_GR.DAT

OUTPUT DATA FOR THEORETICAL MODEL

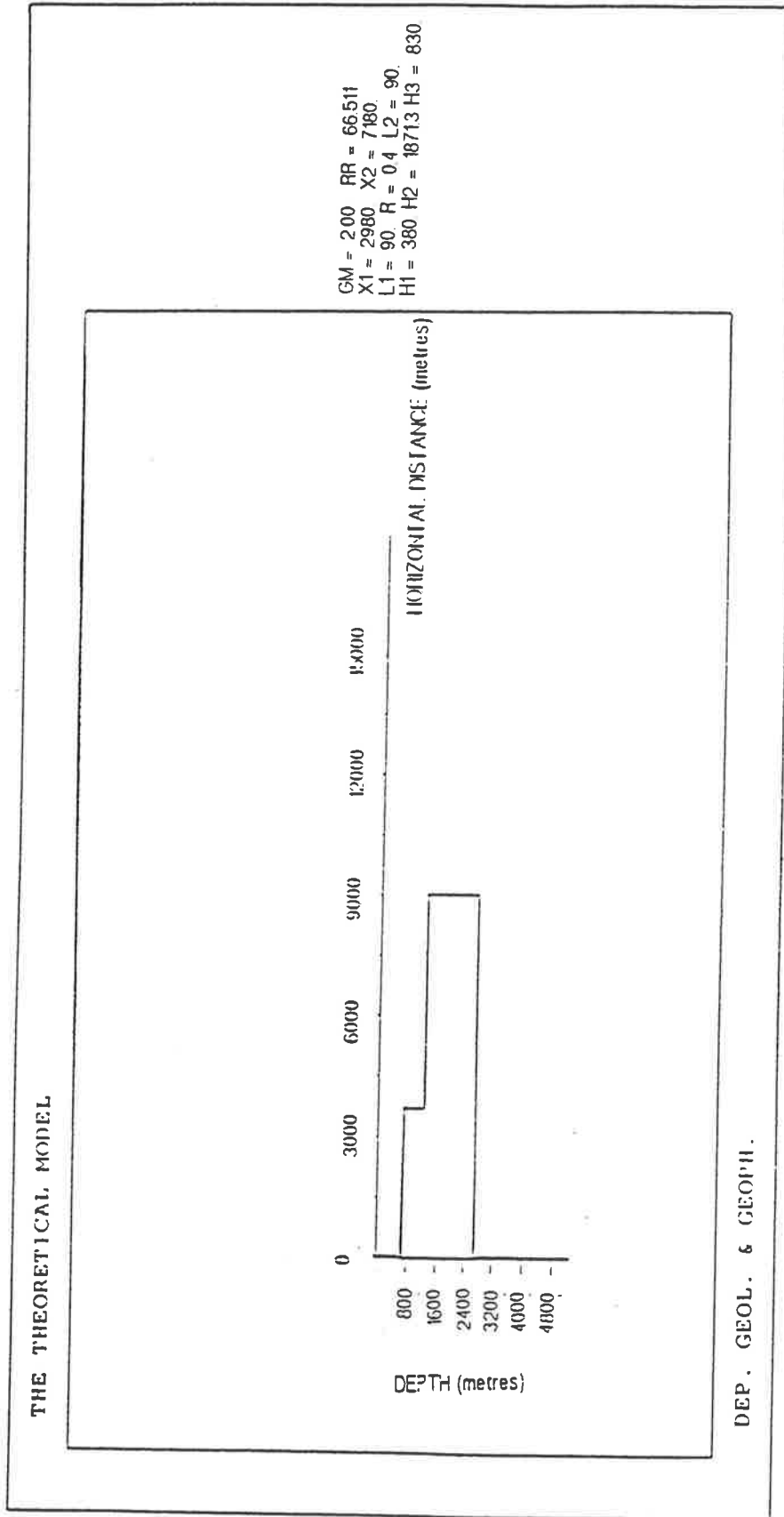
DIFF	DEPTH1	DEPTH2	DEPTH3	DENSITY	ANGLE1	ANGLE2	EAST1	EAST2	K
2.00	380.0	1871.3	830.0	0.400	90.0	90.0	2980.0	7180.0	4.

Calculated gravity	Observed gravity	Easting
23.49357	90.00000	0.0
22.96408	89.00000	1250.0
21.65198	88.00000	2375.0
20.54088	87.00000	2750.0
19.46707	86.00000	3000.0
18.39872	85.00000	3250.0
17.26544	84.00000	3625.0
16.75294	83.00000	3875.0
15.81460	82.00000	4500.0
14.35006	81.00000	5500.0
13.01202	80.00000	6125.0
12.30019	79.00000	6375.0
11.45860	78.00000	6625.0
10.98735	77.00000	6750.0
9.95718	76.00000	7000.0
8.86019	75.28000	7250.0
6.80563	74.00000	7750.0
5.96250	72.48000	8000.0
4.41423	70.51000	8625.0
3.77633	70.00000	9000.0
2.34051	69.00000	10500.0
1.53621	68.00000	12500.0

### C.3.4 Output Plot from File PLOT1.PLT



### C.3.5 Output Data from file PLOT2.PLT





## C.4 Eromanga Basin - Line no.3; One Fault

### C.4.1 Gravity Data from File OBS\_GRAV.DAT

328715.	96.05
329715.	95.7
330715.	95.3
331715.	94.8
332715.	94.35
333715.	93.75
334715.	92.
335715.	89.
336715.	83.
337715.	78.
338715.	75.5
339715.	73.75
340715.	72.8
341715.	71.72
342715.	71.75
343715.	71.6

## C.4.2 Output Data from File OUT\_INF.DAT

### INITIAL DATA

	Minimum	Maximum	Step
First fault			
Easting :	336350.0	336500.0	10.0
Depth :	600.0	820.0	10.0
Angle :	60.0	100.0	10.0
Density :	0.35	0.50	0.05
Step of Gmax:	1.0		
Max of K:	7		

### OUTPUT DATA

DIFF	DEPTH1	DEPTH2	DENSITY	ANGLE1	EAST1	K
0.60	730.00	2427.14	0.40	80.00	336410.00	5.
0.60	740.00	2437.14	0.40	80.00	336410.00	5.
0.60	740.00	2437.14	0.40	80.00	336400.00	5.
0.61	730.00	2427.14	0.40	80.00	336420.00	5.
0.61	730.00	2427.14	0.40	80.00	336400.00	5.
0.61	720.00	2417.14	0.40	80.00	336410.00	5.
0.61	720.00	2417.14	0.40	80.00	336420.00	5.
0.62	740.00	2437.14	0.40	80.00	336420.00	5.
0.62	750.00	2447.14	0.40	80.00	336400.00	5.
0.62	740.00	2437.14	0.40	80.00	336390.00	5.

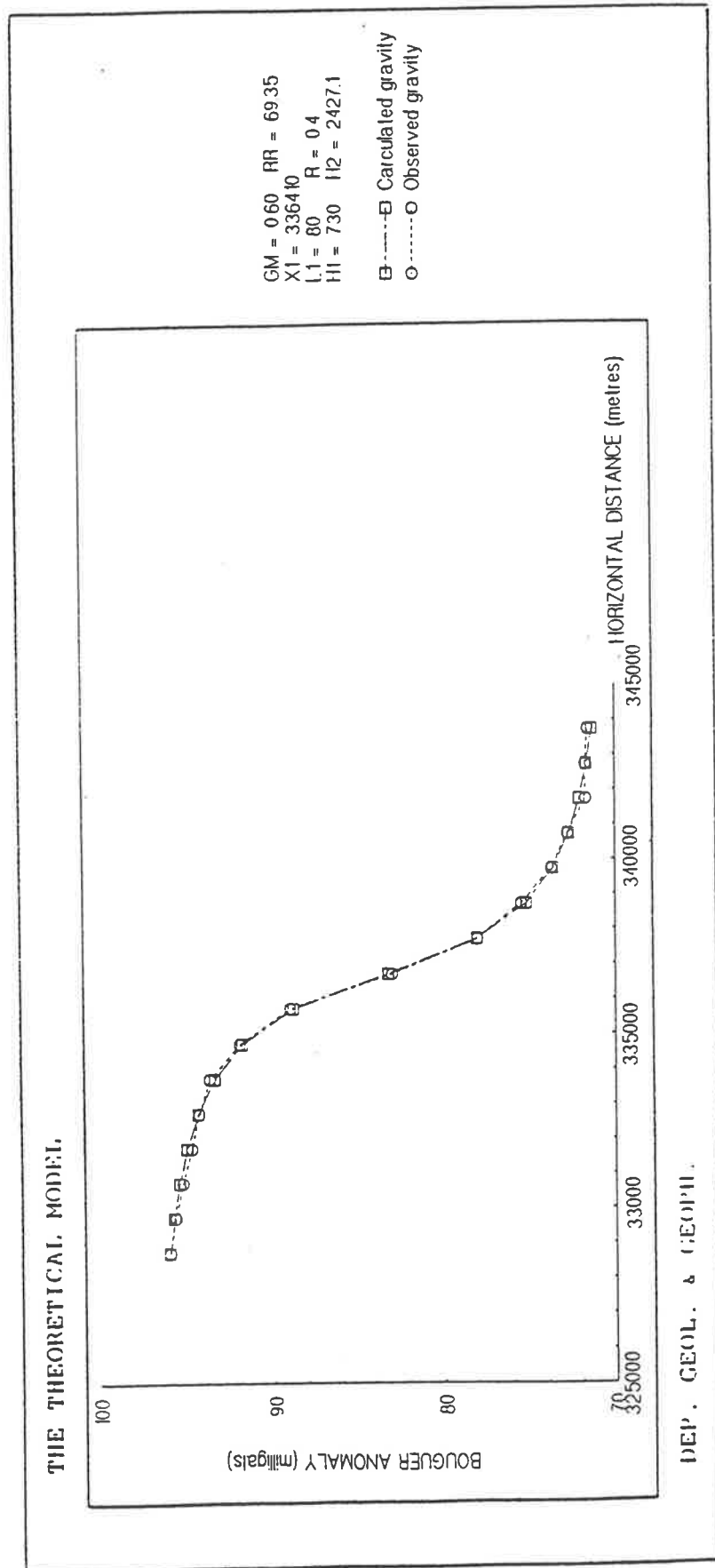
### C.4.3 Output Data from File OUT\_GR.DAT

OUTPUT DATA FOR THEORETICAL MODEL

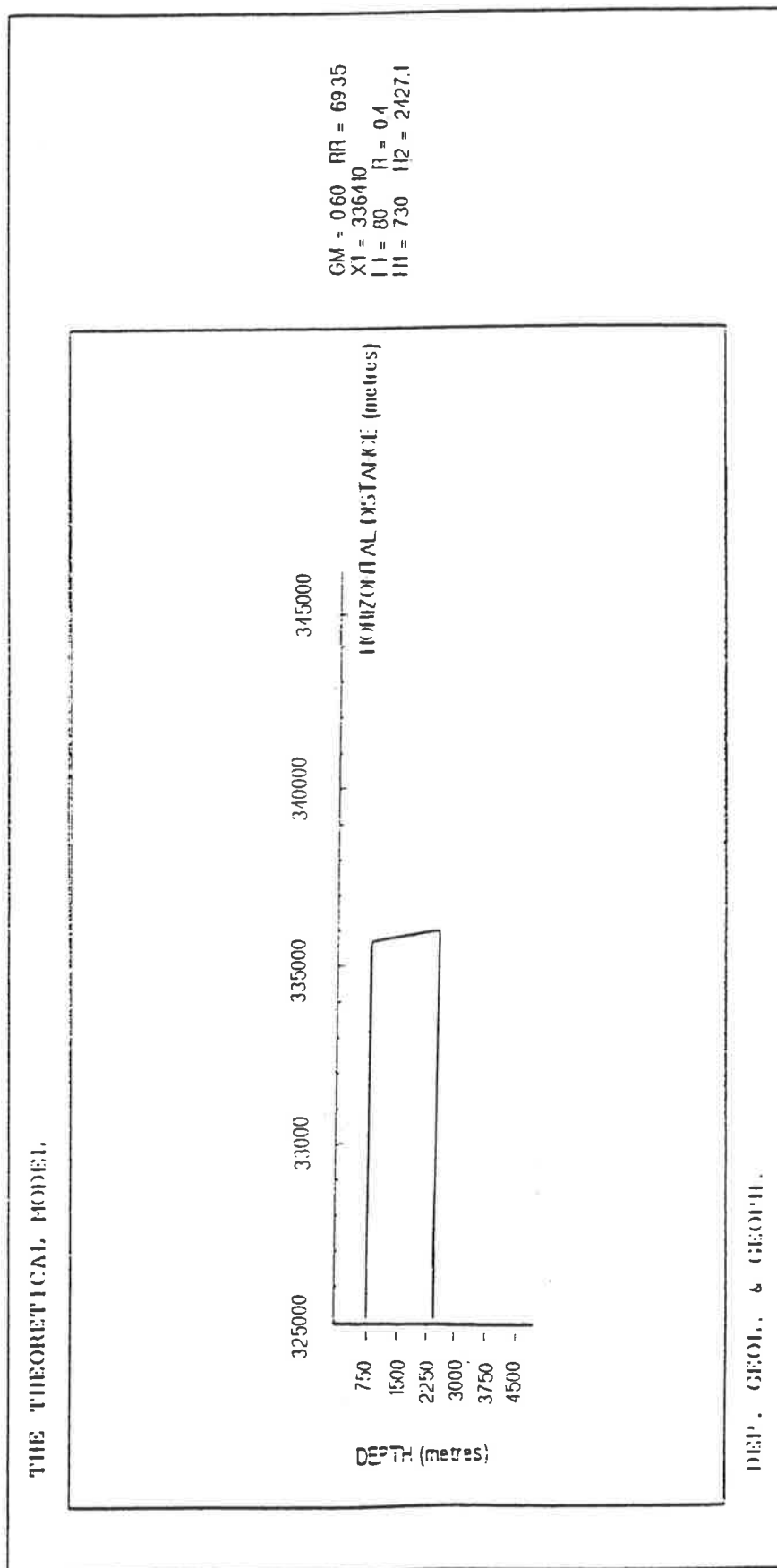
DIFF	DEPTH1	DEPTH2	DENSITY	ANGLE1	EAST1	K
0.60	730.00	2427.14	0.40	80.00	336410.00	5.

Calculated gravity	Observed gravity	Easting
26.69138	96.05000	328715.0
26.44953	95.70000	329715.0
26.13249	95.30000	330715.0
25.70018	94.80000	331715.0
25.07954	94.35000	332715.0
24.12508	93.75000	333715.0
22.51518	92.00000	334715.0
19.47497	89.00000	335715.0
13.86991	83.00000	336715.0
8.68700	78.00000	337715.0
5.85744	75.50000	338715.0
4.29995	73.75000	339715.0
3.36070	72.80000	340715.0
2.74539	71.72000	341715.0
2.31526	71.75000	342715.0
1.99923	71.60000	343715.0

C.4.4 Output Plot from File PLOT1.PLT



# C.4.5 Output Data from file PLOT2.PLT



## C.5 Eromanga Basin - Line no.3; Two Faults

### C.5.1 Gravity Data from File OBS\_GRAV.DAT

328715.	96.05
329715.	95.7
330715.	95.3
331715.	94.8
332715.	94.35
333715.	93.75
334715.	92.
335715.	89.
336715.	83.
337715.	78.
338715.	75.5
339715.	73.75
340715.	72.8
341715.	71.72
342715.	71.75
343715.	71.6

## C.5.2 Output Data from File OUT\_INF.DAT

### INITIAL DATA

	Minimum	Maximum	Step
First fault			
Easting :	336300.0	336600.0	20.0
Depth :	560.0	780.0	20.0
Angle :	70.0	100.0	5.0
Second fault			
Easting :	337700.0	338000.0	20.0
Angle :	70.0	100.0	5.0
Density :	0.35	0.50	0.05
Step of Gmax:	1.0		
Max of K:	7		

### OUTPUT DATA

DIFF	DEPTH1	DEPTH2	DEPTH3	DENSITY	ANGLE1	ANGLE2	EAST1	EAST2	K
0.52	700.0	2397.1	2060.0	0.400	90.	90.	336500.	337730.	5.
0.52	700.0	2397.1	2060.0	0.400	90.	90.	336500.	337750.	5.
0.52	700.0	2397.1	2060.0	0.400	90.	90.	336500.	337710.	5.
0.52	700.0	2397.1	2060.0	0.400	90.	90.	336500.	337770.	5.
0.52	700.0	2397.1	2060.0	0.400	90.	90.	336500.	337790.	5.
0.53	680.0	2377.1	2030.0	0.400	90.	90.	336460.	337790.	5.
0.53	700.0	2397.1	2150.0	0.400	90.	90.	336520.	337790.	5.
0.53	700.0	2397.1	2050.0	0.400	90.	90.	336480.	337710.	5.
0.53	680.0	2377.1	2030.0	0.400	90.	90.	336460.	337770.	5.
0.53	700.0	2397.1	2060.0	0.400	90.	90.	336480.	337790.	5.

### C.5.3 Output Data from File OUT\_GR.DAT

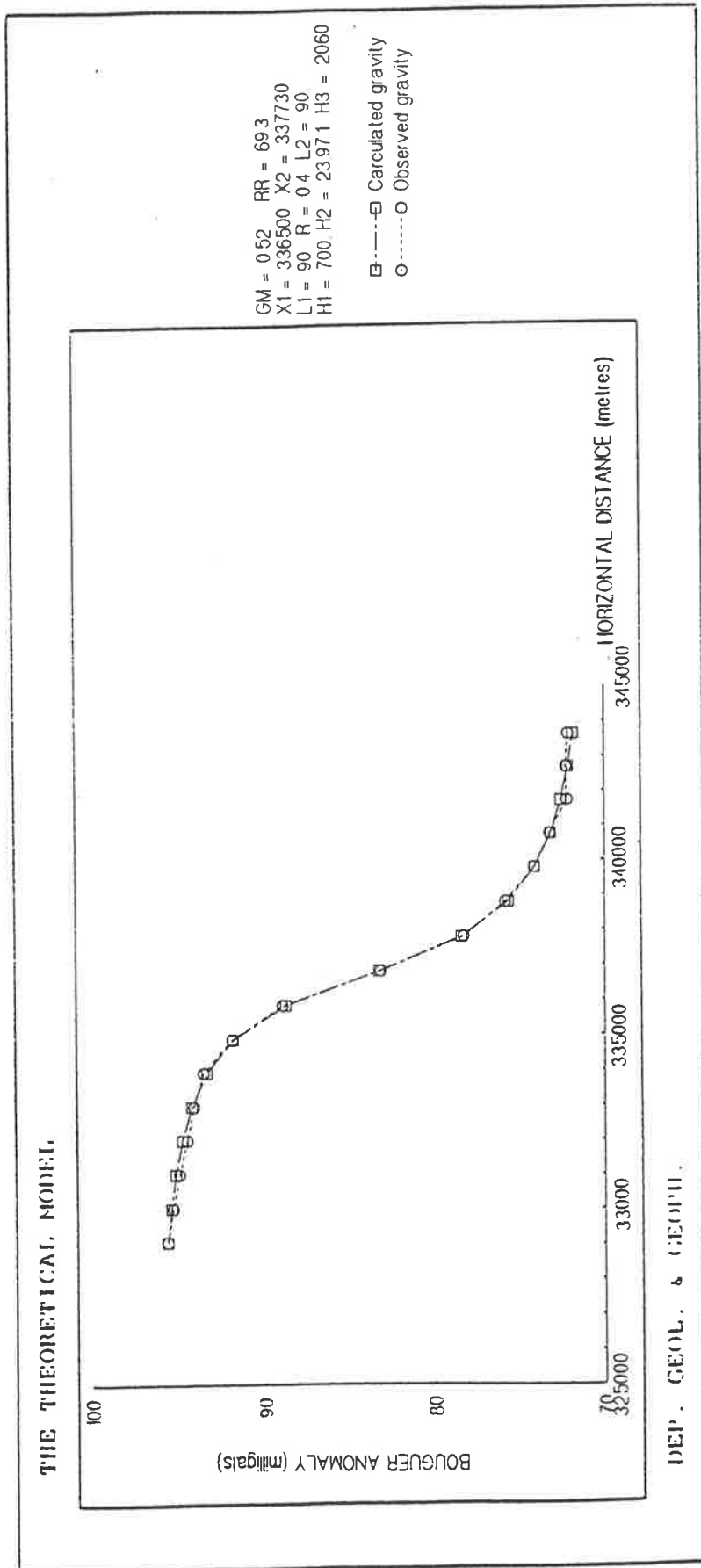
O U T P U T   D A T A   F O R   T H E O R E T I C A L   M O D E L

DIFF	DEPTH1	DEPTH2	DEPTH3	DENSITY	ANGLE1	ANGLE2	EAST1	EAST2	K
0.52	700.0	2397.1	2060.0	0.400	90.	90.	336500.	337730.	5.

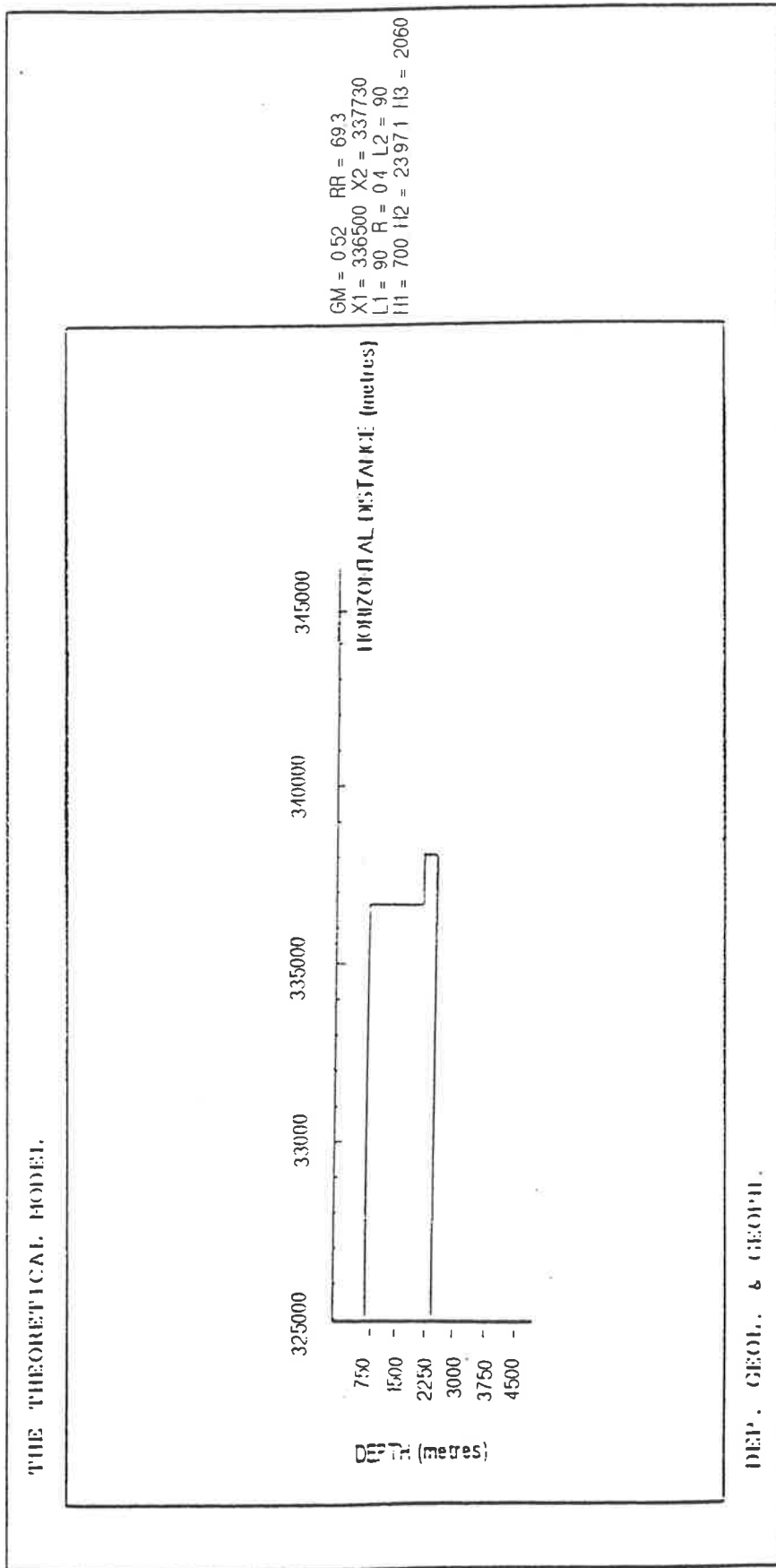
Calculated gravity	Observed gravity	Easting
26.74262	96.05000	328715.0
26.50897	95.70000	329715.0
26.20249	95.30000	330715.0
25.78379	94.80000	331715.0
25.18013	94.35000	332715.0
24.24363	93.75000	333715.0
22.63718	92.00000	334715.0
19.52525	89.00000	335715.0
13.80283	83.00000	336715.0
8.81797	78.00000	337715.0
6.02781	75.50000	338715.0
4.41267	73.75000	339715.0
3.42427	72.80000	340715.0
2.77920	71.72000	341715.0
2.33189	71.75000	342715.0
2.00579	71.60000	343715.0



### C.5.4 Output Plot from File PLOT1.PLT



C.5.5 Output Data from file PLOT2.PLT



## C.6 Eromanga Basin - Line no.11

### C.6.1 Gravity Data from File OBS\_GRAV.DAT

333950.	79.81
334700.	79.63
335450.	79.71
336250.	79.48
337000.	78.28
337500.	76.6
338000.	72.73
338750.	69.13
339500.	67.92

## C.6.2 Output Data from File OUT\_INF.DAT

### INITIAL DATA

	Minimum	Maximum	Step
First fault			
Easting :	337300.0	337450.0	10.0
Depth :	105.0	230.0	10.0
Angle :	20.0	60.0	10.0
Density :	0.40	0.55	0.05
Step of Gmax:	1.0		
Max of K:	5		

### OUTPUT DATA

DIFF	DEPTH1	DEPTH2	DENSITY	ANGLE1	EAST1	K
0.17	175.00	837.87	0.50	40.00	337380.00	3.
0.17	195.00	797.61	0.55	40.00	337390.00	3.
0.17	165.00	827.87	0.50	40.00	337400.00	3.
0.17	165.00	827.87	0.50	40.00	337390.00	3.
0.17	205.00	807.61	0.55	40.00	337380.00	3.
0.18	205.00	807.61	0.55	40.00	337370.00	3.
0.18	175.00	837.87	0.50	40.00	337390.00	3.
0.18	135.00	871.51	0.45	40.00	337400.00	3.
0.18	135.00	871.51	0.45	40.00	337390.00	3.
0.18	195.00	797.61	0.55	40.00	337380.00	3.

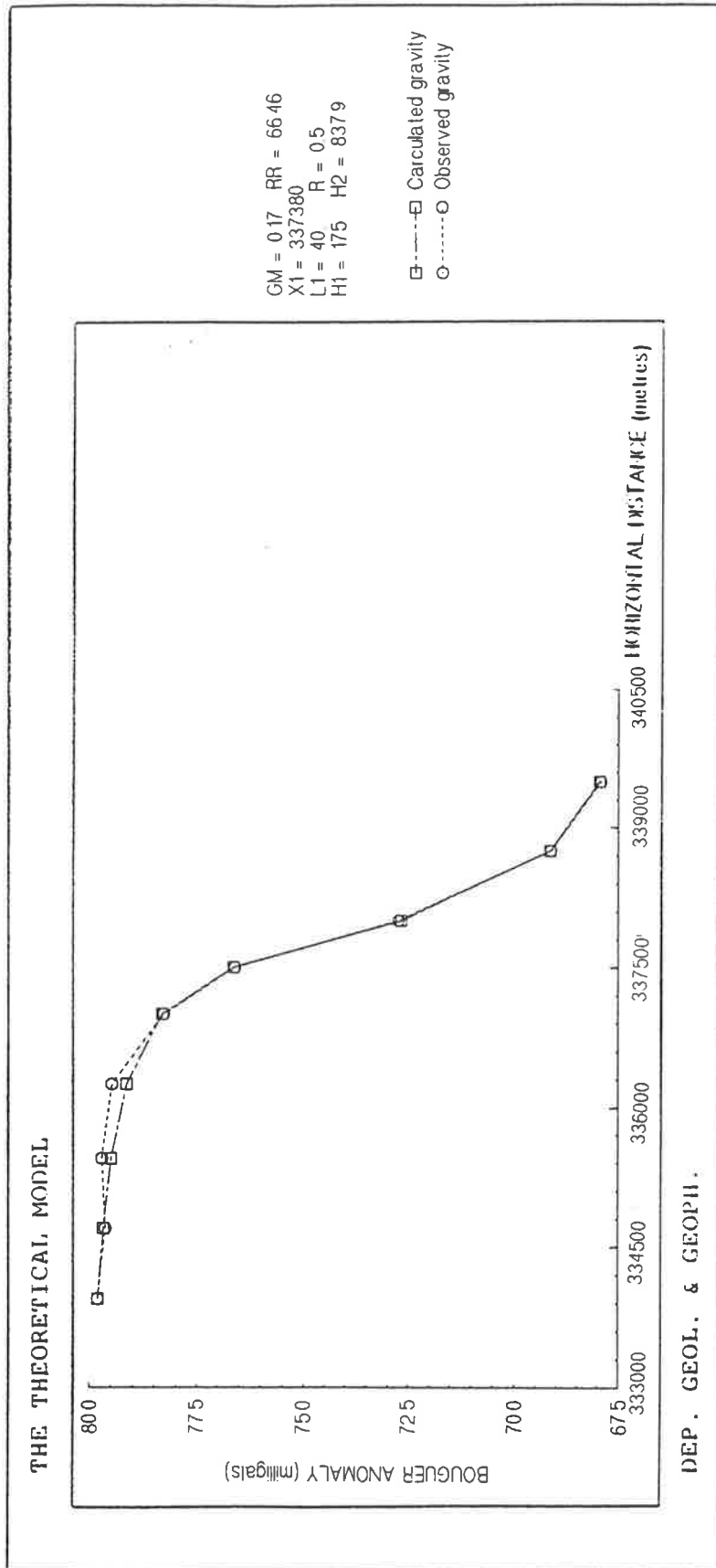
### C.6.3 Output Data from File OUT\_GR.DAT

OUTPUT DATA FOR THEORETICAL MODEL

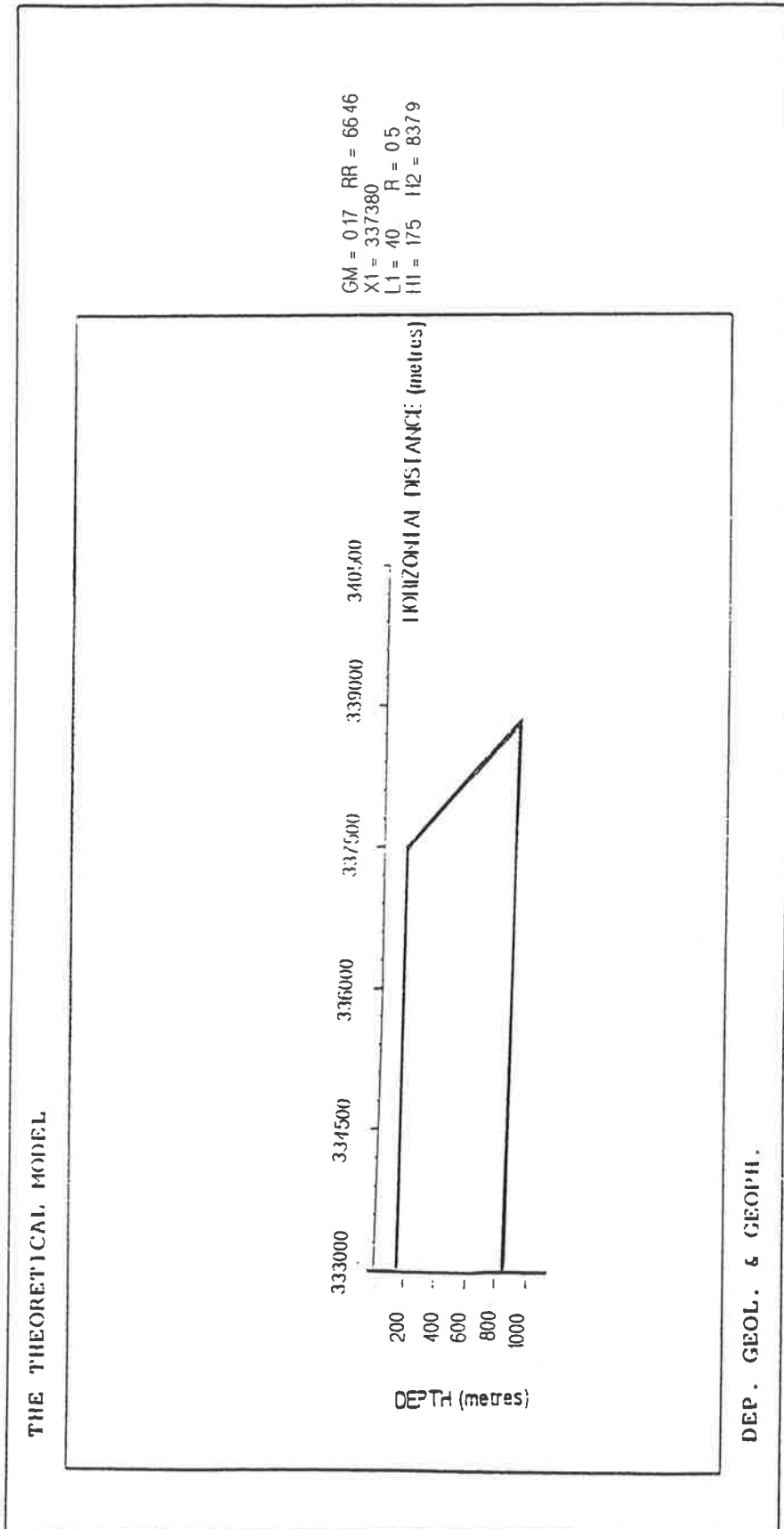
DIFF	DEPTH1	DEPTH2	DENSITY	ANGLE1	EAST1	K
0.17	175.00	837.87	0.50	40.00	337380.00	3.

Calculated gravity	Observed gravity	Easting
13.34862	79.81000	333950.0
13.22926	79.63000	334700.0
13.04276	79.71000	335450.0
12.67907	79.48000	336250.0
11.86591	78.28000	337000.0
10.18273	76.60000	337500.0
6.20497	72.73000	338000.0
2.69109	69.13000	338750.0
1.49143	67.92000	339500.0

### C.6.4 Output Plot from File PLOT1.PLT



# C.6.5 Output Data from file PLOT2.PLT



# Appendix D

## Abbreviations

### General

A.M.G.	Australian Map Grid
cm	centimetres
E	east
eq.	equation
Fig.	figure
g	grams
$\text{g cm}^{-3}$	grams per cubic centimetre
km	kilometres
m	metres
mGal	milligal (unit of gravitational acceleration)
my	million years before the present
N	north
no.	number
N.T.	Northern Territory
S.A.	South Australia



S.I.	International System of metric units
W	west
W.A.	Western Australia

# Bibliography

ANDERSON, E.M., 1942, *The Dynamics of Faulting and Dyke Formation with Application to Britain*: Oliver & Boyd, London 1942.

ANDERSON, E.M., 1951, *The Dynamics of Faulting, Britain*: Oliver & Boyd.

ANGELIER, J., 1984, *Tectonic Analysis of Fault Slip Data*: *Journal of Geophysical Research*, vol.89, no.B7, pp. 5835-5848.

ANGELIER, J., 1989, *From Orientation to Magnitudes in Palaeostress Determinations Using Fault Slip Data*: *Journal of Structural Geology*, Vol.11.

BARTER, C.J. & MARLIN, C.D. et al., 1987, *The Ludvig Users Guide Version 4.0 April 1987*: University of Adelaide, University Computing Service.

BARTER, C.J. & MARLIN, C.D. et al., 1990, *The Ludvig Users Guide Version 5.0 April 1990*: University of Adelaide, University Computing Service.

BHASKARA RAO, D. & PRAKASH, J., 1990, Interpretation of Gravity Anomalies Over an Inclined Fault of Finite Strike Length with Quadratic Density Function: *Exploration Geophysics* (1990), Vol.21, pp. 169-173.

BHATTACHARYYA, B.K., 1978, Computer Modeling in Gravity and Magnetic Interpretation: *Geophysics* Vol.43 No.5, pp. 912-929.

BILLINGS, M.P., 1972, *Structural Geology*: New York, Prentice-Hall Geology Series.

BULTER, B.C.M. & BELL, J.D., 1988, *Interpretation of Geological Maps*: Logman Scientific & Technical, New York.

CHINNERY, M.A., 1966, Secondary Faulting: *Can. J. Earth Sci.* 3.

CHMIELEWSKI, H., *Miedzynarodowy Uklad Jednostek Miar*: Panstwowe Wydawnictwa Szkolnictwa Zawodowego, Warszawa 1974.

COOCSON, G.G., 1987, *Magnetic Tape Operations Users Guide for VAX/VMS, Version 1.0*: University of Adelaide, University Computing Services.

DAVIS, T.M., 1971, A Filtering Technique for Interpretating The Gravity Anomaly Generated by a Two-Dimentional Fault: *Geophysics* Vol.36 No.3, pp. 554-571.

DUNKIN, J.W. & LEVIN, F.K., 1971, Isochrons for a Three-Dimentional Seismic System: *Geophysics* Vol.36 No.6, pp. 1099-1137.

FAJKLEWICZ, Z. & CZUBEK, J., 1972, *Zarys Geofizyki Stosowanej*: Wydawnictwa Geologiczne, Warszawa.

FAJKLEWICZ, Z., 1980, Mikrograwimetria Gornicza: Wydawnictwo Slask, Katowice 1980.

FINLAYSON, B., 1978, Para Fault Gravity Survey, West Adelaide: South Aust. Dept. Mines and Energy.

GORSKOV, G.P., Obshchaya geologia: Izdatelstvo Moskovskogo Universiteta, 1957.

HANCOCK, P.L., 1985, Brittle Microtectonics - Principles and Practice: Journal of Structural Geology, Vol.7, nos.3/4, pp. 437-457.

HUESTIS, S.P. and ANDER, M.E., 1983, IDB-2 A Fortran Program for Computing Extremal Bounds in Gravity Data Interpretation: Geophysics Vol.48 No.7, pp. 999-1010.

HOWCHIN, W., 1928, A Geological Sketch-Section of the Sea cliffs on the Eastern Side of Gulf St. Vincent, from Brighton to Sellick's Hill, with Descriptions: Trans. R. Soc. S. Austr., 47, pp. 279-315.

HOWCHIN, W., 1929, The Geology of South Australia: Published Privately, Adelaide.

HOWCHIN, W., 1930, The Building of Australia and the Succession of Life: Vol.3, Govt. Printer, Adelaide.

KIEK, T. & JONES, C.R., 1986, Zeta Plotting Users Guide, Version 3.0 Dec 1986: University of Adelaide, University Computing Service.

KOZERA, A. & STAJNIAK, J., Geofizyka Ogolna: Wydawnictwa Geologiczne - Warszawa 1971.

KSIĄZKIEWICZ, M., 1968, Geologia Dynamiczna: Wydanie Trzecie Rozszerzone, Wydawnictwa Geologiczne, Warszawa.

KUMARAPELI, P.S. & SAULL, V.A, 1966, The St. Lawrence Valley System: A North American Equivalent of the East African Rift Valley System: Canadian Journal of Earth Sciences, vol.3.

LEVORSEN, A.I., 1972, Geologia Ropy Naftowej i Gazu Ziarnego: Wydawnictwa Geologiczne, Warszawa.

LEGRAS, J., 1974, Praktyczne Metody Analizy Numerycznej: Wydawnictwo Naukowo-Techniczne, Warszawa.

LEITNER, R., 1970, Zarys Matematyki Wyższej dla Inżynierów: Wydawnictwo Naukowo-Techniczne, Warszawa.

LIPINSKI, E. & SWINIARSKI, R., 1977, Podstawy Informatyki - Fortran & Modelowanie Cyfrowe: Wydawnictwa Politechniki Warszawskiej, Warszawa.

MALTMAN, A., 1990, Geological Maps - an Introduction: Van Nostrand Reinhold, New York.

McGRATH, P.H., 1990, Dip and Depth of Density Boundaries Using Horizontal Derivatives of Upward - Continued Gravity Data: Geophysics, Vol.56, no.10 (October), pp. 1533-1542.

McQUILLIN, R. & BACON, M. & BARRCLAY, W., 1979, An Introduction to Seismic Interpretation: London, Graham & Trotman Limited.

MOORE, JMcM., 1979, Tectonics of the Najd Transcurrent Fault System, Saudi Arabia: J. Geol. Soc. London.

MOORE, P.S & MOUNT, T.J., 1982, Eromanga Basin Symposium: Adelaide, South Australia.

MORRIS, D. & SULTZBACH, R.A., 1967, Gravity Data Reduction and Interpretation Using a Digital Computer, a Case Study: Mining Geophysics, Vol.2, pp. 630-641.

MOSZYNSKI, K., 1971, Rozwiazywanie Rownan Rozniczkowych Zwyczajnych na Maszynach Cyfrowych: Wydawnictwo Naukowo-Techniczne, Warszawa.

NECAS, J., 1974, Pamieci Maszyn Cyfrowych w Systemach Informacyjnych: Wydawnictwo Naukowo-Techniczne, Warszawa.

PAINE, J.W., 1987, VAX Routines for Gridding and Countouring: Unpublished Internal Report, Department of Geology and Geophysics, University of Adelaide.

PAINE, J.W., 1987, Gamma User Guide: Unpublished Internal Report, Department of Geology and Geophysics, University of Adelaide.

RAO, B.S.R. & RADHAKRISHNA MURTHY, I.V., 1974, Gravity Interpretation by Characteristic Curves: Andhra University.

RIAD, S., 1977, Shear Zones in North Egypt Interpreted from Gravity Data: Geophysics Vol.42 No.6, pp. 1207-1214.

SELBY, J. & LINDSAY, J.M., 1982, Engineering Geology of the Adelaide City Area: Department of Mines and Energy Geological Survey of South Australia, Bulletin 51.

TALWANI, M. & EWING, M., 1960, Rapid computation of gravitational attraction of three-dimensional bodies of arbitrary shape: Geophysics, Vol.25 No.1, pp. 203-205.

TELFORD, W.M. & GELDART, L.P. & SHERIFF, R.E. & KEYS, D.A., Applied Geophysics: Cambridge

University Press.

THYSSEN-BORNEMISZA, S., 1964, Reconnaissance Survey Using Average Horizontal Gradients of Gravity: *Geophysics* Vol.30 No.4, pp. 661-666.

VERHOOGEN, J. & TURNER, J. & WEISS, L.E., 1969, *The Earth an Introduction to Physical Geology*: University of California at Berkeley.

WADEY, P., 1982, Zeta-1453 Plotting: Local Publication No. 415, January 1982: University of Adelaide, Computing Centre.

WARD, L., K., 1946, The Occurrence, Composition, Testing, and Utilisation of Underground Water in South Australia, and the Search for Further Supplies: *Bull.. geol. Surv. S. Aust.*, 23.